Optical Manipulation and the Angular Momentum of Light.

Anna T. O'Neil

Thesis for the degree of
Doctor of Philosophy

School of Physics and Astronomy,
University of St Andrews,
St Andrews, Fife,
Scotland

September 7, 2001

$\pi \in ?$

Declarations

(i) I, Anna Taylor O'Neil, hereby certify that this thesis, which is approximately 35000 words in length, has been written by me, that it is the record of work carried out by me and that it has not been submitted in any previous application for a higher degree.

Date 7th Sept. 2001 Signature of candidate

(ii) I was admitted as a research student in October 1998 and as a candidate for the degree of Ph. D. in October 1998; the higher study for which this is a record was carried out in the University of St Andrews and the University of Glasgow between 1998 and 2001.

Date 7th Sept. 2001 Signature of candidate

(iii) We hereby certify that the candidate has fulfilled the conditions of the Resolution and Regulations appropriate for the degree of Ph. D. in the University of St Andrews and that the candidate is qualified to submit this thesis in application for that degree.

Date 7th Sept. 2001 Signature of supervisors

In submitting this thesis to the University of St Andrews I understand that I am giving permission for it to be made available for use in accordance with the regulations of the University Library for the time being in force, subject to any copyright vested in the work not being affected thereby. I also understand that the title and abstract will be published, and that a copy of the work may be made and supplied to any *bona fide* library or research worker.

Date 7th Sept. 2001 Signature of candidate

Acknowledgements

I'd like to thank my supervisors Miles Padgett (University of Glasgow) and Wilson Sibbett (University of St Andrews) for all their time and understanding. Especially for managing to keep me sane throughout — in spite of everything!

I'd like to thank my family: Mum, Dad, my brothers Rick and Tom; my in-laws, Penny, Terry, Tuan, Samantha, Simon, Alex, Luke, Charlotte, and Rebecca.

Thanks to all my friends for making it an enjoyable experience. The climbing/squash crew: Johannes, Miles, Martin, Kenton, Gail and Paul (I'm still hoping for a game, Heather!) The St Andrews bunch: Jochen, Graham, Dave, Keith & Karen, Kishan, Gavin, Jacqueline, Shannon, Colin, Alan, Tanya, John-Mark and Cameron. The LIS group: for allowing me to be their social secretary and an Honorary member, sorry about the last few months' lack of nights out! Optics, the Gravvy-wavers, PPE, and everyone at Glasgow University's Department of Physics and Astronomy for making me so welcome. In particular, Graham, Lynne, Steven, John, Ian, Iain, Stephen and Bryan. Thanks to Michael for being my token biologist friend, who according to a certain individual will make me a more rounded human being (that is: if physicists are human, huh Steve!) Thanks, also, to the EPSRC for the financial support.

And finally, but by no means least, to my husband Toby××
(who is probably glad it's all over bar the shouting, err viva! (ahem)).

Abstract

This thesis consists primarily of an investigation into the action of laser light on particles held within optical tweezers. I present work on a dynamic method of measuring both the axial and lateral efficiencies of optical tweezers using Laguerre-Gaussian laser modes. I have developed a new and straightforward way of using an aperture within optical tweezers to rotate particles. I demonstrate a new method for trapping metal particles which is interesting for the insight it gives into the fundamental properties of light. Finally, I show the different ways spin and orbital angular momentum interact with a particle placed off-axis in a Laguerre-Gaussian beam. In addition to the work on optical tweezers I also explain a novel method for producing any type of pure laser mode from a Hermite-Gaussian laser mode. A summary of my conclusions together with some ideas for future work is included.

Publications

Journal Articles

1. A. T. O'Neil and J. Courtial, Mode transformations in terms of the constituent Hermite-Gaussian or Laguerre-Gaussian modes and the variable-phase mode converter, *Opt. Commun.*, **181**, 35–45, (2000).

2. A. T. O'Neil and M. J. Padgett, Three-dimensional optical confinement of micron-sized metal particles and the de-coupling of the spin and orbital angular momentum within an optical spanner, *Opt. Commun.* **185**, 139–143, (2000).

3. A. T. O'Neil and M. J. Padgett, Axial and lateral trapping efficiency of Laguerre-Gaussian laser modes in inverted optical tweezers, *Opt. Commun.* **193**, 45 –50, (2001).

4. A. T. O'Neil, I. MacVicar, L. Allen and M. J. Padgett, The intrinsic and extrinsic nature of the orbital angular momentum of a light beam, submitted to *Phys. Rev. Lett.* in June 2001, accepted November 2001.

5. A. T. O'Neil and M. J. Padgett, Rotational control within optical tweezers using a rotating aperture, submitted to *Opt. Lett.* in August 2001.

Articles in Conference Proceedings

6. A. T. O'Neil and M. J. Padgett, Manipulation of metallic particles in optical tweezers, in *Proc. of Conference on Lasers and Electro-Optics, CLEO®*, Baltimore, CThK49, May 1999.

7. A. T. O'Neil and M. J. Padgett, Efficiency for axial trapping of metallic particles using optical tweezers, in *Proc. of Quantum Electronics* 14, *QE*-14, Manchester, September 1999.

   ⋆ Winner of the Alan Gibson Prize 1999.

8. A. T. O'Neil and M. J. Padgett, Three-dimensional trapping of metallic particles in inverted optical tweezers, in *Highlights of Physics Research and R.& D.*, RAL, Oxon, November 1999.

   ⋆ Winner of the Cavendish Medal (Physics) 1999.

9. A. T. O'Neil and M. J. Padgett, Transfer of orbital angular momentum to metal particles confined using optical tweezers, in *Proc. of SPIE, Lase, Photonics West*, San Jose, January (2001).

10. A. T. O'Neil, I. MacVicar, L. Allen and M. J. Padgett, The nature of the spin and orbital angular momenta of light displayed by use of optical tweezers, in *Proc. of Quantum Electronics and Photonics* 15, *QEP*-15, Glasgow, September 2001.

11. A. T. O'Neil and M. J. Padgett, Rotational control in optical tweezers using a rotating aperture, in *Proc. of Quantum Electronics and Photonics* 15, *QEP*-15, Glasgow, September 2001.

Contents

List of Figures

List of Tables

Chapter 1

Introduction

This thesis provides a description of research relating to the development and use of particular laser beam specifications that play an important rôle in the interaction between light and microscopic particles. The techniques developed, in addition to being useful tools, further the knowledge of the fundamental properties of light.

This introduction is followed by a review chapter (Chapter 2) containing a description of the various laser modes used throughout my work together with some methods for producing them. This material is frequently cross-referenced to subsequent sections in the thesis.

In Chapter 3, I describe a new technique for producing any type of pure laser mode from a Hermite-Gaussian laser mode [1]. This gives the flexibility to produce any laser mode which could, possibly in the future, be applied to areas such as trapping and quantum entanglement.

In Chapter 4, I provide a survey of work within the field of optical trapping that led to Ashkin's discovery of optical tweezers [2]. This is followed in Chapter 5 by a description of an extension to previous work on measuring the efficiency (Q) of optical tweezers using Laguerre-Gaussian modes [3, 4, 5]. As well an axial Q-value, I detail a dynamic way of measuring both the axial and lateral Q for a system [6].

In Chapter 6, I describe a new and straightforward way of using an aperture within optical tweezers to rotate particles [7]. Although rotation was initially observed in 1991 [8], I devised a way of rotating refractive objects without the need for a computer-generated hologram or any other specialised components. The simplicity introduced from using only an aperture allowed great flexibility when it came to altering the optical tweezers system, especially when reverting back to a more traditional system.

Chapter 7 details a novel method I have developed for trapping silver particles [9]. Although the trapping of metal particles has been investigated previously [10, 11], the method which I describe is interesting for the insight it gives into the fundamental properties of light. This research yielded unexpected results, and in the subsequent course of my research it opened up new avenues which resulted in the work discussed in Chapter 8.

In Chapter 8, I describe the different ways that spin and orbital angular momentum interact with a particle placed off-axis in a Laguerre-Gaussian (LG) beam [12]. This work served to further my understanding of spin and orbital angular momentum, which again deepened knowledge into the fundamental properties of light. Finally, in Chapter 9 a summary of my conclusions is presented together with some ideas for future work.

Chapter 2

Hermite-Gaussian & Laguerre-Gaussian laser modes

2.1 Introduction

This chapter contains some of the background material required for the rest of this thesis. I discuss Hermite-Gaussian (HG) and Laguerre-Gaussian (LG) laser modes, as well as the angular momentum (AM) of a light beam. I explain the relationship between Hermite- and Laguerre-Gaussian modes. One of the important properties of LG laser modes is the type of angular momentum they possess — orbital AM. Finally, I describe methods of producing LG modes.

2.2 Laser Modes

Laser modes are characterised by their transverse mode profile. A fundamental Gaussian ($TEM_{0,0}$) laser mode can be expressed by Equation (2.1). This equation describes the Gaussian beam in the (x, y)-plane, propagating

in the z-direction [13]:

$$u(x,y,z) = \sqrt{\frac{2}{\pi}}\frac{1}{w(z)}\exp(i\psi(z))\exp\left(-\frac{x^2+y^2}{w^2(z)}\right) \times \exp\left(-ik\frac{x^2+y^2}{2R(z)}\right). \tag{2.1}$$

Here $w(z)$ is the beam radius, $\psi(z)$ is the *Gouy phase shift*[1] and $R(z)$ is the wave front radius of curvature. This beam has a beam waist, denoted w_0, at $z = 0$ and expands to a far-field angle on both sides of the origin along the z-axis. Given w_0 we can define the *Rayleigh range*, z_R, by [13]

$$z_R = \frac{\pi {w_0}^2}{\lambda} \tag{2.2}$$

The Rayleigh range, z_R, is the distance from the origin at which the diameter of the beam, of wavelength λ, has increased to $\sqrt{2}\,w_0$ — at this distance the radius of curvature is at a minimum. Characteristic beam parameters can be obtained from the Rayleigh range [13]:

$$w(z) = w_0\sqrt{1+\frac{z^2}{{z_R}^2}} \tag{2.3}$$

$$\psi(z) = \arctan\left(\frac{z}{z_R}\right) \tag{2.4}$$

$$R(z) = z\left(1+\frac{{z_R}^2}{z^2}\right) \tag{2.5}$$

Examples of high-order laser modes are the various Hermite-Gaussian and Laguerre-Gaussian modes, represented by $\mathrm{HG}_{m,n}$ and LG_p^l respectively, where m, n, l and p are integers. A Hermite-Gaussian beam, $\mathrm{HG}_{m,n}$, has m intensity nulls in the x-direction and n intensity nulls in the y-direction.

Hermite-Gaussian and Laguerre-Gaussian modes are generalisations of the fundamental Gaussian mode shown in Equation (2.1). HG and LG modes

[1]The factors in Equation (2.1) consist of an intensity normalisation factor $\sqrt{\frac{2}{\pi}\frac{1}{w(z)}}$, a Gouy phase shift, the Gaussian beam profile and a phase shift due to the curvature of the beam's phase fronts.

have a larger Gouy phase term, as well as having a different intensity profile defined by Hermite and Laguerre polynomials respectively. For the zero order (fundamental) mode, $N = 0$, these polynomials are equal to unity, recovering the Gaussian form as shown in Equation (2.1).

Ignoring normalisation, Hermite-Gaussian modes have the form [13]

$$\begin{aligned} u_{m,n}(x,y,z) &= \frac{1}{w(z)} \exp(i(N+1)\psi(z)) \exp\left(-\frac{x^2+y^2}{w^2(z)}\right) \\ &\quad \times \exp\left(-ik\frac{x^2+y^2}{2R(z)}\right) H_m\left(\frac{\sqrt{2}\,x}{w(z)}\right) H_n\left(\frac{\sqrt{2}\,y}{w(z)}\right) \end{aligned} \tag{2.6}$$

where $w(z)$,$\psi(z)$ and $R(z)$ are the same as before. The order, N, of the mode is given by the expression

$$N = m + n. \tag{2.7}$$

H_m and H_n are Hermite polynomials of order m and n, respectively, where m and n are integers. The Hermite polynomial, of order k, is given by [14]

$$H_k(x) = \sum_{s=0}^{k/2} \frac{(-1)^s (2x)^{k-2s} k!}{(k-2s)!\,s!}. \tag{2.8}$$

The additional Gouy phase is $N\psi(z)$. Figure 2.1 shows two examples of the intensity profiles calculated for Hermite-Gaussian laser modes.

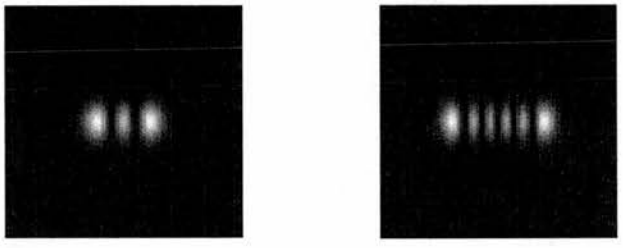

Figure 2.1: (a) $HG_{2,0}$ (b) $HG_{5,0}$

The Laguerre-Gaussian modes are described by [13]

$$\begin{aligned} u_p{}^l(r,\varphi,z) &= \frac{1}{w(z)} \exp(i(N+1)\psi(z)) \exp\left(-\frac{r^2}{w^2(z)}\right) \exp\left(-ik\frac{r^2}{2R(z)}\right) \\ &\quad \times \exp(-il\varphi)\left(\frac{2r^2}{w^2(z)}\right)^{\frac{|l|}{2}} L_p^{|l|}\left(\frac{2r^2}{w^2(z)}\right) \end{aligned} \tag{2.9}$$

where the mode order, N, is given by the expression

$$N = |l| + 2p. \tag{2.10}$$

$L_p^{|l|}$ are generalised Laguerre polynomials. A Laguerre-Gaussian beam, LG_p^l, is characterised by l phase fronts in the *azimuthal*-direction and p intensity nulls in the *radial*-direction. These mode indices p and l are integers with $p \geq 0$ and $-\infty < l < \infty$. The number of radial nodes is $(p+1)$ for $p > 0$. For a given LG beam of index l we have $2\pi l$ cycles of azimuthal phase around the ring. Modes with $l \neq 0$ have an intensity null on the z-axis and an azimuthal phase dependency $\exp(-il\varphi)$ leading to helical phase fronts [15]. The Laguerre polynomial [16] is given by

$$L_p^l(x) = \sum_{s=0}^{n+1} \frac{(-x)^s (l+p)!}{(l-s)!(p-s)!s!}. \tag{2.11}$$

The orbital angular momentum of LG laser modes depends on their azimuthal mode index. The orbital angular momentum carried by the phase fronts is given by

$$\text{Orbital Angular Momentum} = l\hbar \text{ per photon}, \tag{2.12}$$

see [17]. The number of intertwined phase fronts depends upon the value of l. As we can see from Equation (2.12), for a larger l-value there are more phase fronts and thus more orbital AM[2]. In addition to the orbital AM there is also a spin angular momentum given by

$$\text{Spin Angular Momentum} = \sigma\hbar \text{ per photon}, \tag{2.13}$$

see [17]. Here σ is the index indicating the degree of circular polarisation of the light: for right-hand circularly polarised light, $\sigma = +1$; for left-hand circularly polarised light, $\sigma = -1$; and for linearly polarised light, $\sigma = 0$. For many applications Laguerre-Gaussian modes with $p = 0$ are the most useful as $\{\mathrm{LG}_0^l : l = 0, 1, 2, 3, \ldots\}$ forms a set of single annular rings. These beams have an on-axis phase dislocation which is often called an optical vortex [18].

[2]The angular momentum of light is described in Section 2.3.

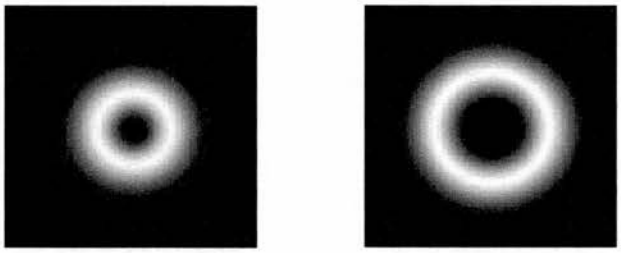

Figure 2.2: (a) LG_0^2 (b) LG_0^5

For example, LG_0^2, shown in Figure 2.2(a), has $2\hbar$ per photon of orbital angular momentum, whilst LG_0^5, shown in Figure 2.2(b), has $5\hbar$ per photon of orbital angular momentum. The LG_0^5 has a larger central hole than the LG_0^2. Looking at Figure 2.2 we see that both of these examples consist of a single annular ring — there are no nodes going out from the centre because $p = 0$. The first order beam, the $l = 1$ mode, is of particular interest since the intrinsic spin AM component can be used to cancel out that of the orbital AM [19]. Table 2.1 shows a variety of laser modes grouped according to their mode order.

In the remainder of this chapter, I explain the types of laser mode, their importance and ways of producing them.

N	Laser Modes			
0	 $HG_{0,0}$		 LG_0^0	
1	 $HG_{1,0}$	 $HG_{0,1}$	 LG_0^{-1}	 LG_0^1
2	 $HG_{2,0}$	 $HG_{1,1}$	 $HG_{0,2}$	
	 LG_0^{-2}	 LG_1^0	 LG_0^2	
3	 $HG_{3,0}$	 $HG_{2,1}$	 $HG_{1,2}$	 $HG_{0,3}$
	 LG_0^{-3}	 LG_1^{-1}	 LG_1^1	 LG_0^3

Table 2.1: Calculated examples of the intensity profiles of Hermite-Gaussian and Laguerre-Gaussian laser modes grouped according to their mode order, N.

2.3 Angular Momentum of Light

A circularly polarised beam of light is known to carry angular momentum, [20, 21]. Circularly polarised Laguerre-Gaussian (LG) modes possess both *orbital* AM and *spin* AM. Each circularly polarised LG beam has an angular momentum of $(l + \sigma)\hbar$ per photon where l is the azimuthal mode index and $\sigma = \pm 1$ for right- or left-handed circularly polarised light. The effects of angular momentum are difficult to measure, since in many instances they are very small[3]. The first attempt to measure the torque produced by spin angular momentum was made by Beth in 1936 [20]. He reported that his findings supported the theory of sign and magnitude. More recently, different groups [23, 19] have worked on orbital AM.

Hermite-Gaussian laser modes are often present in lasers, whereas Laguerre-Gaussian laser modes are less common. This is because cylindrical symmetry is hard to maintain within a laser cavity as any dust or astigmatism compromises the desired symmetry and results in a HG output.

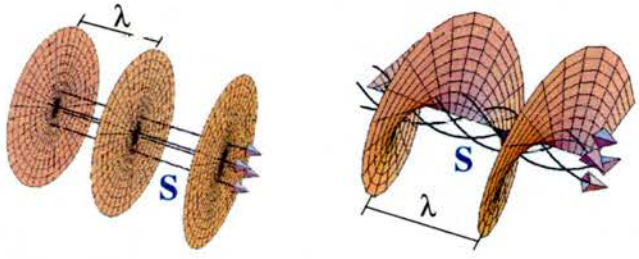

Figure 2.3: THE *Screwthread* POYNTING VECTOR. A Hermite-Gaussian laser beam has plane phase fronts. A Poynting vector, $\boldsymbol{S}$, is perpendicular to the phase fronts, and points along the direction of beam propagation; it is the product of the electric and magnetic fields. In contrast, an $l = 1$ Laguerre-Gaussian laser beam has one helical phase front, and the Poynting vector spirals around the beam's axis.

[3]For example, the angular momentum flux produced by a circularly polarised 10mW He-Ne laser is of the order of 10^{-18}Nm [22].

A laser beam with an azimuthal phase term produces a screwthread Poynting vector, that is, a helical phase front, (see Figure 2.3). As stated earlier, on page 6, the number of intertwined phase fronts depends directly upon the value of l. The Poynting vector is always perpendicular to the phase fronts present in a beam. Hence, if there are helical phase fronts then there is a spiralling Poynting vector, if there are plane phase fronts then the Poynting vector just points straight ahead in the direction of beam propagation.

2.4 How to produce LG laser modes

In this section I describe several different ways of producing a Laguerre-Gaussian laser mode from a Hermite-Gaussian mode. In Section 2.4.1 I describe how to produce pure Laguerre-Gaussian laser modes by using cylindrical lenses [24]. In Section 2.4.2 I discuss how to direct a $TEM_{0,0}$, the fundamental Gaussian mode, onto an appropriate computer-generated hologram [25, 26, 27], thus producing a Laguerre-Gaussian mode. Alternatively, as shown in Section 2.4.3, they can be made by using spiral phase plates [28, 29].

These are all well established production methods for LG modes. A more recent addition was the creation of a laser cavity for efficient production of LG beams [30], which is described in Section 2.4.4. Similar laser cavities have been investigated before [31], but the new design, published in 2000 [30], is the most successful thus far, in that it is an efficient way of producing LG modes. However, it is not clear how far these LG modes will propagate upon exiting the laser cavity [32].

These methods have various pros and cons relating to the production of Laguerre-Gaussian laser modes. In Table 2.2 I list some of the main advantages and disadvantages which influence the choice of method to produce LG modes.

METHOD	PROS	CONS
CYLINDRICAL LENS MODE CONVERTER	Pure LG Mode production	Require higher order HG mode to use it
HOLOGRAMS	Can be used with a fundamental Gaussian mode to produce a LG mode	Superposition of LG Modes
SPIRAL PHASE PLATE	Can be used with a fundamental Gaussian mode to produce a LG mode	Superposition of LG Modes
LASER CAVITY	LG Modes produced straight from laser cavity	Require a special laser cavity, i.e. it can not be used with proprietary bought lasers (e.g. diodes)

Table 2.2: Advantages and disadvantages of various methods for producing Laguerre-Gaussian laser modes

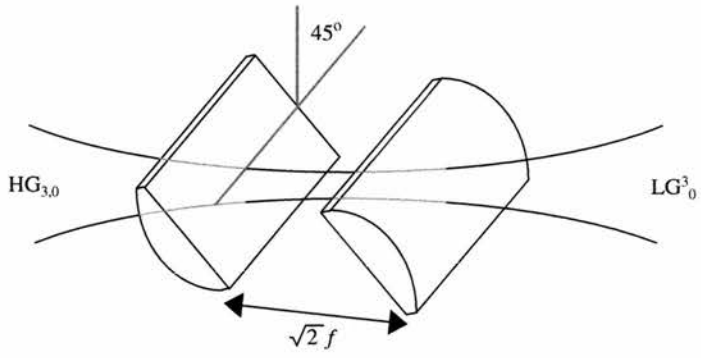

Figure 2.4: THE CYLINDRICAL LENS MODE CONVERTER (CLMC). This is made up of two cylindrical lenses with identical focal length, f. When the lenses are placed $\sqrt{2}f$ apart one gets a $\frac{\pi}{2}$-mode converter and when this Mode Converter is placed with a rotation of 45° with respect to the incident beam it transforms the beam from HG to a LG, or vice versa.

2.4.1 The Cylindrical lens mode converter (CLMC)

Figure 2.4 shows a $\frac{\pi}{2}$-converter. It is made up of two cylindrical lenses with identical focal length, f. The lenses must be placed back-to-back at a distance, $d = \sqrt{2}f$ apart. When the beam waist of the beam, w_0, is midway between the lenses and satisfies the condition $w_0 = \sqrt{(1 + \frac{\sqrt{2}}{2})f\frac{\lambda}{\pi}}$ in the cylindrical lens mode converter the beam can be transformed. When the CLMC is placed at 45° to the incident beam it transforms the beam from Hermite-Gaussian to Laguerre-Gaussian, and vice versa, as the light passes through it. The right lenses must be chosen to ensure that the beam is the correct size for the system to work successfully.

Using this converter, a phase difference of $\frac{\pi}{2}$ is introduced between neighbouring modes[4] of order N, as shown in Figure 2.5. In this way any Hermite-Gaussian beam can be converted to a Laguerre-Gaussian beam. A Hermite-Gaussian beam, $HG_{m,n}$, is converted using a cylindrical lens mode converter

[4]The term *neighbouring* refers to laser modes of the same order with a differing m (or n) value of 1.

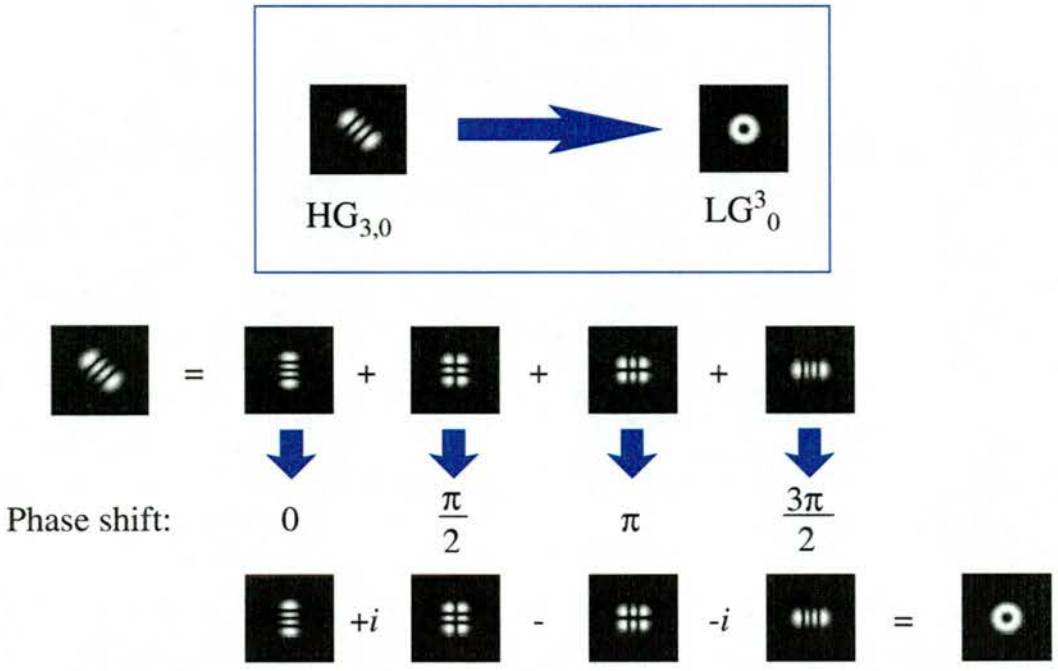

Figure 2.5: THE CYLINDRICAL LENS MODE CONVERTER TRANSFORMATION. This diagram shows how HG modes sum to give LG modes in the CLMC. The phase shift of the modes is given by $(m\text{-}n)\frac{\pi}{4}$.

to a Laguerre-Gaussian laser beam[5], LG_p^l. This transformation is governed by Equation (2.14) relating the $\frac{\pi}{2}$-converter from Hermite-Gaussian mode indices, m and n, to the Laguerre-Gaussian mode indices, l and p.

$$\begin{gathered} HG_{m,n} \Rightarrow LG_p^l \\ \text{where } l = m - n \text{ and } p = \min(m, n) \end{gathered} \tag{2.14}$$

Note that the l-values can be either positive or negative.

Recall that each beam has a mode order, N, associated with it. Hence, equating Equations (2.7) and (2.10), where the respective order of HG and LG beams is defined we see

$$N = m + n = |l| + 2p \tag{2.15}$$

Some examples of conversions with the $\frac{\pi}{2}$-converter are shown in Figures 2.6, 2.7 and 2.8. Transforming $HG_{5,0}$ using Equation (2.14) we obtain LG_0^5

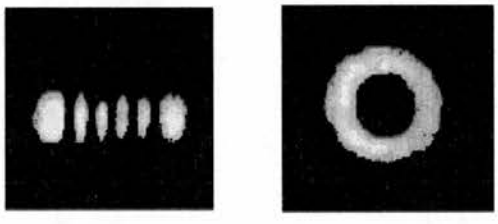

Figure 2.6: The experimental $HG_{5,0}$ mode shown here has five nodes present in the x-direction, and none in the y-direction. Hermite-Gaussian laser modes also have no orbital angular momentum. The LG_0^5 mode, experimentally obtained, has an orbital angular momentum equal to $5\hbar$ per photon. It has a large central hole with no nodes going out from the centre.

(Figure 2.6), from $HG_{3,1}$ we get LG_1^2 (Figure 2.7), and finally from $HG_{3,3}$ we get LG_3^0 (see Figure 2.8). M. J. Padgett *et al.* investigated the intensity and phase structure of these laser modes in 1996 [33].

[5]Once again, l is the azimuthal mode index, and corresponds to the 'ringsize', and p is the radial mode index, and corresponds to the number of rings coming out from the centre of the beam.

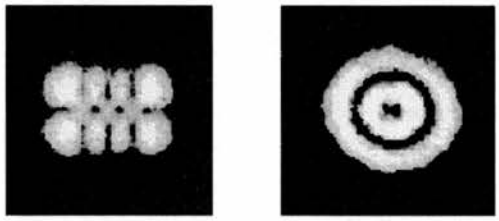

Figure 2.7: The $HG_{3,1}$ mode has three nodes in the x-direction, and one in the y-direction. After transformation, the LG_1^2 mode produced has one node going out from the centre, and $2\hbar$ of orbital angular momentum per photon. There is an azimuthal phase shift of 4π around its ring. These beam profiles were obtained experimentally.

Figure 2.8: Laser modes obtained during an experiment. The $HG_{3,3}$ mode has three nodes in both the x- and y-directions. After producing LG_3^0 we have a laser mode with three nodes going out from the centre, but no orbital angular momentum. There is no azimuthal phase shift in this case.

Cylindrical lens mode converters, including the $\frac{\pi}{2}$-converter, play an important role in the Variable phase-shift mode converter which is described in Chapter 3.

2.4.2 Computer-generated Holograms

Computer-generated holograms are regularly used in practice [34] despite the fact that they do not produce pure Laguerre-Gaussian modes. Holograms only produce superpositions of modes with specific azimuthal mode index l, but different values of radial mode index p.

Holograms can be either reflection or transmission holograms. Reflection holograms reconstruct the desired profile from reflected light coming back

off the surface, whilst transmission holograms are so-called because they reconstruct the desired profile after the light has propagated through the hologram.

Throughout this research transmission holograms were always used. Initially they were made by Jochen Arlt using holographic film [35], but later ones were made using holographic plates by the author. Holograms can be produced to introduce either a phase change or an amplitude variation depending on the design and their development process.

Beams with helical phase fronts are easily produced using holograms. These holograms can simply consist of a interference pattern between a plane-wave input beam and a beam with a prescribed azimuthal phase dependence. This interference results in a diffraction grating with an l-fold dislocation in the centre on the beam axis. Illumination with a fundamental Gaussian mode results in many diffracted orders[6], the zeroth order being the original beam profile, and the first order being a beam which possesses l helical phase fronts intertwined about the beam axis. *Blazing*[7] of a diffraction grating produces mode orders with preferential power levels in one particular order, usually the first order. In Figure 2.9 we can see the pattern used to produce $l = 1, 2, 3, 4$ and 8 Laguerre-Gaussian beams where $p = 0$. When a hologram with an l_{holo}-fold dislocation is illuminated with a beam of azimuthal mode index equal to l_{beam}, the first order diffracted beam has an azimuthal mode index l_{total} given by

$$l_{total} = l_{holo} + l_{beam}$$

In the special case of $l_{holo} = -l_{beam}$ subsequently a beam with a large on axis intensity profile and plane phase fronts is produced.

[6]A diffraction grating converts a single laser mode to produce a mode with many different orders. The zeroth order is not displaced with respect to the original beam, but the other orders are labelled out from this central order, with $\pm 1, \pm 2, \ldots$ etc.

[7]For more information on the blazing of holograms — see Appendix A, Section A.3.

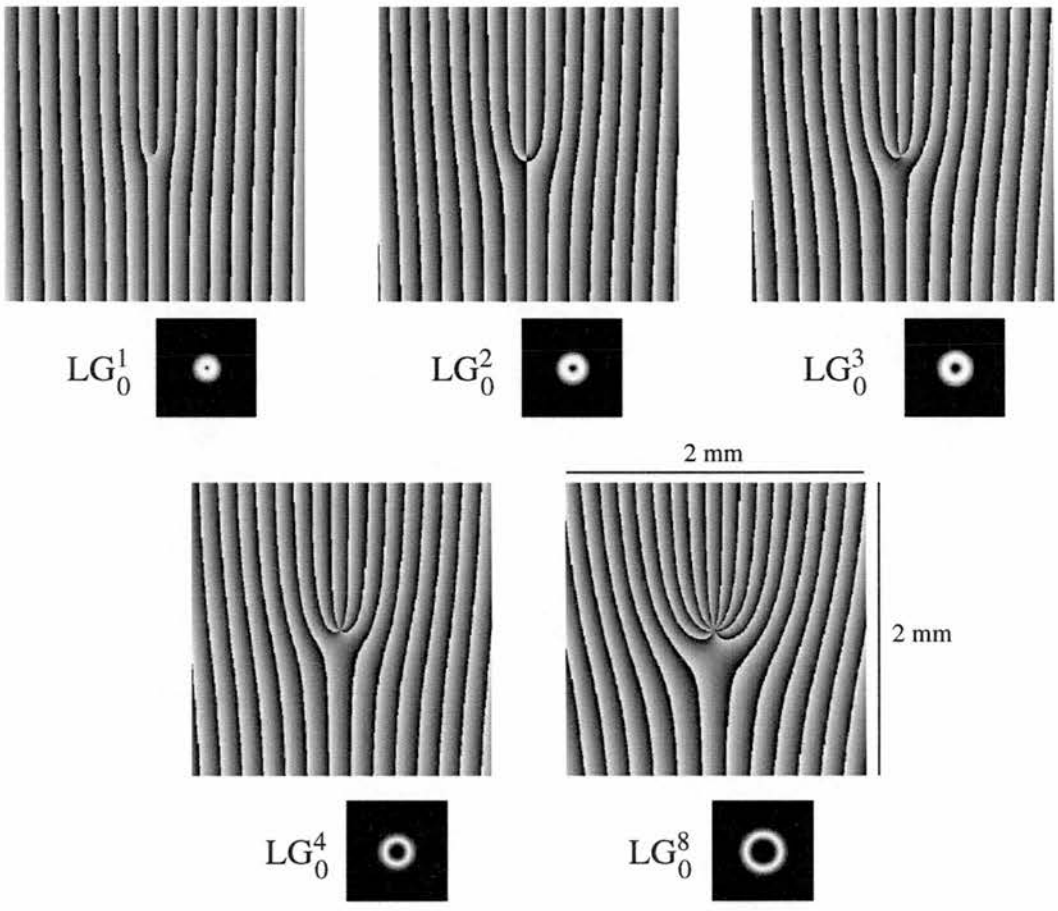

Figure 2.9: The centres of the calculated blazed hologram patterns used to produce the various Laguerre-Gaussian beams shown.

Amplitude Holograms

Amplitude holograms modify the amplitude of the reference beam depending on the calculated pattern. They record an interference of the pattern and a reference beam using the difference in transparency level of the final hologram. The varying transparency levels are what produce the desired output beam. Unfortunately, because of this they are quite lossy, and do not achieve a high transmission.

Phase Holograms

Phase holograms are so-called due to the fact that they alter the phase of the reference beam in order to create the final beam. The phase change is caused by a difference in refractive index, and since the transparency is maintained at a high level the theoretical maximum transmission for a phase hologram is 100% making them a more desirable prospect for this research because of the requirement of a reasonable power level. In practice 100% cannot be obtained, but 35% efficiencies are possible and were more than adequate for this research.

Experimentation using Holograms

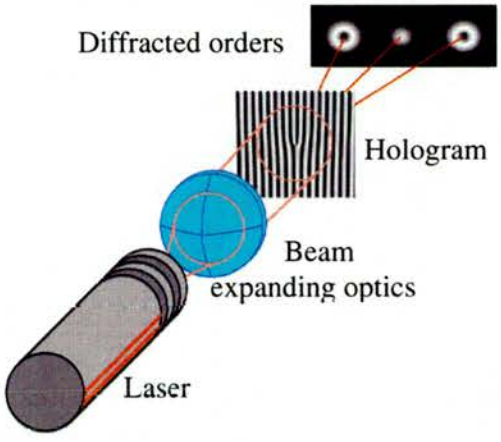

Figure 2.10: HOLOGRAM WITH INCIDENT LASER MODE: The various orders produced when a laser beam is sent through a hologram.

When using a hologram to change the mode profile, the beam size of the fundamental Gaussian is expanded to about one centimetre in diameter. This beam expansion reduces the intensity incident from the laser on the hologram, thus increasing the hologram's lifetime. The beam is directed through the hologram with the centre of the incident laser beam aligned directly with the dislocation present in the hologram's pattern. Beyond the hologram a number of orders of Laguerre-Gaussian laser modes are obtained,

these are shown in Figure 2.10. One can then select, for example using an iris, the first order mode, which, depending on the initial pattern used, gives us a Laguerre-Gaussian laser beam, LG_p^l, where l takes some non-zero integer value $|l| \geq 1$. In most of the work presented here the value of p is 0.

Further information about how to produce holograms and the recipes used during this research can be found in Appendix A. As well as detailing the recipes along with some insight into which recipe performed the best on the holographic plates, I also give information for sourcing the plates and required chemicals.

2.4.3 Spiral Phase plates

Spiral phase plates (see Figure 2.11) are another method of producing Laguerre-Gaussian modes [28, 29]. This method, like the holograms, produces a superposition of Laguerre-Gaussian modes. A spiral phase plate is a variable thickness component which at one radial section has zero thickness, and whilst moving this radial line around the circle the thickness increases gradually until, when one moves around 2π of the circle, there is a step height of $(n-1)l\lambda$. Once again, n is the refractive index, l is the azimuthal mode index and λ is the specific wavelength of electromagnetic radiation, e.g. light, that the spiral phase plate is designed for. A laser beam is used with the spiral phase plate in a similar manner to when using a hologram. A fundamental Gaussian beam is incident on the spiral phase plate at the central point of the dislocation. The beam goes through the plate to produce a superposition[8] of Laguerre-Gaussian beams which can then be used for experimental purposes, and is actually ideal for millimetre waves [29].

[8]This technique, similar to the hologram technique, produces LG modes that are a superposition of azimuthal index, l, with constant radial mode index, p.

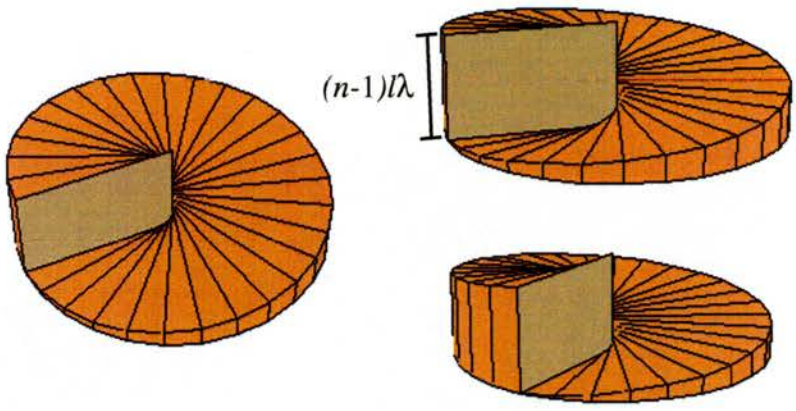

Figure 2.11: A SPIRAL PHASE PLATE: Material composition and size depends upon the phase plate's specific use.

2.4.4 Laser cavities

This was originally an unusual way of producing LG modes. Laser cavity designs had occasionally been used before. For example, in [31], a Dove prism was introduced into a ring cavity design. These designs have not, as yet, been very successful. Despite the physics being sound, they appear to lack practical viability.

A group in Israel [30], designed a laser cavity where the back mirror is replaced by a reflective spiral phase element and in the cavity between the gain medium and the output coupler is a cylindrical lens. This lens is paired with another on the outside beyond the laser cavity which is used to collimate the beam. This system, using a large gain medium, produces LG modes, with a high power of 1.2 W for a CO_2 laser, $\lambda = 10.2\mu$m. For a fundamental Gaussian, their reduced efficiency gave a power output of 0.9 W. This system can be used in many applications to input a LG beam directly from a stable laser cavity.

The reason that in this case the production of higher-order Laguerre-Gaussian beams is more efficient than the production of the fundamental

Gaussian beams is that a much greater region of the gain medium within the laser cavity is used. This additional gain results in greater amplification of the mode for each round trip in the laser cavity, and hence a subsequently 33% higher value on release from the CO_2 laser [30].

2.5 Summary

In this chapter I have discussed the types of laser modes which are available. I have described their attributes, given examples of the various modes and given ways of producing them. The content is intended as useful background material which underlies the research described in this thesis.

Chapter 3

The Variable Phase-shift Mode Converter

3.1 Introduction

Hermite-Gaussian and Laguerre-Gaussian laser modes were described in Chapter 2. In this chapter I show how the variable phase-shift mode converter allows intermediate superpositions of Hermite-Gaussian and Laguerre-Gaussian laser modes to be produced. I then go on to show how the analogy between polarisation and laser modes can be employed to construct a variable phase-shift mode converter.

In this chapter I also discuss the theory of the optical components used to build a variable phase-shift mode converter, see Section 3.3. The results obtained with such a set-up are given in Section 3.5. This chapter contains material that was the basis for a paper published in Optics Communications [1], although here I give examples for $HG_{1,0}$ and $HG_{2,2}$ in addition to the $HG_{3,0}$ demonstrated there. Theoretical calculations, as well as the actual experimental results, are shown to agree favourably.

3.2 Analogy between Polarisation of light & Laser Modes

As stated in this chapter's introduction one can describe the polarisation of a light beam as a superposition of two orthogonal polarisations. Figure 3.1[1] shows the decomposition of various types of polarised light in terms of two orthogonal linear polarisations. In the same way the mode structure of a light beam can be described in terms of superpositions of orthogonal Hermite-Gaussian or Laguerre-Gaussian laser modes [36]. Figure 3.2 outlines the decomposition of various Hermite-Gaussian and Laguerre-Gaussian modes in terms of orthogonal Hermite-Gaussian modes. By comparing Figures 3.1 and 3.2 we can see clearly the analogy between polarised light and laser modes.

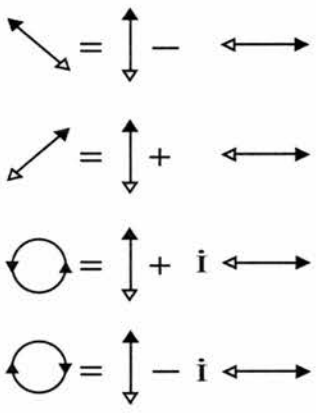

Figure 3.1: Polarisation of light and how to produce circularly polarised light. The light and dark ends have opposite phase.

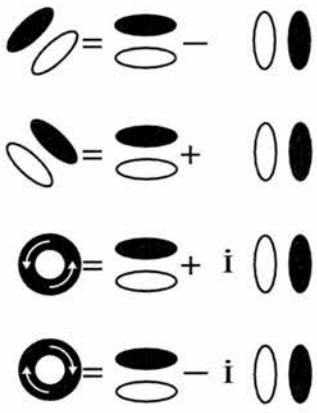

Figure 3.2: How to produce first-order LG modes from HG modes. The light and dark lobes have 0 and π phase respectively.

This analogy goes much deeper. The Poincaré sphere for polarised light [36] is shown in Figure 3.3. Given the analogy between polarised light and laser

[1]Once again, the i term is equivalent to a $\frac{\pi}{2}$ phase shift (see Figure 2.5).

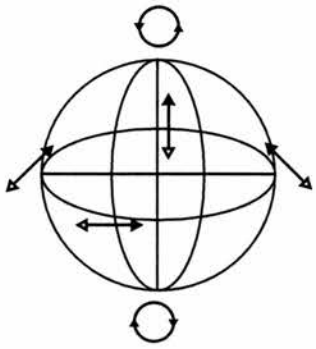

Figure 3.3: The Poincaré Sphere of polarised light.

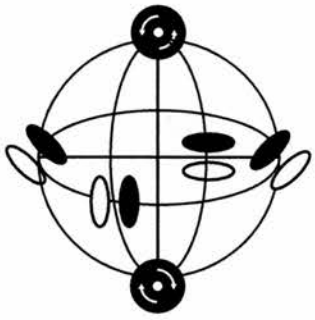

Figure 3.4: The laser mode equivalent of the Poincaré sphere [36].

modes one can draw an equivalent of that sphere, as shown in Figure 3.4. I am able also to draw definite parallels between the following optical components

- A $\frac{\pi}{2}$ mode converter (for modes) $\equiv$ a quarter-wave $\left(\frac{\lambda}{4}\right)$ plate (for polarisation).
- A π mode converter or a Dove prism $\equiv$ a half-wave $\left(\frac{\lambda}{2}\right)$ plate.

Propagation of light beams through optical elements which preserve the mode order were described in [37] in terms of constituent Hermite-Gaussian modes. That paper describes the matrices for the phase and intensity structure of monochromatic light and the transformation between different mode structures. Hermite-Gaussian laser modes are shown to be mathematically analogous to linearly polarised light. In addition, propagation of light beams can also be described in terms of superpositions of Laguerre-Gaussian modes [1]. Laguerre-Gaussian laser modes are mathematically analogous to circularly polarised light (see Table 3.1).

Wave Plate	Quarter ($\frac{\lambda}{4}$)	Half ($\frac{\lambda}{2}$)
Matrix multiplication	$\begin{bmatrix} 1 & 0 \\ 0 & -i \end{bmatrix} \begin{bmatrix} E_x \\ E_y \end{bmatrix}$	$\begin{bmatrix} 1 & 0 \\ 0 & -1 \end{bmatrix} \begin{bmatrix} E_x \\ E_y \end{bmatrix}$

Mode Converter	$\frac{\pi}{2}$	π
Matrix multiplication	$\begin{bmatrix} 1 & 0 \\ 0 & -i \end{bmatrix} \begin{bmatrix} E_{\mathrm{HG}_{1,0}} \\ E_{\mathrm{HG}_{0,1}} \end{bmatrix}$	$\begin{bmatrix} 1 & 0 \\ 0 & -1 \end{bmatrix} \begin{bmatrix} E_{\mathrm{HG}_{1,0}} \\ E_{\mathrm{HG}_{0,1}} \end{bmatrix}$

Table 3.1: JONES AND MODE MATRICES AND VECTORS. Analogy between waveplates for polarised light and mode converters for first-order laser modes.

3.3 Theory of the components in the variable phase-shift mode converter

The variable phase-shift mode converter is made up of two cylindrical lens mode converters, see Figure 2.4 in Section 2.4.1 for a reminder, and two Dove prisms, see Figure 3.5, along with extra lenses to obtain the correct beam size as it propagates through the system.

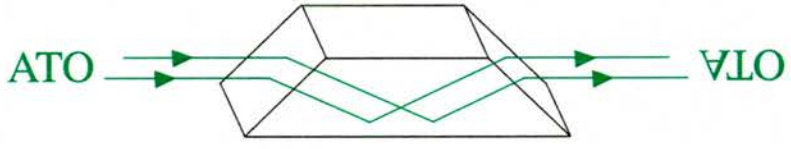

Figure 3.5: THE DOVE PRISM. The path of the light rays as they pass through the Dove prism is shown. The rays get switched over reversing the handedness of the amplitude cross-section of the light as they pass through. For our purposes, it is important that the image is flipped about the horizontal axis because the angle of the Dove prism is $\theta = 0$. This is equivalent to a cylindrical lens mode converter with the lenses placed $2f$ apart, i.e. a π-converter.

3.3.1 Cylindrical Lens Mode Converter

In Chapter 2, I discussed ways of producing Laguerre-Gaussian laser modes. The cylindrical lens mode converter is a way of producing pure Laguerre-Gaussian laser modes from Hermite-Gaussian laser modes, as described in Section 2.4.1.

In general, a Φ-converter introduces a phase difference of Φ between 'neighbouring' HG modes of the same order, i.e modes whose m (or n) index differs by 1. For example, if initially all the HG modes of order $N = 2$ have a phase 0, then upon propagation through a Φ-converter, in the simplest case, the $HG_{0,2}$ mode now has for example a phase $-\Phi$, the $HG_{1,1}$ mode now has a phase 0, and the $HG_{2,0}$ mode now has a phase $+\Phi$. The general equation for this phase shift imparted to a mode with indices m, n is

$$\text{Phase shift introduced by a } \Phi\text{-converter} = (n - m)\frac{\Phi}{2}, \qquad (3.1)$$

see Figure 3.6. This figure illustrates the phase change introduced by a Φ-mode converter for HG modes of order $N = 1$.

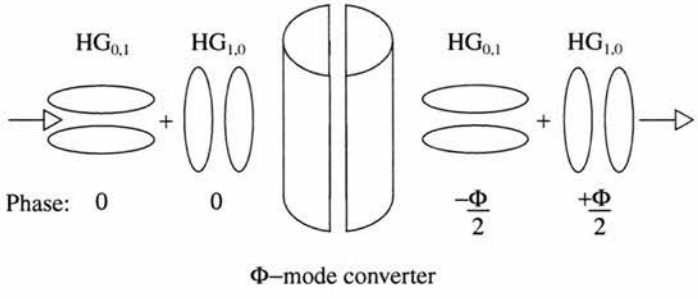

Figure 3.6: Phase shift introduced by a Φ-mode converter. (The phase of each mode is indicated under each of them.) On propagation through the mode converter one mode has a phase shift of $-\frac{\Phi}{2}$ and the other has a phase shift of $+\frac{\Phi}{2}$.

The $\frac{\pi}{2}$-converter

Recall (from Section 2.4.1) that the $\frac{\pi}{2}$-converter is made up of two cylindrical lenses with identical focal length, f. These lenses must be placed a distance

$d = \sqrt{2}f$ apart at 45° to the incident beam, thus producing a pure Laguerre-Gaussian beam from a pure Hermite-Gaussian beam and vice versa.

Using this converter a phase difference of $\frac{\pi}{2}$ is introduced between neighbouring modes of order N. For example, if I have Hermite-Gaussian laser modes of order $N = 1$, the neighbouring modes are given as $\mathrm{HG}_{0,1}$ and $\mathrm{HG}_{1,0}$. These modes get a subsequent phase difference of $\frac{\pi}{2}$ between the two modes, after travelling through the converter, this produces a Laguerre-Gaussian mode. In this way any Hermite-Gaussian beam can be converted to a Laguerre-Gaussian beam. The equations relating the $\frac{\pi}{2}$-converter's transformations from Hermite-Gaussian mode indices, m and n, to the Laguerre-Gaussian mode indices, l and p were described in Equation (2.14). Recall

$$\mathrm{HG}_{m,n} \Rightarrow \mathrm{LG}_p^l$$
$$\text{where } l = m - n \text{ and } p = \min(m, n).$$

The π-converter

The π-converter introduces a phase difference, $\Phi = \pi$ between 'neighbouring' laser modes. This acts in the same way as a Dove prism, and is analogous to the Half-wave plate in the case of polarisation.

3.3.2 Beams of Higher Order

In the case of laser modes the variable phase shift mode converter works for higher order modes as well as the first order modes which are analogous to polarisation. Each beam has a mode order, N, associated with it. This was defined in Equation (2.15) as

$$N = m + n = |l| + 2p.$$

Table 2.1 shows all the intensity profiles for each of the mode orders for $N = 0, 1, 2, 3$. In Table 3.2 I calculate the corresponding modes for orders

N	$HG_{m,n}$	LG_p^l
0	$HG_{0,0}$	LG_0^0
1	$HG_{0,1}$ $\boxed{HG_{1,0}}$	LG_0^{-1} $\boxed{LG_0^1}$
2	$HG_{0,2}$ $HG_{1,1}$ $HG_{2,0}$	LG_0^{-2} LG_1^0 LG_0^2
3	$HG_{0,3}$ $HG_{1,2}$ $HG_{2,1}$ $\boxed{HG_{3,0}}$	LG_0^{-3} LG_1^{-1} LG_1^1 $\boxed{LG_0^3}$
4	$HG_{0,4}$ $HG_{1,3}$ $\boxed{HG_{2,2}}$ $HG_{3,1}$ $HG_{4,0}$	LG_0^{-4} LG_1^{-2} $\boxed{LG_2^0}$ LG_1^2 LG_0^4

Table 3.2: MODE ORDERS. Here we can see the mode order for various HG and LG beams. The boxed HG modes are the input modes used for the results in this chapter. The boxed LG modes are those produced for the special case of a $\frac{\pi}{2}$-converter placed at 45° to the HG mode.

from $N = 0, 1, \ldots, 4$. Any mode of order N can be expressed as the sum of $(N+1)$ Hermite-Gaussian or Laguerre-Gaussian modes of that order. Such a mode can be expressed as

$$\begin{bmatrix} E_{N,0} \\ E_{N-1,1} \\ \cdots \\ E_{1,N-1} \\ E_{0,N} \end{bmatrix},$$

where $E_{m,n}$ is the complex amplitude coefficient of the Hermite-Gaussian mode, $HG_{m,n}$.

3.4 The variable phase-shift mode converter

The diagram in Figure 3.7(a) shows polarised light going through a system of wave plates. In Figure 3.7(a) the final half-wave plate and quarter-wave plate can be orientated to give us a full set of polarisations, including elliptical polarisations, on the Poincaré sphere, see Figure 3.3. The following comparisons, along with the relevant spin angular momentum (SAM) and

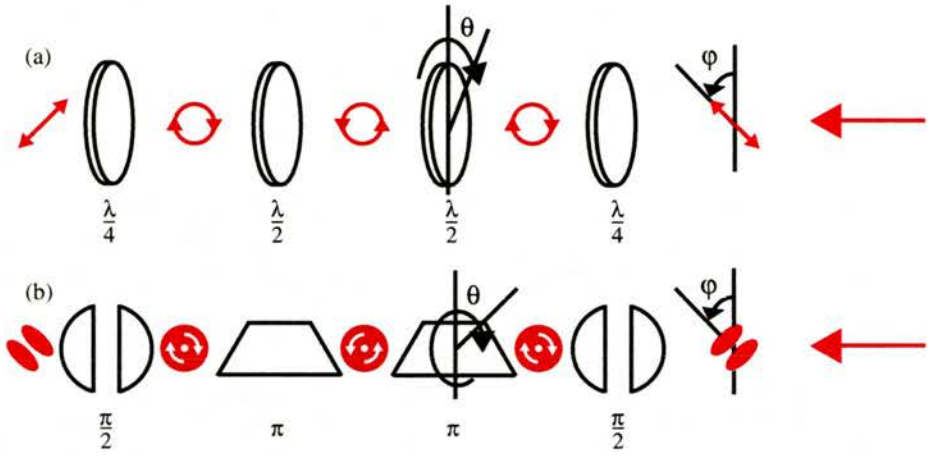

Figure 3.7: (a) A variable phase-shift wave plate comprising a combination of quarter- and half-wave plates. Also shown are the polarisation states throughout the system for the simple example of the incident light being linearly polarised at 45° and the half-wave plates being rotated with respect to each other through an angle $\theta = 0°$. (b) Here we see a combination of $\frac{\pi}{2}$ and π mode converters that makes up a variable phase-shift mode converter. In this system I have the angles of rotation for the mode converter and Dove prism denoted by φ and θ respectively throughout. The laser modes are shown for angles of $\theta = 0°$ and $\varphi = 45°$.

orbital angular momentum (OAM) components, can be made:

- Linearly Polarised Light (SAM $= 0$) $\equiv$ HG modes (OAM $= 0$).
- Circularly Polarised Light (SAM $= \hbar$) $\equiv$ LG modes (OAM $= l\hbar$).
- Elliptically Polarised Light $\equiv$ Intermediate laser modes.

Figure 3.8 shows the positions of linear, elliptical and circular polarisations on the Poincaré sphere. Since polarised light can be directly compared with first order laser modes it is valid for the variable phase-shift mode converter (VPMC). When I replace the HWP with a π-converter and the QWP with a $\frac{\pi}{2}$-converter the transformation is similar. We can see the laser mode equivalent of the Poincaré sphere in Figure 3.9.

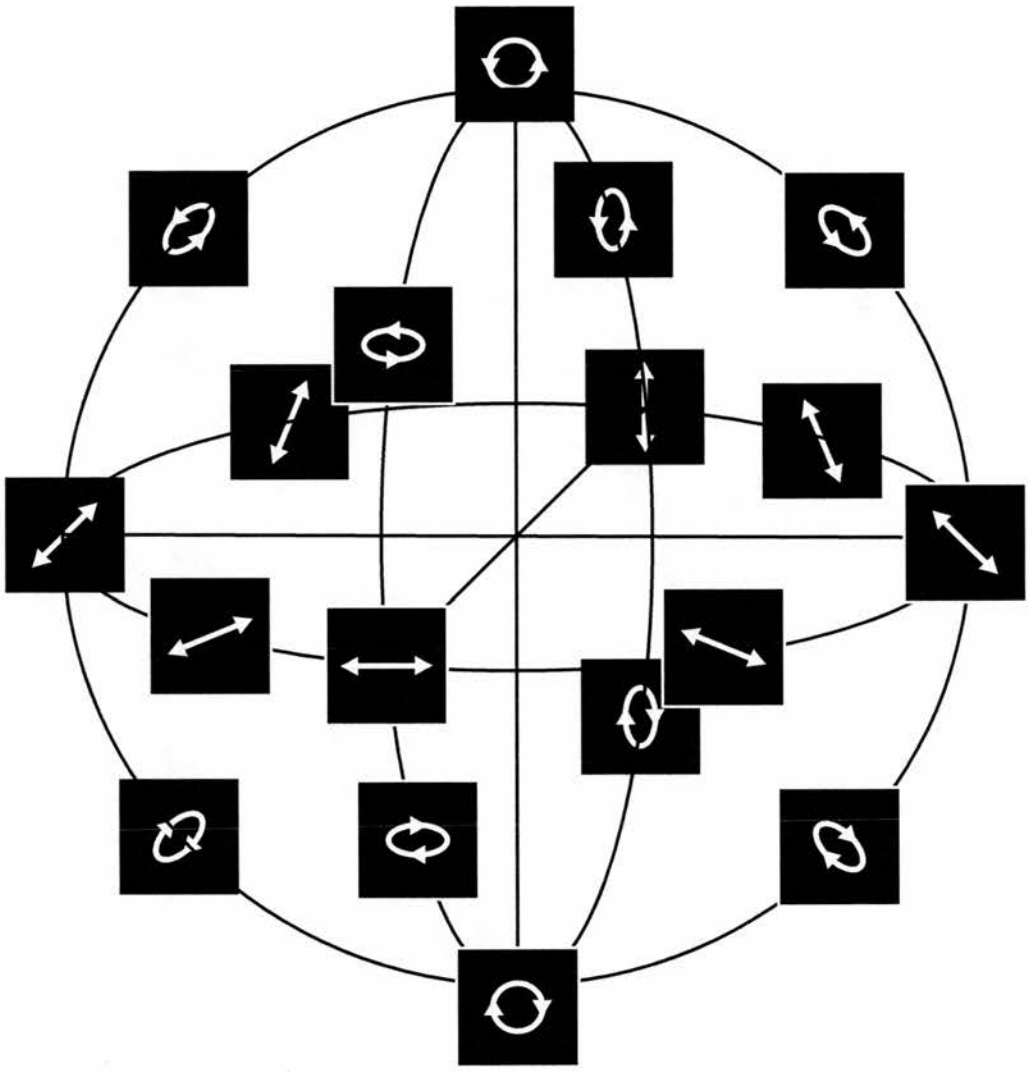

Figure 3.8: Poincaré sphere showing Linear, Elliptical and Circular Polarisations.

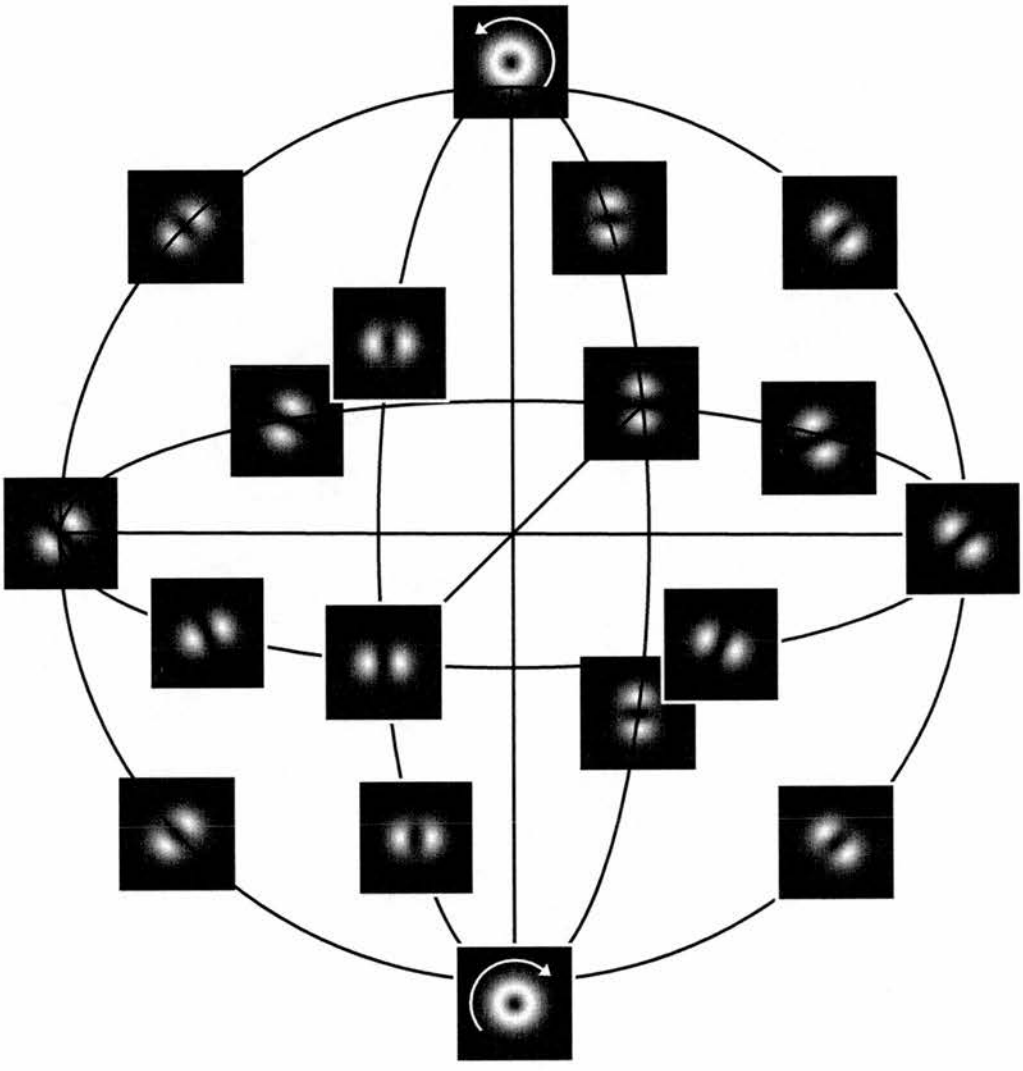

Figure 3.9: Poincaré sphere equivalent showing first-order modes.

3.4.1 How the variable phase-shift mode converter works

A $\frac{\pi}{2}$-mode converter introduces a phase difference of $\frac{\pi}{2}$ between neighbouring HG modes[2]. In general, as stated previously, a Φ-converter introduces a phase shift of Φ. The first-order modes are analogous to the polarisation states described, but as far as laser modes go it holds for higher orders as well.

One can introduce specific rotations of LG modes using a π-mode converter, a Dove prism can be used to perform this function. When a LG laser mode is incident on a Dove prism it is flipped as described in Figure 3.5. When two Dove prisms are placed next to one another with a rotation difference of θ there are two actions of flipping resulting in a rotation of the mode by 2θ, see Figure 3.10. An LG mode has a cylindrical intensity distribution

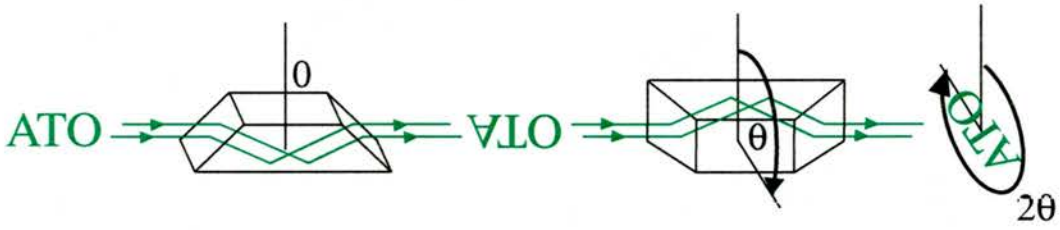

Figure 3.10: A rotation introduced by the flipping action of two nested Dove prisms.

with an azimuthal phase term consequently rotating a LG beam through an angle 2θ, which is equivalent to a phase delay of $2\theta \cdot l$. In general the input beam is a superposition of LG modes of many orders, these modes have different integer values of l; a different phase shift, due to the dependency on l, is given to each LG mode depending on their order. This phase shift is the basis of the variable phase-shift mode converter.

[2]Once again, *neighbouring* modes are those modes of the *same* order, N, which differ by m or $n = 1$.

Conversion of HG modes to LG modes is achieved using a $\frac{\pi}{2}$-converter placed at an angle of 45° to the HG mode, see Section 2.4.1. It is then easy to rotate the LG modes as previously described (see Figure 3.10) using two Dove prisms, by any specific angle. Having done this, conversion back to a HG mode is done using another $\frac{\pi}{2}$-converter and I can achieve any intermediate mode I wish, see Figure 3.11.

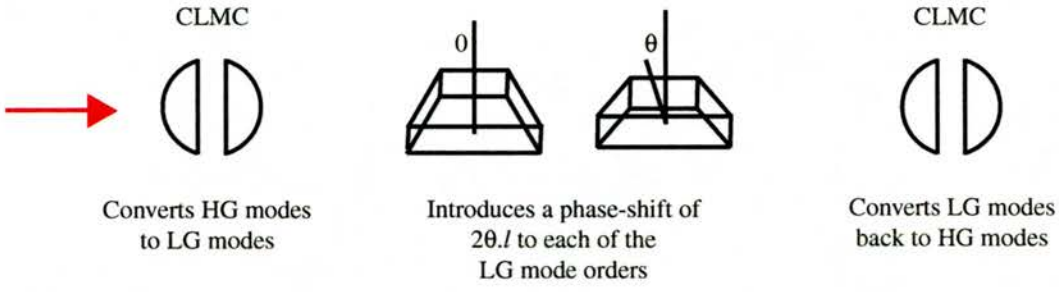

Figure 3.11: The variable phase-shift mode converter described in three stages. The conversion of HG to LG modes, the rotation of these LG modes including a phase-shift depending on their order, and the subsequent conversion back to HG mode.

3.4.2 Mode Converter Example

For the rotation angle, $\varphi = 45°$, in the variable phase-shift mode converter, the original Hermite-Gaussian mode is converted to a Laguerre-Gaussian mode upon propagation through the first $\frac{\pi}{2}$-mode converter, it is then rotated by 2θ when the Dove prisms are placed an angle of θ apart. This rotated LG mode then goes through the second $\frac{\pi}{2}$-mode converter and is converted back to a Hermite-Gaussian mode.

Providing I have a Hermite-Gaussian laser mode incident at the required angle on the first cylindrical lens mode converter then I can achieve specific mode types. These different laser modes are created using specific angles for the optical system's components. The angle θ acts on the DP, whilst φ is the rotation angle for the CLMC. The specific angles specified allow

production of all laser modes Hermite-Gaussian and Laguerre-Gaussian and those in between. For example, using angles of $\theta = 0, \frac{\pi}{4}, \ldots \pi$ and $\varphi = 0°, 90°$ acting on a Hermite-Gaussian laser mode I maintain a Hermite-Gaussian laser mode. If I have angles of $\theta = \frac{\pi}{2}$ and $\varphi = 45°$ acting on a Hermite-Gaussian laser mode I get a Laguerre-Gaussian laser mode. Finally, using angles of $\theta = \frac{\pi}{2}$ and $\varphi = 22.5°$ I form an intermediate laser mode.

The Poincaré sphere equivalent of first order modes is shown in Figure 3.9. This shows all the theoretical calculations for an $l = 1$ Laguerre-Gaussian mode. They are displayed in their correct positions on the Poincaré sphere equivalent. This demonstrates how the mode changes as you move through different angles around the sphere.

3.5 Results obtained with the Variable phase-shift mode converter

In this section I compare the theoretical and experimental results obtained using a variable phase-shift mode converter. The agreement of these results with that of the theory indicates that this experiment was successful. The apparatus is shown in Figure 3.12. A schematic of the equipment with focal lengths of specific lenses is shown in Figure 3.13.

In the following pages I include the results for the input Hermite-Gaussian modes, $HG_{1,0}$, $HG_{3,0}$ and $HG_{2,2}$. The theoretical and experimental results for $HG_{1,0}$ are displayed in Figure 3.14 and Figure 3.15 respectively. Theoretical and experimental results for $HG_{3,0}$ are displayed in Figure 3.16 and Figure 3.17 respectively. Theoretical and experimental results for $HG_{2,2}$ are displayed in Figure 3.18 and Figure 3.19 respectively.

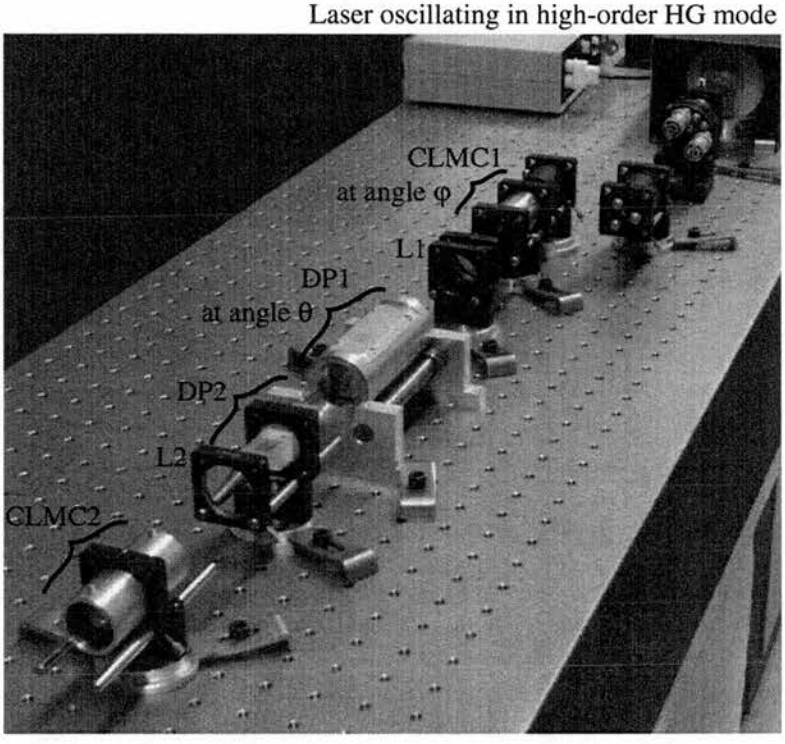

Figure 3.12: The experimental setup for the mode converter. CLMC1 and CLMC2 are the cylindrical lens mode converters, DP1 and DP2 are the Dove prisms, and L1 and L2 are lenses placed back to back.

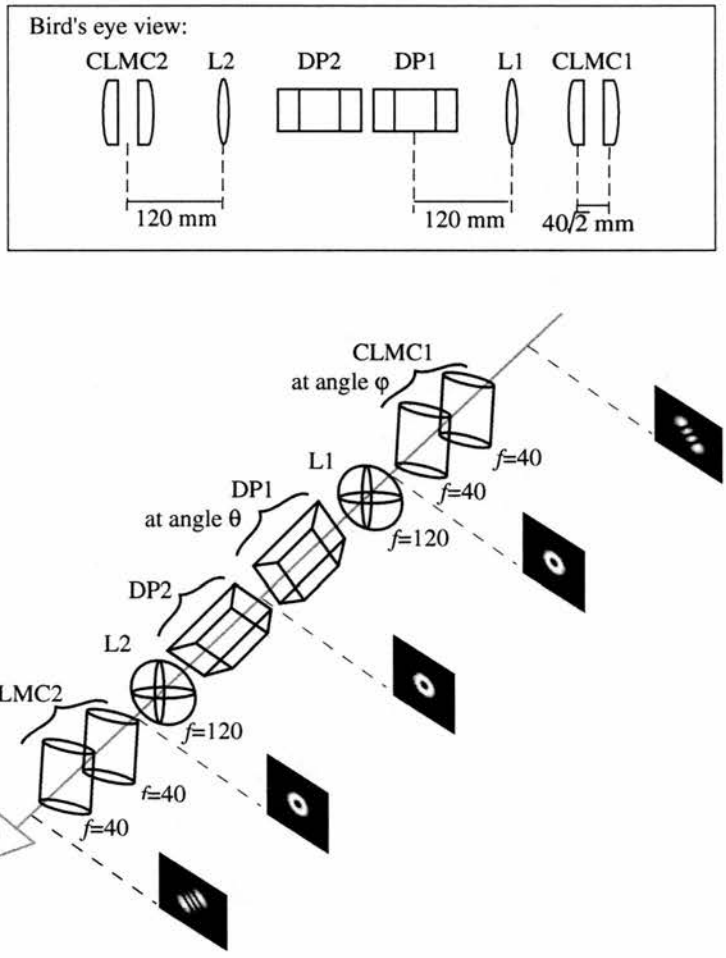

Figure 3.13: A schematic of the setup for the mode converter. This shows the focal length (in mm) of all the lenses used.

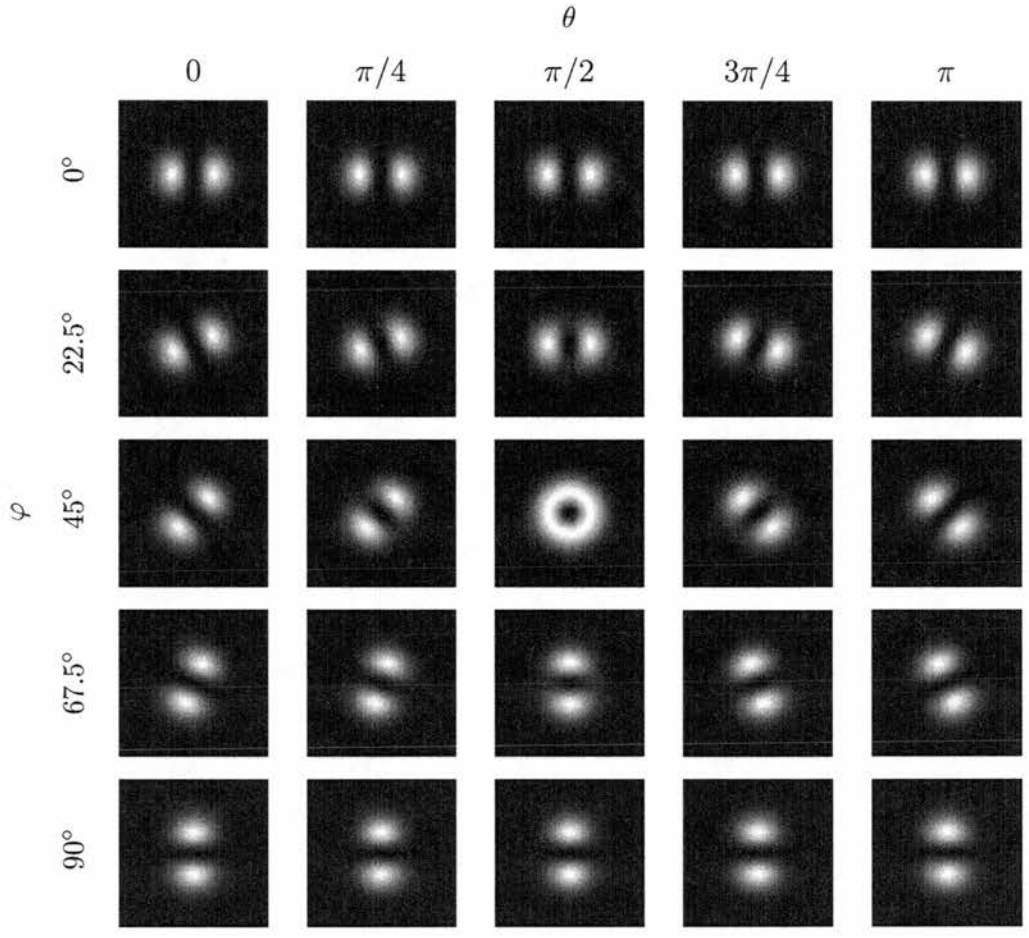

Figure 3.14: Theoretical calculations for $l = 1$. The angles θ and φ are the required angles for the DP and CLMC respectively.

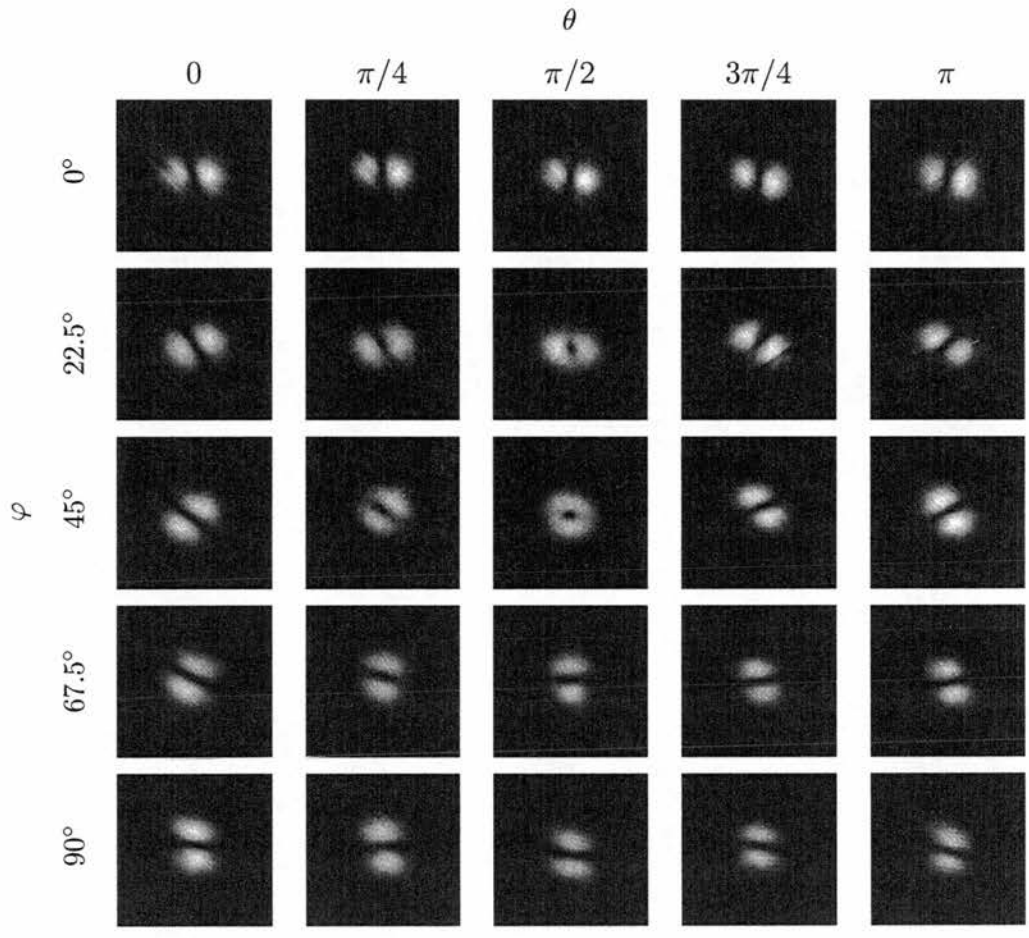

Figure 3.15: Experimental results for $l = 1$. The angles θ and φ are the required angles for the DP and CLMC respectively.

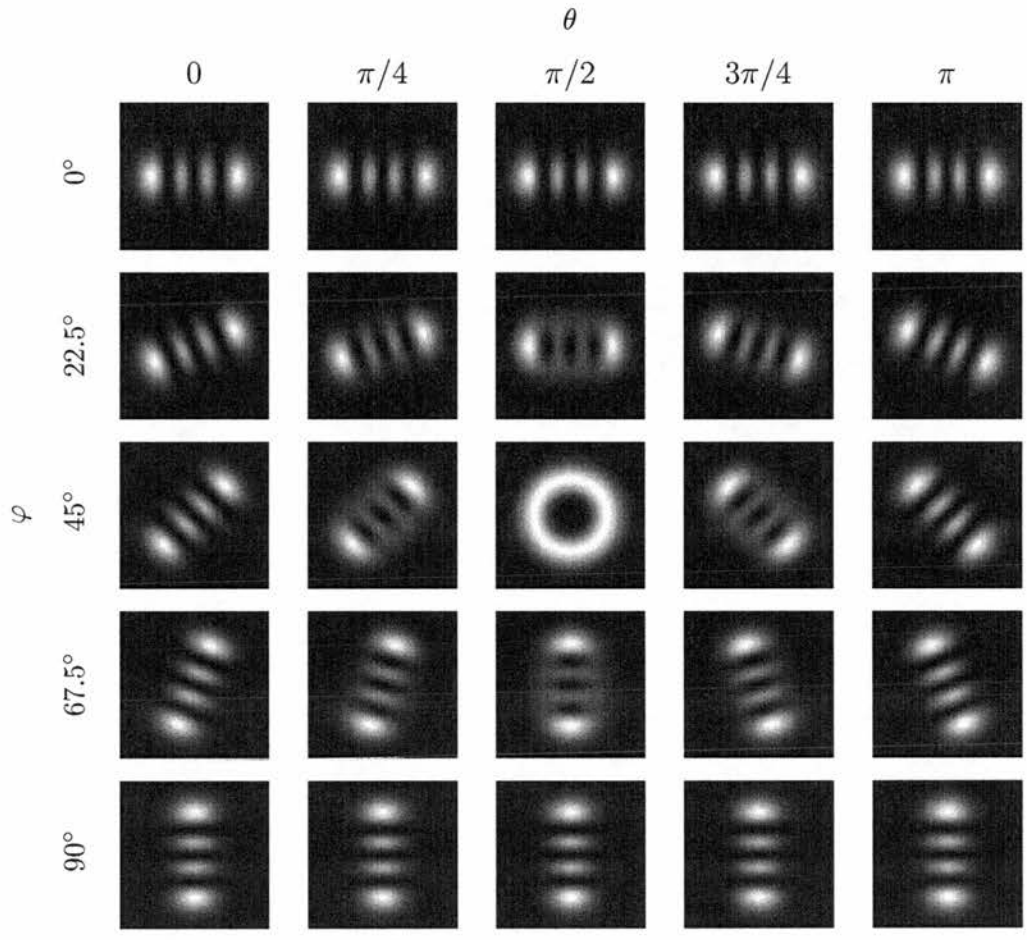

Figure 3.16: Theoretical calculations for $l = 3$. The angles θ and φ are the required angles for the DP and CLMC respectively.

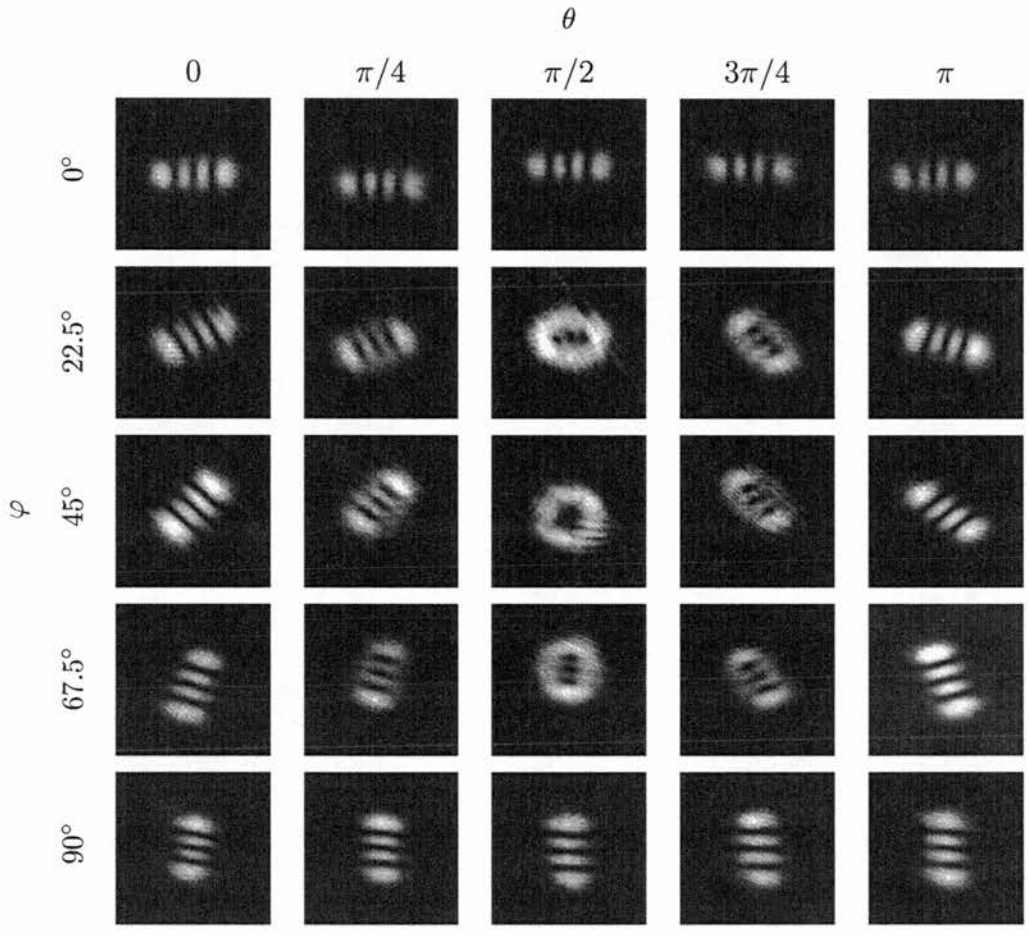

Figure 3.17: Experimental results for $l = 3$. The angles θ and φ are the required angles for the DP and CLMC respectively.

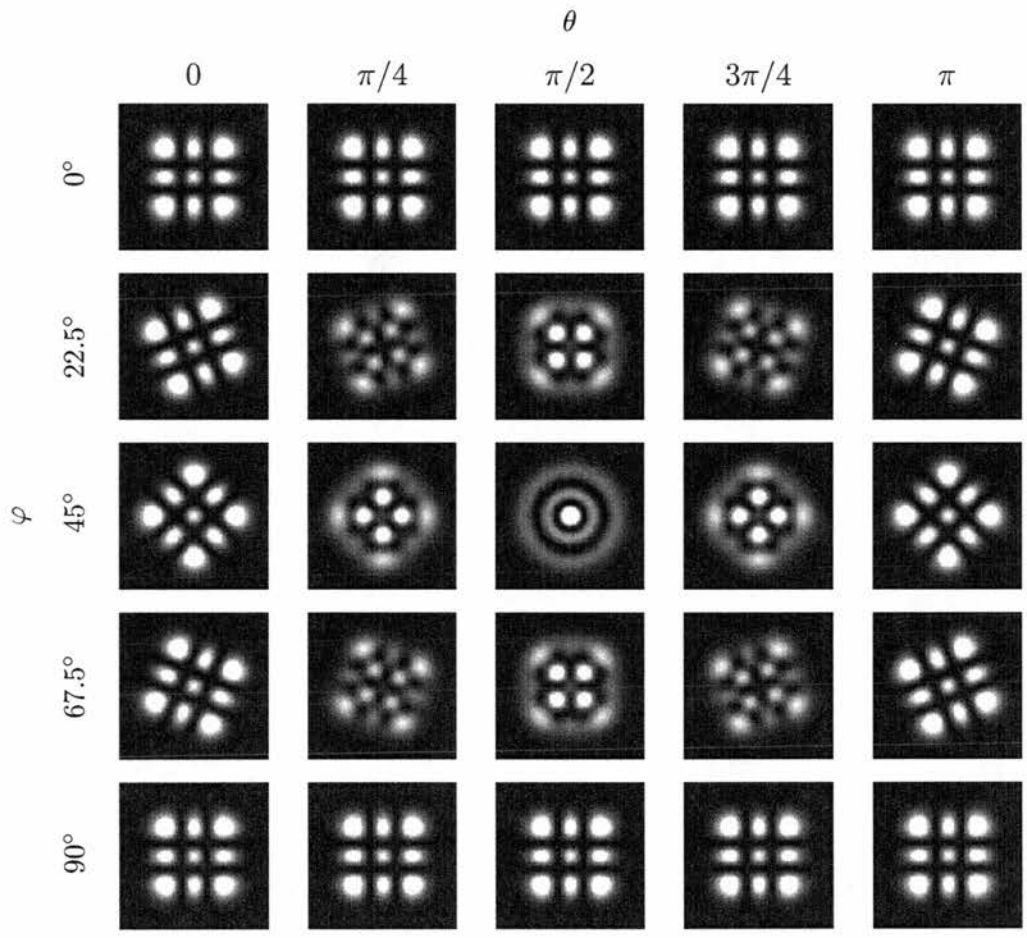

Figure 3.18: Theoretical results for $l = 0$ and $p = 2$. The angles θ and φ are the required angles for the DP and CLMC respectively.

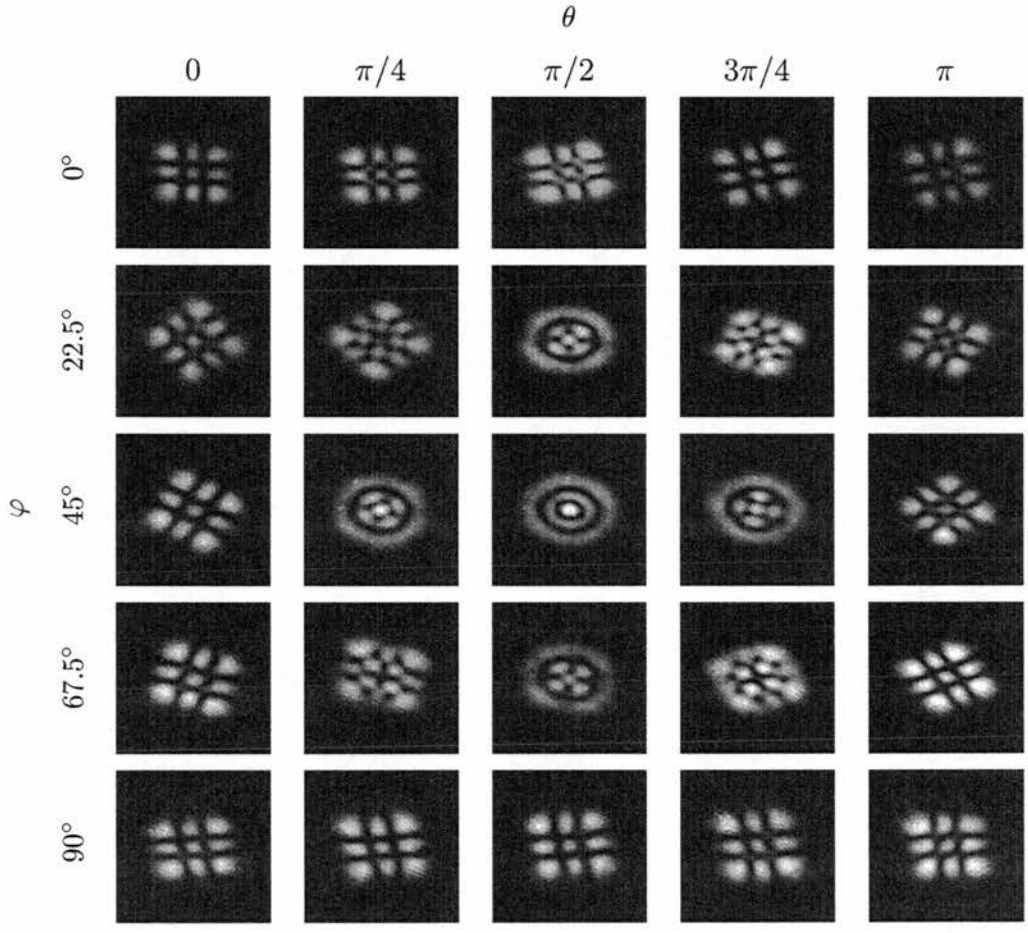

Figure 3.19: Experimental results for $l = 0$ and $p = 2$. The angles θ and φ are the required angles for the DP and CLMC respectively.

3.6 Summary

I have described the parallels between polarisation of light and laser modes. These parallels are summarised in Table 3.3. I then described how these

POLARISATION	MODE
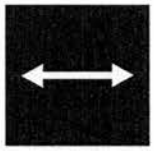 Linear	 Hermite-Gaussian
 Elliptical	 Intermediate
 Circular	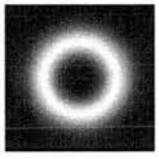 Laguerre-Gaussian

Table 3.3: Analogy between Polarisation and Laser modes.

analogies can be employed to construct a variable phase-shift mode converter based on simple optical components.

3.7 Conclusion

This proved an interesting experiment which explored the analogy between polarisation and laser modes further. The physical description of how to

produce the intermediate modes was useful to provide. One of its suggested future uses in which it may prove invaluable is for physically testing out the theories of quantum entanglement [38, 39], but that requires further research.

Chapter 4

Optical Tweezers Explained – Their Evolution

4.1 Introduction

Optical tweezers use modern laser technology to grasp and move microscopic particles. These have been adapted to further include optical spanners which, an extension of the theme, uses laser light to rotate objects held within an arrangement of optical tweezers [2]. Progress within the last twenty years, from their inception to the making of a viable product, which is now widely available, has been significant. A complete commercial optical tweezers set up is currently available from Cell Robotics [40] and P.A.L.M [41]. Their uses are extensive, and there are many applications in which these devices may be implemented with great effect. The tweezers are proving to be particularly helpful in microbiology and medicine, when manipulating living cells in sterile surroundings.

Recently, research has been additionally focused on to the trapping of metallic particles, which by the nature of their reflective properties are more difficult to trap with light. This research requires the use of some techniques

which allow us to get around this problem. This chapter includes the background, recent developments, my research and potential areas for progress in the future.

4.2 Background: The Development Of Optical Tweezers

4.2.1 In the Beginning: Low and High Index Spheres

Over thirty years ago in 1970 Ashkin was describing the ability of trapping and accelerating particles by the radiation pressure of light [42]. He managed to trap micron-sized particles within an optical potential well. He achieved this with a fundamental ($TEM_{0,0}$) mode CW laser light in the green. Initial experimentation was carried out using a single laser beam focused down through a cell containing water and transparent latex spheres of 0.59 μm, 1.31 μm, and 2.68 μm in diameter. This glass cell was 120 μm thick and allowed the argon ion laser to be moved to trap individual spheres. A particle positioned away from the central beam axis underwent forces that were described by Ashkin as:

> "The sphere is simultaneously drawn into the beam axis and accelerated in the direction of the light. It moves off with a limiting velocity of microns per second until it hits the front surface of the glass cell where it remains trapped in the beam. If the beam is blocked, the sphere wanders off by Brownian motion" [42].

When mixing the spheres, the 2.68 μm diameter spheres were successfully trapped, whilst the 0.59 μm spheres remained free to move by Brownian motion, see Figure 4.1.

It was recognised that the radiation pressure could produce large forces without the thermal effects produced previously during experimentation. In

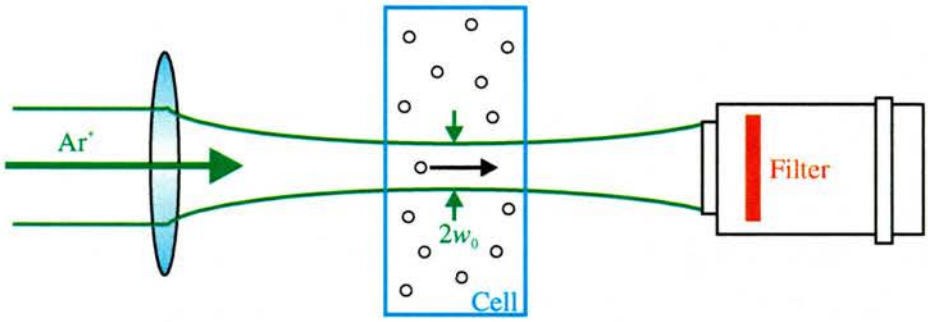

Figure 4.1: Viewed by the microscope on the right, particles were trapped and accelerated within the cell, and moved in the direction of beam propagation [42].

earlier experiments these thermal effects prevented effective study of the radiation pressure, and are known as radiometric forces. Radiometric forces were created by a temperature gradient between the sphere and its surrounding solution. When the particle moves by radiation pressure alone this is called *photophoresis*[1] [42, 43]. By suspending transparent particles in a similarly transparent medium, the radiometric forces can be reduced, because of this they worked at much higher power densities than previously reported [43, 44].

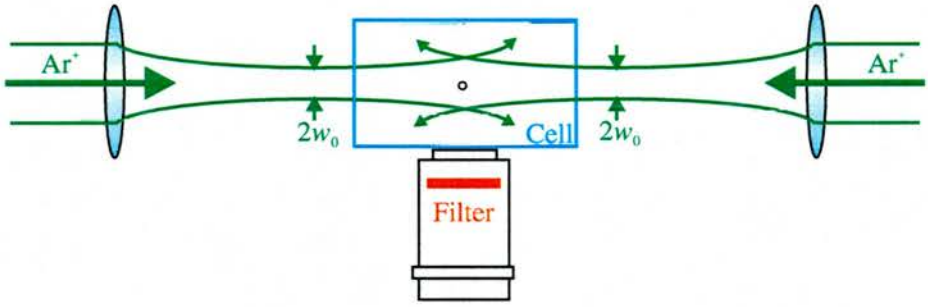

Figure 4.2: Two counter-propagating laser beams hold a particle within the cell at the point where the radiation forces balance [42].

[1] "Photophoresis is the net transfer of momentum to a particle with a temperature gradient due to gas molecules rebounding from the hotter side with greater momentum than from the colder side. The 'photo' prefix implies that the temperature gradient is due to absorbed radiation. *c. f.* N. A. Fuchs, *The Mechanics of Aerosols* (Pergamon Press, Oxford, 1964, p54" [43].

Using high index spheres in a low index medium showed, as described above, that the off-axis sphere accelerated towards the centre of the beam and was forced along in the direction of propagation. The refraction of the light passing through the sphere caused a change in momentum that moved the sphere towards the most intense portion of the beam, where it was then held on the beam axis. Ashkin then hypothesised that if low index spheres were placed in high index medium, then the spheres would be pushed away from the most intense part of the beam, i.e. *out* of the beam. Experimentation proved this to be the case; bubbles of gas were used in a high index medium. Results suggested a way of forming an optical potential well with the radiation pressure of two opposing laser beams. It was possible to optically levitate particles at the point where the radiation forces of the two beams balance as shown in Figure 4.2.

4.2.2 Optical Levitation

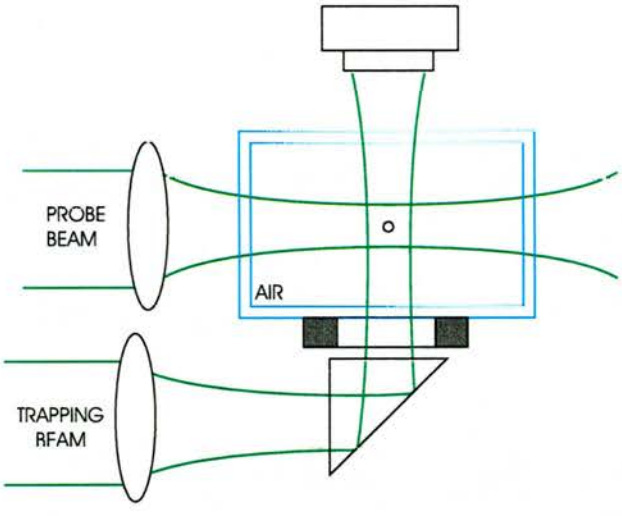

Figure 4.3: OPTICAL LEVITATION OF A PARTICLE. The particle moved up due to the force of radiation pressure, until it was equalled by that of gravity upon it, where it then is held. Probing with an additional beam from the left allowed investigation of the magnitude of these forces [45].

Ashkin described the movement of two sizes of spheres in the beam, subjected to a radiation pressure, the larger ones moved across the cell faster than those which were smaller. Explanations were given as to the differing forces exerted on the spheres, as well as the optical levitation of them. This was published detailing how to achieve optical levitation using a single-beam optical bottle [45]. The strengths of optical restoring forces within the system were measured using a second beam as a probe to exert an additional horizontal force on the system, see Figure 4.3.

After using the radiation pressure to trap latex spheres Ashkin used the knowledge he gained to deflect neutral atoms out of an atomic beam [46]. Ashkin's work furthered other avenues, and proved very helpful for other research projects; such as trapping, cooling and manipulating atoms [47].

4.3 Optical Tweezers

Arthur Ashkin first developed optical tweezers in 1986 [2]. He and his colleagues achieved optical trapping of dielectric particles ranging from 25 nm to tens of microns in diameter. A very tightly focused laser beam was directed down onto a sample from above, and particles were trapped on the beam axis near the focus, which was stable in all three dimensions. Optical tweezers were formally described as *a single-beam gradient force trap* [2, 47]. This laser beam has been used to trap microscopic particles; those of a biological nature, such as cells, organelles and bacteria; and many others, like silica spheres, or metallic particles. A description of the trapping forces involved can be found in Section 4.3.1.

Single-beam gradient force traps can restrict a variety of particle dimensions, ranging from as little as 25 nm to 200 μm in diameter. In this, the simplest possible trap, only one beam was brought to a diffraction-limited focus. The optical tweezers were constructed by focusing the Gaussian profile

of a Hermite-Gaussian $TEM_{0,0}$ mode laser beam through a microscope objective of high numerical aperture (NA). This pioneering work continued, and in 1987 Ashkin and Dziedzic used optical tweezers on a biological sample [48]. An argon ion laser formed the trap, producing several hundred milli-Watts of power using green wavelengths. A successfully monitored, and predicted, increase in the light scattered at 90° from the trapping region was observed as single virus cells became trapped at the beam focus. After several days of repeating the experiment with the virus culture, it was discovered that the scattered light readings would occasionally increase exponentially. The tobacco mosaic virus used was effectively an asymmetric Rayleigh particle, having dimensions significantly less than the wavelength of light. When the solution was inspected particles were found that were large in comparison to those of the virus. They appeared to move rapidly, up to a few hundred microns per second, then stopped, and regularly reversed their direction as they neared the edge of the trapping region. Unintentionally, they had discovered that optical tweezers were extremely effective at trapping the bacteria that contaminated their solution. Their work led to many experiments being carried out to discover how many different species of bacteria could be successfully trapped.

As a general rule the samples being trapped were held in solution[2]. The solution serves a few purposes, the particle is then partially buoyant allowing easier lifting, the particle is cooled by heat transfer to the surrounding medium, and it serves as a damping force to allow easier trapping of the particle.

The main problem with using laser light to trap biological cells was that even brief exposure times could cause irreparable damage to the sample, often causing complete destruction of the cell; termed *optication* [49]. There has, as a result, been a move to use infra-red lasers [50, 51, 52] for this work, which

[2]Particles or cells were often suspended in water.

results in virtually damage-free irradiation of many particles. The reason for this is that the wavelength is sufficiently different to that of the absorption peaks for the cells. Power up to approximately 100 mW can be sustained with out causing serious damage. Reproduction of cells through a number of generations could occur within the trap, with additional cells being held as well. Up to six cells at one time could be trapped. Using higher powers the optical tweezers can hold and manoeuvre a bacterium up to 500 μm s^{-1} across the plane, significantly better than through their motion alone.

The decision to change from visible to near-infrared wavelengths was sensible because visible light is readily absorbed by the cells. The longer infrared (IR) wavelengths, however, were not as damaging since the cells were almost transparent to the IR radiation. This slight alteration in wavelength was not significant to require modification of the microscope; being optimised for visible wavelengths they worked well with near IR too. Ashkin, however, found that although yeast and bacteria could reproduce in traps of up to Power $\approx$ 80 mW, there was a loss in flexibility in the membranes of erythrocytes after ten to 20 minutes exposure [48]. Block also observed that the bacterium *E. Coli* lost mobility after only several minutes exposure in a trap of P $\approx$ 50 mW [53, 49]. Many experiments were then performed using optical tweezers, as everyone began to realise their potential.

In Chapter 2 the properties of laser beams were discussed, and so now the trapping forces involved in optical tweezers will be explained.

4.3.1 The Trapping Forces

Optical-ray diagrams demonstrate where the origin of each of the trapping forces lie. In Figure 4.4, we can see that momentum components act from the centre of the sphere and cause the sphere to be pushed slightly downwards. In Figure 4.5, the sphere moves towards the most intense point of the light, where the origin of the gradient force is situated. The gradient force is

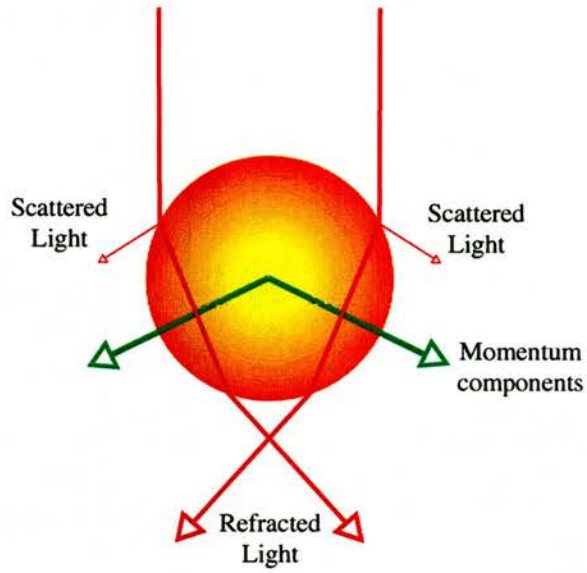

Figure 4.4: ORIGIN OF LATERAL TRAPPING xy-FORCE [49].

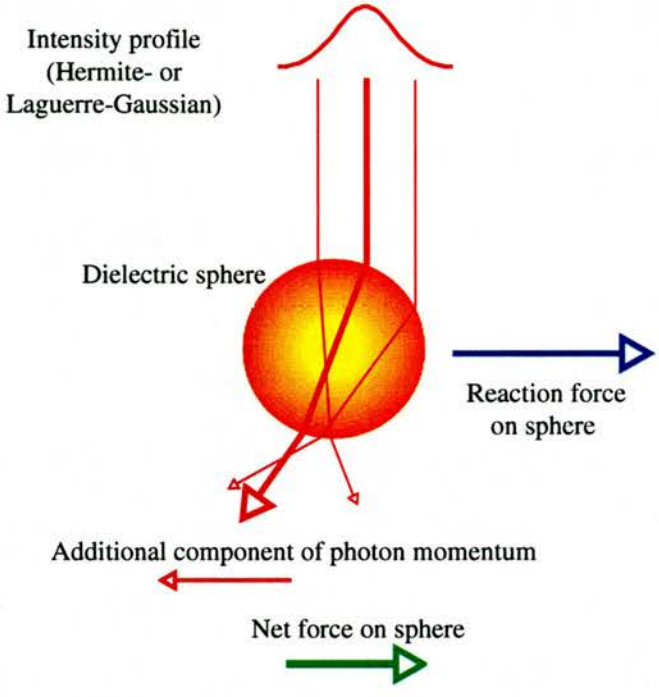

Figure 4.5: GRADIENT TRAPPING (xy-)FORCES.

the sole provider of lateral trapping; the scattering force acts only along the longitudinal direction. Figure 4.6, shows a sphere located just below

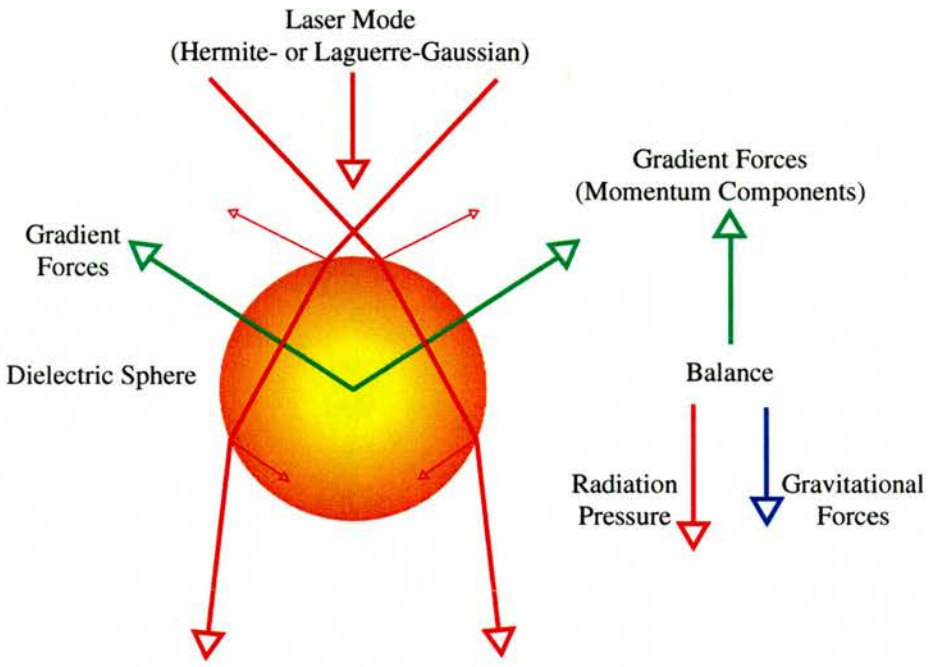

Figure 4.6: ORIGIN OF LONGITUDINAL TRAPPING z-FORCE [49].

the focus of a highly convergent beam. The light rays from above are largely due to lateral momentum having a relatively small component of longitudinal momentum. Having passed through the sphere, the rays become parallel with only longitudinal momentum. The sphere moves up slightly, maintaining the balance by conservation of momentum in the z-direction. Stability of the trap is achieved as long as the light is sufficiently convergent and is passing through an object which is transparent to the wavelength of light used. The object, when placed just below the focus, is held in a stable trap. Above the focus, the scattering and gradient forces have the same sign. Within this trap the object's refractive index, n, must be more than the surrounding medium, n_b; otherwise the gradient forces will reverse sign and the trap becomes unstable.

Calculation of the trapping force proves difficult for all but the simplest geometries. High local curvature at boundaries creates substantial gradient

forces; thus enabling optical tweezers to grasp the edges of *large* objects[3]. Radiation pressure forces depend on the object's exact shape as well as the direction and shape of the laser beam. As most cells have an irregular shape it is difficult to calculate the trapping forces due to the complicated geometries involved.

Overheating whilst a cell is being irradiated can result in the *opticution* [49] of the sample. This can occur easily if we consider that a milli-Watt laser can produce MW cm^{-2} of power density when brought to a diffraction-limited focus. To prevent such an occurrence the sample is effectively water-cooled by the surrounding solution. In this case, the diameter of the focused beam when trained on the sample covers such a small volume that the heat is quickly transferred into the water and causes much less damage to the sample.

4.3.2 The Equations for each of the Trapping Forces

In this section I have the equations for the various forces shown in Figure 4.7. These formulae [2] are valid for Rayleigh particles[4]; Mie particles require more complicated formulae[5].

The gravitational force, $F_{gravity}$, on a particle (or sphere) is given by

$$F_{gravity} = \frac{4}{3}\pi r^3 (\rho - \rho_b) g \tag{4.1}$$

where ρ is the density the particle, ρ_b is the density of the solution in which the particle is suspended, and r is the radius of the particle.

[3]In this context, large implies dimensions greater than the wavelength used.

[4]A particle whose dimensions are small compared with the wavelength of light of the radiation incident upon it.

[5]Mie-scattering formula takes into account the size, shape, refractive index, and absorptivity of the scattering particles. It includes Rayleigh scattering as a special case. It is easier to use ray-optics to work out the physics involved in this case.

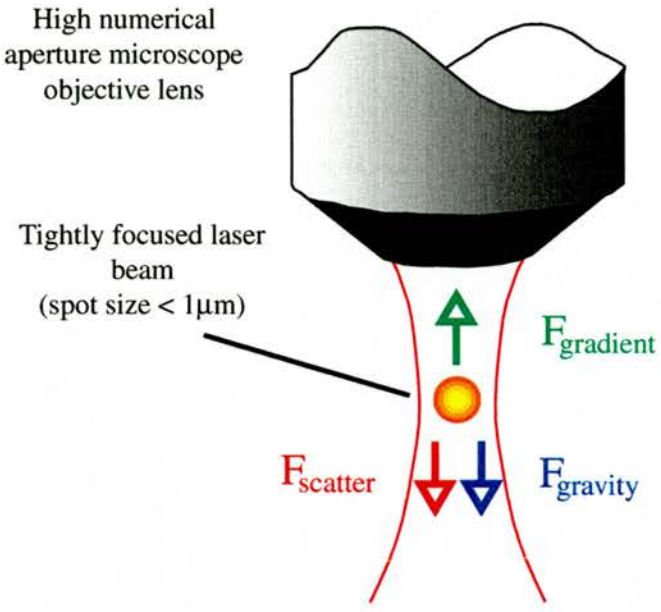

Figure 4.7: FORCES ACTING ON RAYLEIGH PARTICLES. Here we can see the gradient and scattering forces acting on the Rayleigh particle. Also shown is the force due to gravity.

The gradient force, $F_{gradient}$, due to radiation pressure on a sphere is

$$F_{gradient} = -\frac{n_b^3}{2} r^3 \left\{ \frac{\left(\frac{n}{n_b}\right)^2 - 1}{\left(\frac{n}{n_b}\right)^2 - 2} \right\} \Delta E^2 \tag{4.2}$$

where n is the refractive index of the particle, n_b is the refractive index of the solution, and ΔE is the gradient of the electric field. Here r is the same as before.

The Rayleigh scattering force, $F_{scatter}$, on a particle is given by

$$F_{scatter} = \frac{I_0}{c} \frac{128\pi^5 r^6}{3\lambda^4} \left\{ \frac{\left(\frac{n}{n_b}\right)^2 - 1}{\left(\frac{n}{n_b}\right)^2 + 2} \right\} n_b \tag{4.3}$$

where I_0 is the light intensity, λ is the wavelength of light and c is the speed of light. Here n, n_b and r are as previously stated.

The drag force, F_{drag}, due to the viscosity of the liquid is

$$F_{drag} = 6\pi\eta r v \tag{4.4}$$

where, η is the coefficient of viscosity and v is the velocity of the particle. Once again, r is the radius of the particle.

In general, only optical trapping of dielectric particles had been widely achieved, although optical trapping of metallic Rayleigh particles, 36 nm in diameter, was demonstrated in 1994 [54]. The scattering force is not a significant factor in the behaviour of Rayleigh particles — this is not the case for larger particles.

4.3.3 Necessary Conditions for Optical Tweezers

Light is refracted, reflected and absorbed by a trapped particle; the important fact, in the *conventional operation* of optical tweezers, is that the light is *refracted* as it passes through the sphere. Certain criteria must be satisfied for optical tweezers to work [49]:

- The laser beam must be transmitted through the back of the objective such that the microscope can work normally.
- The beam must fill (or slightly overfill) the back of the aperture of this lens giving maximal convergence of the light, the smallest possible focal spot, and hence the large field gradient.
- The beam must be brought to a diffraction-limited focus at the specimen plane, where the sample is being viewed.

For easier use of the optical tweezers the xyz-position of the focus can be altered using external controls. These controls enable the specimen to be moved independently to the laser beam. The beam spot's image must be visible on the microscopic object so that it can be correctly aligned.

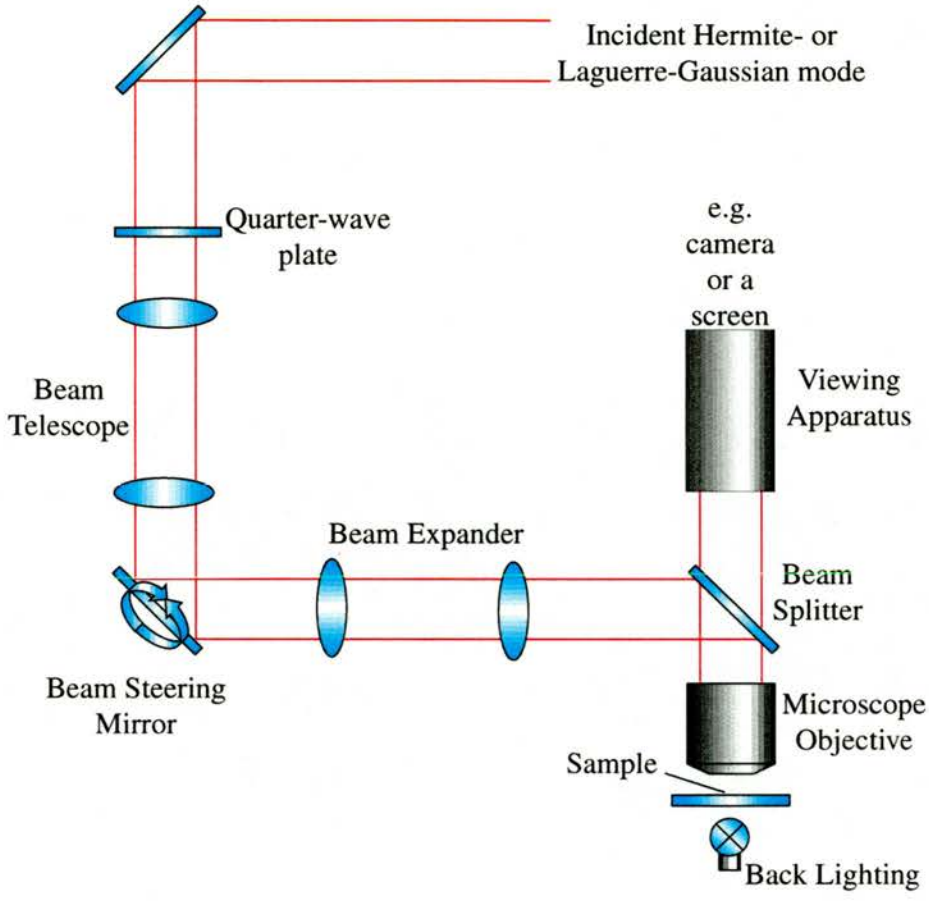

Figure 4.8: SCHEMATIC DIAGRAM OF OPTICAL TWEEZERS. Optical tweezers allow a particle to be held by a laser beam at the focus of the microscope objective. When the laser beam moves the particle moves with it. Optical tweezers are also possible using Laguerre-Gaussian modes.

Further important developments are still being made. In Figure 4.8 we can see the design of the optical tweezers and improvement of them is ongoing. Increased trapping efficiency was achieved by the use of a Laguerre-Gaussian (LG)[6] laser mode [5]. When using a LG $l = 3$ mode the power required to trap many different sizes of particles is reduced by as much as half compared

[6]A Laguerre-Gaussian laser beam has radial symmetry as opposed to the rectangular symmetry of the Hermite-Gaussian (HG) mode. There is also an additional component of angular momentum related with it, called *orbital angular momentum*.

to that of the fundamental Hermite-Gaussian $HG_{0,0}$[7] mode. This results in less damage to biological samples [5].

This enhanced trapping efficiency is caused by the absence of on-axis rays. Rays in line with the axis are not refracted, they apply radiation pressure to the sides of the sphere, but have no contribution to the axial trapping force [55]. Higher order LG modes produce a greater trapping force per unit power than that of the fundamental HG mode or a fundamental LG mode. Using constant laser power for both the fundamental and higher order LG modes, I get the same trapping force, but can use an objective lens with a lower numerical aperture (NA) for the higher order modes, therefore resulting in an increased working distance (WD) of the objective.

Conjugate Planes of optical tweezers

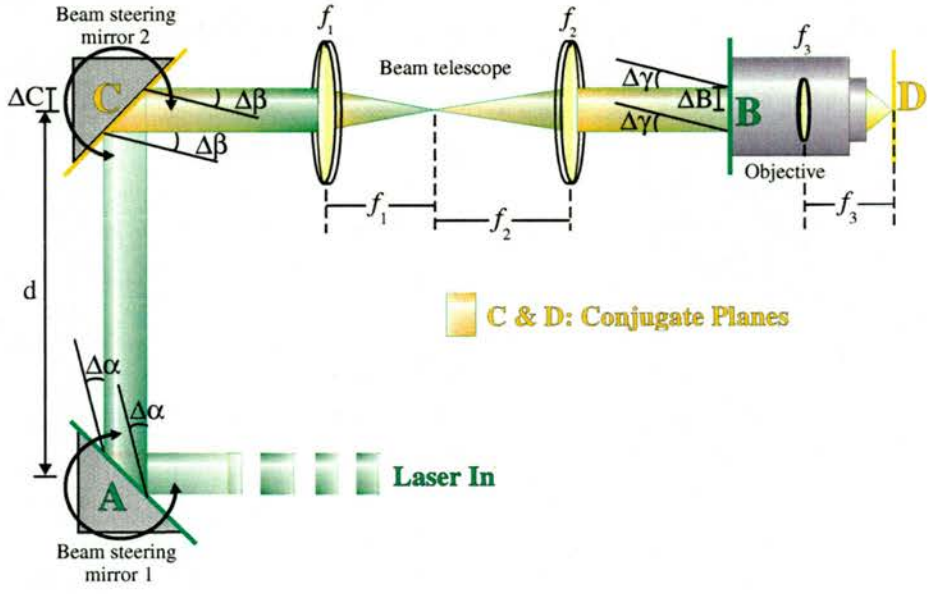

Figure 4.9: Configuration needed to *steer* the beam correctly within the optical tweezers.

[7]Hermite-Gaussian laser modes are the usual ones to be found in a working laser. More details of both the Hermite-Gaussian and Laguerre-Gaussian laser modes can be found in Chapter 2.

Figure 4.9 shows the conjugate planes needed in an optical tweezers set up. Adjustment of the folding mirror (Beam steering mirror 1 in Figure 4.9), causing an angular shift at plane A, translates a lateral motion to the focus in plane B. This allows the beam to be sent through the back aperture of the objective. Movement of the second beam steering mirror repositions C, translating equivalent motion to D. The movement of the conjugate pair depends upon the characteristics of the beam telescope. The values of focal length of each lens within the telescope dictate the translation of the beam from each of the pairs. Angular movement of plane A some angle, $\Delta\alpha$ say, produced a movement of plane B equal to $\Delta\mathrm{B} = \frac{f_1}{f_2} \cdot d \cdot \Delta\alpha$. The similar rule applied to motion between planes C and D, but one must take account of the additional lens of focal length f_3 in the objective. Now given an angular shift at C, of some angle $\Delta\beta$, that causes a lateral shift at D given by the equation:

$$\Delta D = \frac{F_1}{F_2} \cdot F_3 \cdot \Delta\beta$$

4.4 Applications of Optical Tweezers

Optical tweezers have proved useful in many areas, from biology and medicine to nanotechnology. The fact that particles can be trapped using reduced laser power [5] is of particular significance in medicine, where cells can be quite sensitive to over-exposure, and can suffer *optication* [49]. Using near-IR radiation to trap biological cells has made it possible to produce one-to-one fusion of these cells within an enclosed chamber preventing the widespread damage of previous techniques [56].

Optical trapping has also been used on metal particles [10, 11, 9]. For transparent particles refraction of the light through the particle produces a suitable gradient force to trap it within the tweezers arrangement. Metal, on the other hand, was considered difficult to trap using an optical set-up,

because of its reflective properties. Having used a circularly scanning laser beam of a $TEM_{0,0}$ mode, the entrapment of an iron particle was achieved in 1992 [10]. The laser beam scanned quickly across the sample and created a cage around it. Repulsive radiation forces, reflected back and forth in all directions, produce this cage around the particle.

There are many applications which have been demonstrated using optical tweezers, some with profound impact on other fields. A couple of relevant ones are explained in this section. Optical spanners [19] is particularly relevant because it uses LG modes which are useful when trapping metallic particles. Interferometric optical tweezers [57] could also be applicable to metallic particles because it may be possible to channel metallic particles down the troughs produced by this configuration.

4.4.1 Rotation using Optical Tweezers

This can be split into three distinct sections of research. They are:

1. Angular Momentum Transfer, otherwise known as optical spanners. Research papers: He *et al.* 1995 [22], Simpson *et al.* 1997 [19], Friese *et al.* 1996 [23].

2. Special Laser modes. Research papers: Sato *et al.* 1991 [8], Paterson *et al.* 2001 [58].

3. Radiation Pressure. Research papers: Ashkin 1970 [42], 1978 [47] and 1980 [59].

Optical Spanners (Angular Momentum Transfer)

Laguerre-Gaussian laser modes, with their orbital angular momentum component are essential for the operation of optical spanners. In Figure 4.10

Laguerre-Gaussian laser modes were used to transfer its orbital angular momentum to the trapped particle. This orbital angular momentum caused rotation of the particle, hence the name *optical spanners.*

To produce optical spanners we have:

$$\underbrace{\text{Laguerre-Gaussian laser mode}}_{\text{orbital angular momentum}} + \text{Optical Tweezers} = \text{Optical Spanners}$$

The phase structure of the LG beam used in optical spanners is very im-

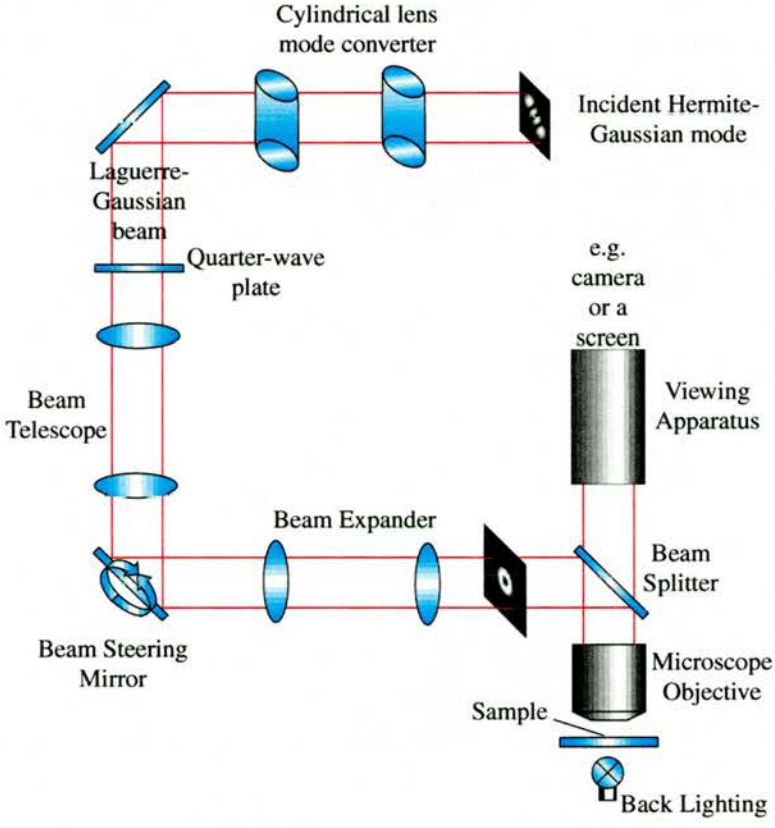

Figure 4.10: Optical arrangement used including a Laguerre-Gaussian laser mode, known as OPTICAL SPANNERS [19].

portant. A Mach-Zehnder interferometer shown in Figure 4.11 could be used to analyse a laser beam's phase structure. It consists of a cylindrical lens mode converter used to create a LG beam from the original high order HG

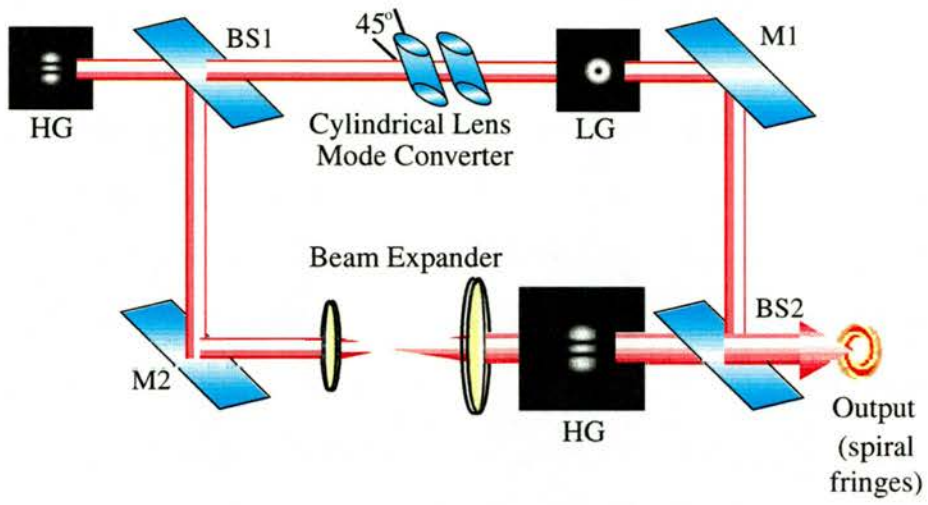

Figure 4.11: THE MACH-ZEHNDER INTERFEROMETER.

beam which is sent in its original form through a beam expander to interfere with the LG beam at the other end. The output, a spiral pattern, gives us information as to the order of the LG beam and its phase. This method is useful as an easy unambiguous way of identifying the LG beam present.

The angular momentum transferred to the particle can be used to rotate the particle. Total angular momentum is given by:

$$\text{Total angular momentum (AM)} \;=\; \text{Spin AM} \;+\; \text{Orbital AM}.$$

If a $l = 1$ Laguerre-Gaussian laser mode is used the spin AM and the orbital AM can either sum or cancel out the other term. When the orbital angular momentum cancels out the spin AM there is no rotation:

$$\text{Total angular momentum} \;= \hbar - \hbar = 0 \text{ per photon}$$

When the orbital angular momentum adds to the spin AM there is fast rotation:

$$\text{Total angular momentum} \;= \hbar + \hbar = 2\hbar \text{ per photon}$$

These calculations support Equation (2.12) on page 6.

Optical Tweezers using Special Laser Modes.

In 1991, Sato *et al.* [8] did research with special laser modes to allow the rotation of particles in optical tweezers. In 2001 Paterson *et al.* [58] reported that the interference of two beams enables the rotation of particles and in Chapter 6 the results of my research in this area are presented.

Radiation Pressure

The fact that light carries angular momentum and can exert force on electrically neutral objects was suggested by Kepler in the 17th Century. Eventually, in the 19th Century, Maxwell provided his theory of electromagnetism to substantiate this claim. He found that the forces involved were very small and, hence, difficult to measure. This early theory did not suggest that there could be applications using this phenomenon. The invention of the laser [60, 61] allowed these forces to be exploited [42, 47, 59]. Many articles since Ashkin first reported the exploitation of the radiation pressure [42] have been produced exploiting this topic, notably, optical tweezers [2] and atom trapping [62, 63].

4.4.2 Metal particle trapping

There have been a number of methods suggested for achieving trapping of metallic particles. In the most part, they suffer from certain limitations, such as requiring small particle size or trapping in two dimensions only. In Table 4.1 there is a summary of various approaches. In Chapter 7 I present a description of my research done in this area [9].

			
Sasaki *et al.* 1992 SCANNING BEAM Mie (μm) particle 2D TRAPPING	Sato *et al.* 1994 ANNULAR BEAM Mie (μm) particle 2D TRAPPING	Furukawa & Yamaguchi 1998 CREEPING WAVE Rayleigh (nm) particle 3D TRAPPING	O'Neil & Padgett 2000 ANNULAR BEAM Mie (μm) particle 3D TRAPPING

Table 4.1: The various methods of Metal Particle trapping and their attributes [10, 11, 64, 9].

4.5 Conclusion

Optical tweezers are available commercially, and are widely used throughout the scientific community. I believe their applications to date, however, are not yet fully realised. On the basis of work carried out in this thesis, I hope that, although presently lacking application in the area of metal particle trapping, further uses can be developed touching new and exciting areas of research.

Chapter 5

Lateral and Axial Trapping Efficiency of Laguerre-Gaussian Modes

5.1 Introduction

In this chapter, I describe how to use an inverted optical tweezers arrangement to measure both the lateral and axial trapping efficiency obtained with Gaussian and high-order Laguerre-Gaussian beams. These results confirm that, for larger particles, the axial trapping is improved by using a Laguerre-Gaussian beam but, contrary to earlier suggestions (outlined later), that the lateral efficiency is unchanged. I show that this latter observation is compatible with a ray-optical model of the trapping mechanism.

5.2 Background and motivation

As discussed in Chapter 4 optical tweezers have many uses. In 1986, after more than a decade of related research, Ashkin and co-workers used a tightly

focused beam of laser light to trap a glass sphere in three dimensions [2]. This technique is now commonly referred to as optical tweezers and is widely used in many biological applications, some of which were described in Chapter 4, such as measuring the compliance of bacterial tails [53], the measurement of the forces exerted by single muscle proteins [65] and the stretching of single strands of DNA [51].

Optical tweezers rely on the extremely large gradient in the electric field generated in the region of a tightly focused laser beam. Any dielectric particle in the vicinity of the focus experiences a force, directed towards the region of highest field. At optical frequencies, a dielectric material is one that has a predominantly real refractive index. If the laser beam is focused tightly enough then the *gradient force* can overcome that due to gravity and light scattering such that the particle becomes trapped in three dimensions [2]. For transparent particles a few microns in diameter, suspended in water or alcohol, a few milliwatts of laser power focused with an oil-immersion microscope objective is sufficient to form a robust trap. Lateral and axial forces of a few hundred piconewtons can be generated which allow particles to be manipulated at speeds of the order of a few tens of microns per second [49].

The trapping efficiency of optical tweezers is usually described in terms of a dimensionless parameter, Q [66], which relates the force on the sphere, F_{trap}, to the power of the laser, P, and the refractive index of the surrounding medium, n_m:

$$F_{trap} = \frac{n_m Q P}{c}. \tag{5.1}$$

A Q-value of $Q = 1$ corresponds to all of the light beam's momentum being transferred to the particle.

In principle, it is possible to calculate the Q-value corresponding to any particular experimental geometry. In practise this is problematic since the particles are typically comparable in size to the optical wavelength, making a ray-optic calculation [67] inaccurate. Similarly, the typical particle is too

large[1] to allow a precise calculation of the trapping forces based on electromagnetic theory [2] and in any event neither approach allows easily for the aberrations in the focusing optics or irregularities in particle shape. Consequently, proposed tweezers configurations need to be assessed experimentally to determine the Q-values for particle displacement in the axial and lateral directions. However, although not completely reliable, the ray-optical model of optical tweezers does provide useful insight into the trapping mechanism.

Although most optical tweezers have used a fundamental Gaussian mode as the trapping beam, investigations using other beam types have also been performed. For example, rectangularly symmetric high-order Gaussian modes have been used to fix the rotational alignment, within the trap, of asymmetric red blood cells [8]. More generally, using a ray-optic model, Ashkin considered the theoretical trapping efficiency resulting from different beam profiles. Specifically, he pointed out that, since the trapping force results from a change in ray direction, it is only the off-axis, large NA, rays that contribute to the axial trapping force. Indeed, his calculations predicted that modest improvements in Q-axial (z-trapping) were possible using a TEM_{01}^{*} *doughnut* mode, which has no on-axis rays. Such beams have also been used to trap low-index hollow spheres [69] and to confine metal particles within the centre of the ring [11, 70].

Radially symmetric modes like the TEM_{01}^{*} *doughnut* mode are best described in terms of Laguerre-Gaussian modes [13, Chapter 16, p647–648] which, like the Hermite-Gaussian modes, form a complete orthogonal set. Laguerre-Gaussian modes are normally characterised by an $\exp(il\varphi)$ azimuthal phase dependence and the corresponding helical phase fronts carry an orbital angular momentum of $l\hbar$ per photon [17][2], where l is the azimuthal

[1]For particles of diameter $d \geq 10\lambda$ electromagnetic theory does not work and one must use a geometrical ray-optic model [68] for Q-value calculations. For particles of diameter $d \leq \lambda$ one can use electromagnetic theory to calculate trapping efficiencies.

[2]Equation 2.12 in Chapter 2 on page 6.

mode index. Indeed, this orbital angular momentum has been transferred to partially absorbing particles held in optical tweezers [22, 19]. However, for non-absorbing dielectric particles, no transfer of orbital angular momentum takes place and the interest in the use of Laguerre-Gaussian beams lie solely in their annular intensity profiles. The radius of maximum intensity, $r_{I_{max}}$, for a Laguerre-Gaussian mode is given by

$$r_{I_{max}} = \sqrt{\frac{z_R\, l}{k}}, \tag{5.2}$$

see [71]. Previously, Simpson *et al.* used a ray-optical argument to calculate the relative axial trapping efficiency of Laguerre-Gaussian modes of different azimuthal mode index [55]. As might be expected, they predicted an increase in axial trapping efficiency as the azimuthal index was increased. However, in all such cases one needs to be careful how beam size is defined since, ultimately, the maximum NA of the trapping rays is limited not only by the choice of mode but by the design of the microscope objective and the refractive index of sphere and medium (n and n_b).

Experimentally, a number of groups have investigated the use of Laguerre-Gaussian modes in optical tweezers. The TEM_{01}^{*} mode, which has the same intensity profile as the $l = 1$ Laguerre-Gaussian mode, was reported to result in a 20% improvement [8] in lateral trapping efficiency. An $l = 3$ mode has also been used within an optical tweezers and changes in the fluctuations in backscattered light suggested a doubling of the axial trapping efficiency [72]. In a non-inverted tweezers configuration, Simpson *et al.* measured the minimum power required to support different spheres against gravity and demonstrated similar improvements in axial trapping efficiency [5].

In this chapter, I describe how I used a dynamic method to measure the axial and, for the first time, the lateral trapping efficiency obtained with Laguerre-Gaussian beams when used in the more commonly employed inverted tweezers geometry.

5.3 Experimental arrangement

In this work I used an inverted tweezers geometry which is favoured by most biologists. The Laguerre-Gaussian beam enters the objective lens from below, this allows easy access to the sample cell. This is an important consideration since, within an inverted geometry, the light scattering force (particularly that due to the on-axis rays) acts to support the trapped particle against the pull of gravity. Consequently, one might expect that use of a Laguerre-Gaussian mode would result in less improvement.

This optical tweezers system, as in other chapters, is based on a $\times 100$, Zeiss Plan Neofluar, oil immersion objective with an NA=1.3. The trapping laser is a frequency-doubled Nd:YVO_4 solid state laser, with a 100 mW, fundamental (i.e. $l = 0$) output at 532 nm. Computer-generated holograms[3] were inserted into the collimated beam to produce Laguerre-Gaussian modes with $l = 2$ and $l = 3$. An iris was used to select the appropriate diffraction order so that the trapping beam could be quickly switched between the zero-order, $TEM_{0,0}$ Gaussian beam and the first-order Laguerre-Gaussian beam. The particles themselves were 1.1, 2 and 5 μm diameter silica spheres suspended in a water solution and sealed within a sample cell comprising of a microscope slide, a 70 micron spacer and a coverslip. A beam steering mirror allows the trap position to be controlled and the trapped particle moved to the centre of the visual field. The sample cell was mounted upon a piezo-controlled x-y-z translation stage that could either be driven manually, or from a programmable voltage source, enabling specific movements to be defined and repeated, see Figure 5.1. A schematic of the experimental apparatus is shown in Figure 5.2.

[3]See Appendix A.

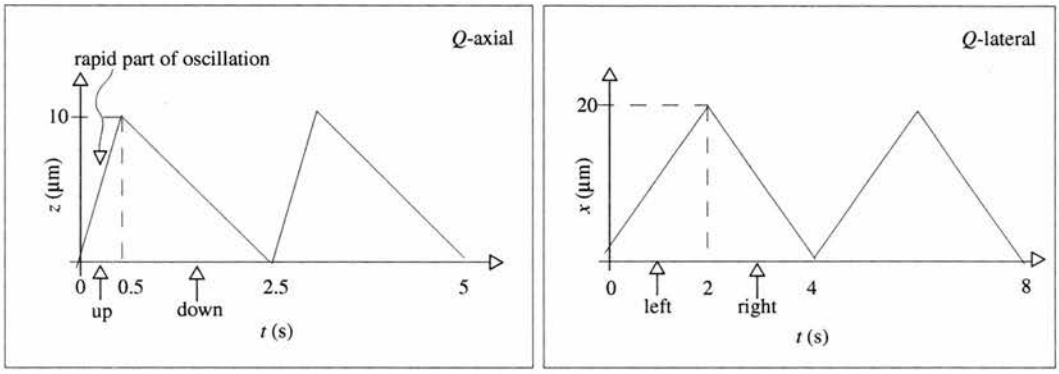

Figure 5.1: Time-dependent displacement in the vertical and horizontal direction of the piezo-controlled translation (PZT) stage for the measurement of axial and lateral Q-values, respectively. A signal generator was used to apply a triangular voltage signal to the PZT stage, where it was translated into a proportional displacement. In the case of Q-axial an asymmetric displacement function was used. The strength of the trap was tested during the fast, upwards, movement, whilst the purpose of the downward movement was simply to return to the starting position sufficiently slowly so as not to recapture the sphere.

5.4 Results

In keeping with the approach adopted by many other groups [3, 4], the trapping efficiency was assessed by measuring the maximum speed at which particles could be moved, before escape, and relating this to the calculated drag force, F_{drag}, acting on the particle moving through the viscous fluid. Once the particle is more than a few diameters away from the sample cell walls, the drag force, F_{drag}, is related to the viscosity of the fluid, η, the velocity, v, and the diameter of the particle, d, by

$$F_{drag} = 3\pi\eta v d, \tag{5.3}$$

see [3]. For power levels in excess of a few milliwatts, the performance of the trap is such that the force acting on the particle due to gravity is small compared to the drag force and consequently can be ignored.

Equating the drag force at the moment of escape to the trapping force

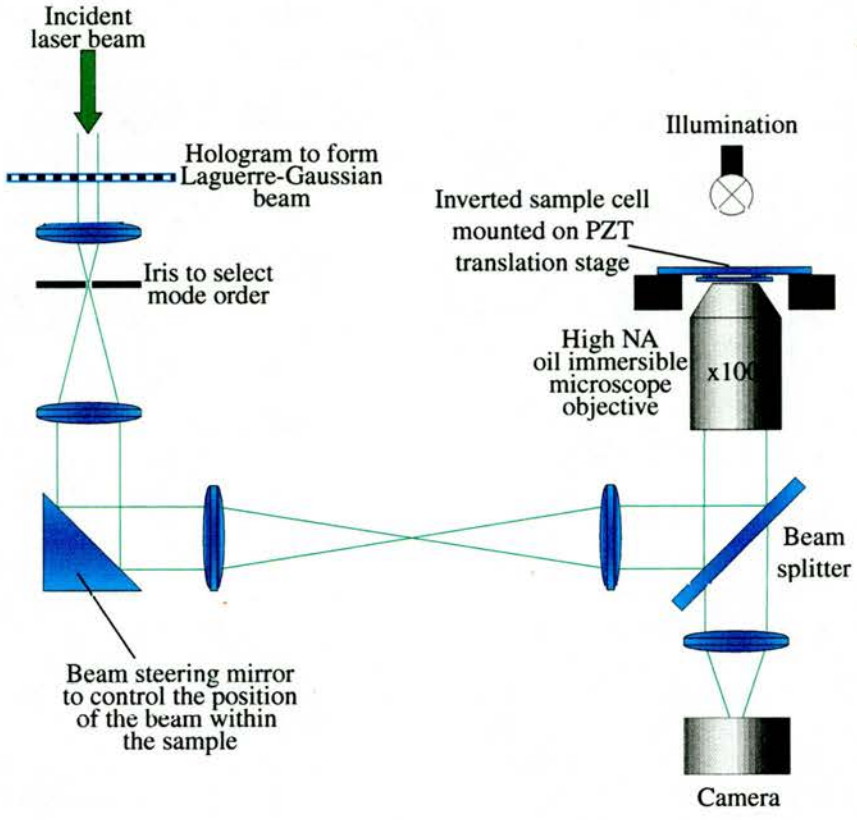

Figure 5.2: The arrangement of the inverted optical tweezers used in this work.

gives a simple relation, including power, P, to calculate the trapping efficiency, Q, of

$$Q = \frac{c}{n_m} \cdot \frac{3\pi\eta v d}{P}. \tag{5.4}$$

Clearly, to obtain an accurate value of the trapping efficiency it is necessary to make an accurate measurement of the laser power. This itself can prove difficult since most microscopes objectives exhibit transmission losses of the order of 50% and their extremely high NA means the tightly-focused transmitted beam is difficult to collect onto a power meter. Furthermore, the need to maximise the NA of the focused beam means that the back-aperture of the objective lens is typically overfilled, again resulting in a loss which is difficult to quantify. For these measurements, I used two identical objective lenses, in the arrangement shown in Figure 5.3, which focus and then re-collimate the beam so that their combined transmittance can be accurately measured. From this I infer that the transmission at 532 nm of each of the objective lenses is in the range 48–52%, depending on the mode order of the laser beam. For all subsequent power measurements, taken whilst using the tweezers, I inserted the second objective, assumed that any aperturing of the laser beam occurs at the first objective lens, and hence that the laser power in the sample plane is approximately twice the power measured through the second objective lens (given the 50% collection efficiency).

For all measurements, a particle was selected at random, moved to the centre of the field of view and lifted approximately 13 microns off the bottom of the cell. The sample cell was repeatedly moved sideways, to assess lateral trapping, or up and down to assess axial trapping. In both cases the movement was uniform over a finite range. The speed of the sample cell was gradually increased until the particle fell out of the trap. The ability to change quickly between zero-order Gaussian and first-order Laguerre-Gaussian beams[4] allowed direct comparison between the two beam types

[4]There were additional ND filters added for the zero-order HG beam to allow power

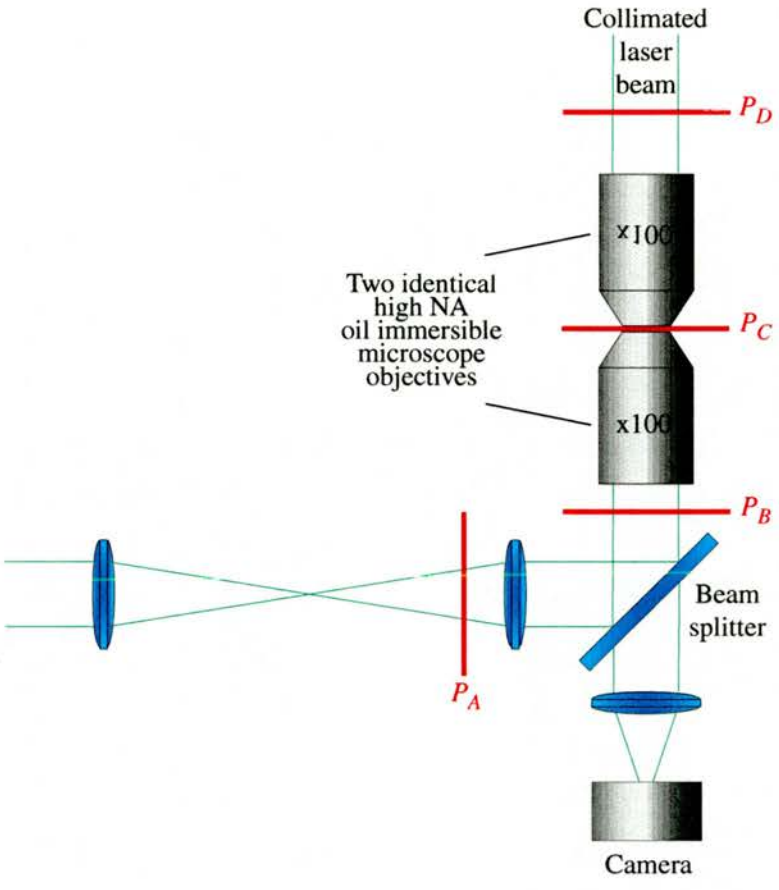

Figure 5.3: A second objective was used to re-collimate the laser light so that an accurate power measurement in the sample plane can be obtained. Measuring P_A, P_B and P_D one can then calculate the power at the sample, P_C, for each of the beam profiles. From then on by measuring P_A for each particle, and checking it at the end of each particle set with the ratio of P_A to P_D, one can ensure that the measured power at the sample is always accurate.

to be made on the same trapped particle. This whole process was then repeated for between 10 and 30 particles. Table 5.1 shows the average values of Q-lateral and Q-axial obtained for a $TEM_{0,0}$ Gaussian beam and the Laguerre-Gaussian beams with $l = 2$ and $l = 3$ for 1.1, 2 and 5 μm diameter silica spheres suspended in water. Figure 5.4 shows a histogram which summarises the mean Q-values obtained for both lateral and axial trapping with

levels at the sample to be equivalent for each laser mode.

	Sphere Diameter					
	1.1μm		2μm		5μm	
Mode	Q-lateral	Q-axial	Q-lateral	Q-axial	Q-lateral	Q-axial
$TEM_{0,0}$	0.0354 ±0.0013	0.0383 ±0.0013	0.0676 ±0.0021	0.0601 ±0.0037	0.1206 ±0.0055	0.1179 ±0.0097
$l = 2$	0.0363 ±0.0025	0.0388 ±0.0015	0.0694 ±0.0041	0.0937 ±0.0090	0.1171 ±0.0028	0.1510 ±0.0064
$l = 3$	0.0147 ±0.0009	0.0213 ±0.0015	0.0580 ±0.0018	0.1453 ±0.0033	0.1198 ±0.0029	0.1859 ±0.0048

Table 5.1: Average values of Q-lateral and Q-axial obtained for a $TEM_{0,0}$ Gaussian beam and the Laguerre-Gaussian beams with $l = 2$ and $l = 3$ for 1.1, 2 and 5 micron diameter silica spheres in water.

relation to particle size.

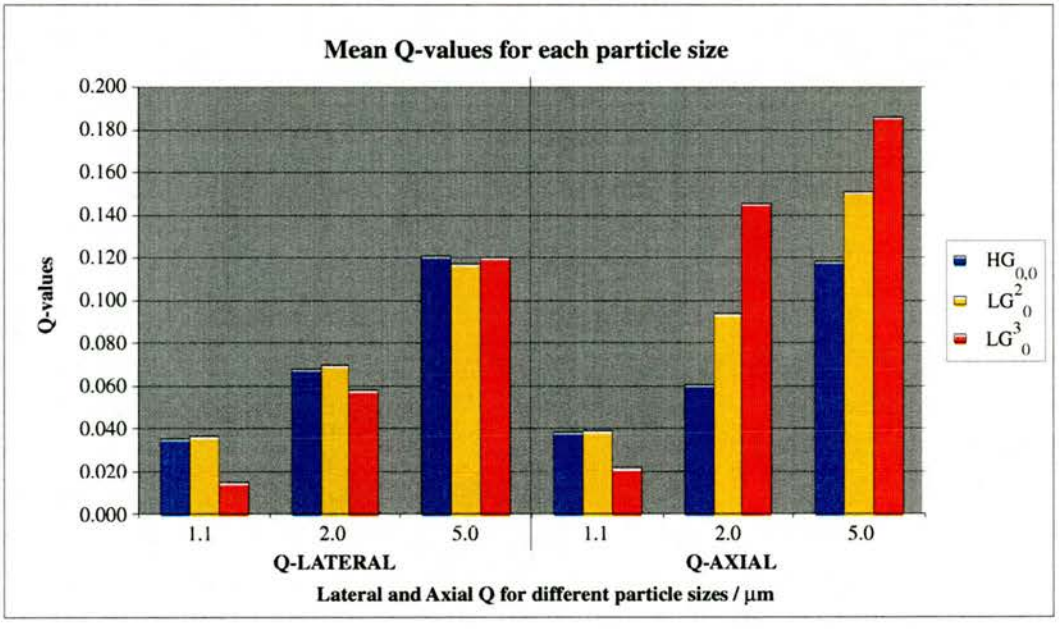

Figure 5.4: Lateral and Axial Q-values. For example, for a beam power of $P = 1$ mW and a $Q = 0.1$, the force on the particle is $F = 0.45$ pN.

Firstly, note that my measured Q-values obtained using the fundamental Gaussian $TEM_{0,0}$ fall within the range reported by other groups [3], indicating that the tweezers arrangement I used is representative of other systems. Regarding the use of Laguerre-Gaussian modes in optical tweezers, the gen-

eral trends within these results show that, compared with a fundamental Gaussian mode, they improve the axial trapping efficiency whilst leaving the lateral efficiency largely unaltered for larger particles. The improvement in axial trapping confirms earlier observations [3], but these new results are the first detailed study of lateral trapping and indicate that a Laguerre-Gaussian beam offers no advantage. Also note that the potential improvement in trapping efficiency is only realised for the 2 and 5 micron spheres. For the 1.1 micron spheres the Laguerre-Gaussian beam is less effective, perhaps not surprisingly, as these spheres are too small to interact with the whole cross section of the Laguerre-Gaussian beam. This last statement is further supported by noting that for the smallest spheres, the $l = 3$ beam performs even worse than the $l = 2$ beam for axial trapping. Figures 5.5 and 5.6 show the lateral and axial trapping efficiencies with respect to sphere size.

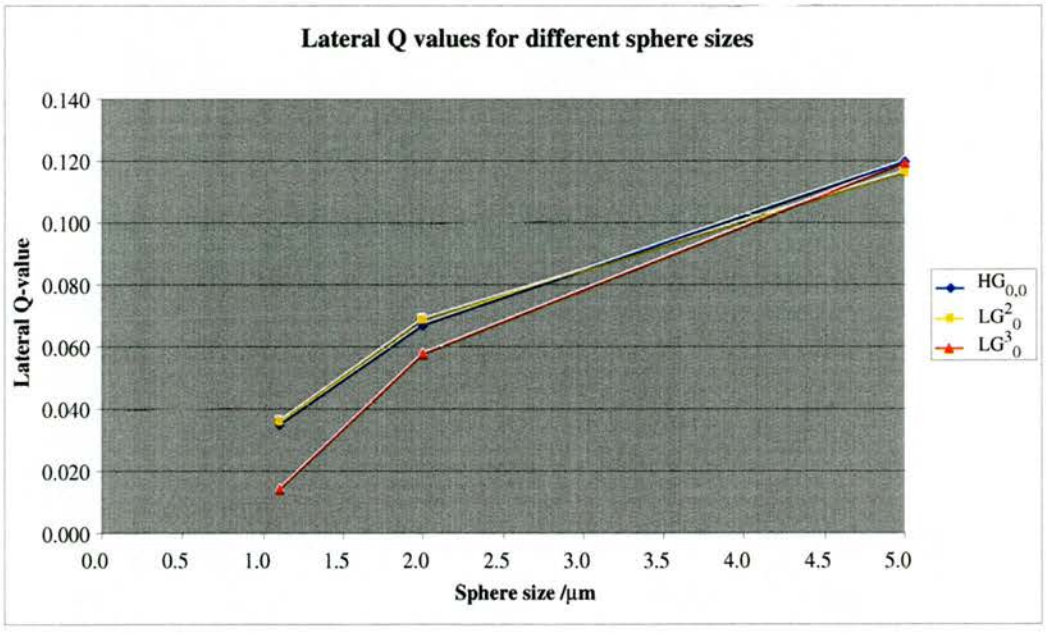

Figure 5.5: Summary of Lateral Q-values with respect to sphere size.

Following similar approaches that have been adopted previously [66, 4], one can apply Snell's law at the sphere-fluid interface to calculate the ef-

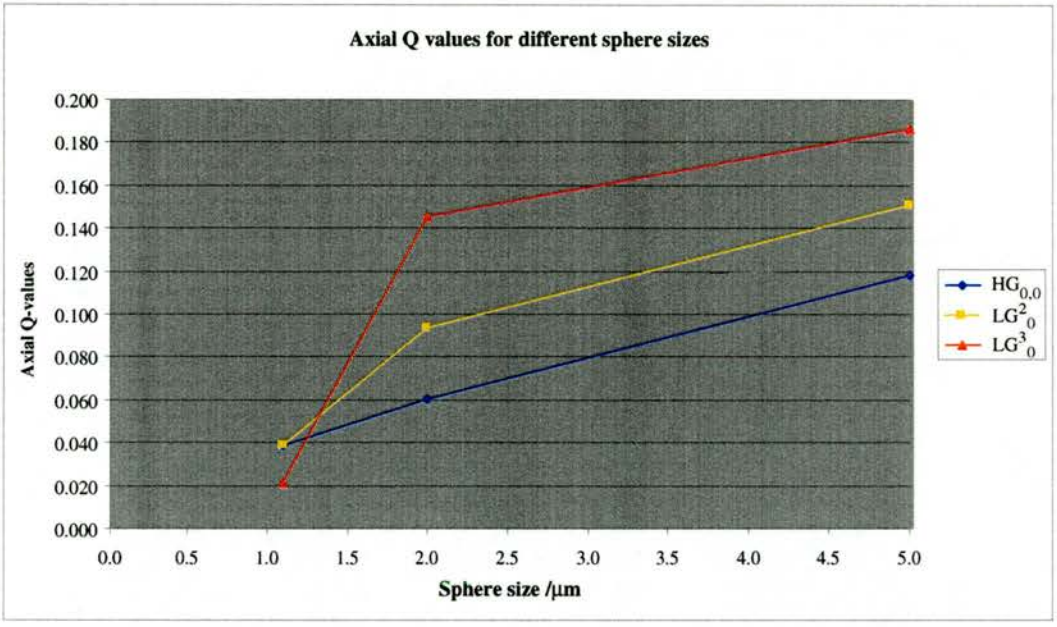

Figure 5.6: Summary of Axial Q-values with respect to sphere size.

fective Q-value for rays at various NA. Figure 5.7, from [6], shows graphs for theoretical calculations of Q-axial and Q-lateral for individual rays after refraction by a sphere with a refractive index of 1.5 immersed in a fluid of refractive index 1.33. In both cases the displacement axis is normalised in terms of sphere radius. The figure shows that the off-axis rays provide significantly greater axial trapping than on-axis rays, but that all rays provide similar levels of lateral trapping. Consequently, in support of the experimental observations, this suggests that Laguerre-Gaussian modes, which have an intensity weighting biased towards off-axis rays, should indeed offer improved axial trapping.

Although the absence of refraction suggests that the on-axis rays do not contribute to the axial trapping force, one must also take into account reflection of the light from the fluid boundary. Taking fused silica spheres in water as an example, a simple calculation based on the Fresnel reflections at the boundary would suggest that the Q-axial for the on-axis rays is of the order

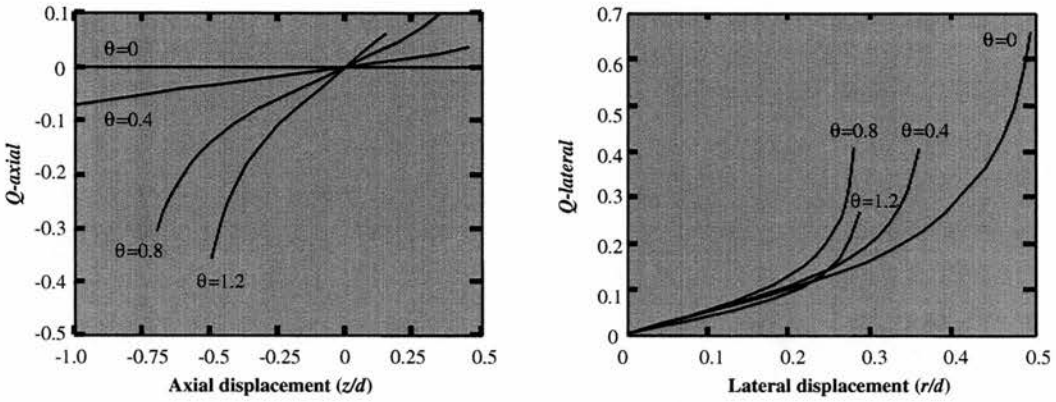

Figure 5.7: Graphs showing Q-values for trapping efficiency, calculated using a ray-optical model, of rays at various angles (in radians) to the optical axis [6]. Displacements are given in multiples of the diameter of the trapped particle, d.

of 0.01. This may explain the small difference observed between inverted and non-inverted tweezers geometry, as this value is not particularly significant in terms of overall tweezers performance.

5.5 Conclusion

In a more complete set of comparative results, I have confirmed earlier predictions and observations that for spheres larger than the focused beam size, the use of a higher order Laguerre-Gaussian mode improves the axial trapping efficiency of optical tweezers. However, in contrast with an earlier preliminary observation [3], there is no improvement in the lateral trapping efficiency. This last observation is compatible with a ray-optical model of the optical tweezers force. The results also demonstrate that for smaller particles, Laguerre-Gaussian modes may be less efficient than a fundamental Gaussian mode. Consequently, I suggest that Laguerre-Gaussian mode should only be considered for conventional trapping experiments for larger particles and if axial rather than lateral trapping efficiency is of paramount importance.

A paper based on the material in this chapter has been published in

Optics Communications [6].

Chapter 6

Rotational control within optical tweezers using a rotating aperture

6.1 Introduction

In this chapter, I demonstrate a simple method for rotational control of objects trapped within optical tweezers that does not require high-order modes, interferometric precision or computer-controlled optical modulators. Inserting a rectangular aperture into the optical beam results in a focused spot which also has rectangular symmetry. I show that an asymmetric object trapped in the beam has its angular orientation fixed such that rotation of the aperture results in a direct rotation of the particle.

6.2 Background

Ashkin demonstrated fifteen years ago that tightly focused laser beams could be used to trap and manipulate micron-sized particles [2], see Chapter 4. So-

called optical tweezers rely on the extremely large gradient in the electric field generated by a tightly focused laser beam. Any dielectric particle in the vicinity of the focus is subject to a force, directed towards the region of highest field. For a very tightly focused laser beam, the gradient force overcomes the gravitational force as well as light scattering; the particle becomes trapped in three dimensions. For particles a few microns in diameter, suspended in water, a few milli-Watts of laser power focused with an oil-immersion microscope objective is sufficient to form a robust trap. Lateral and axial forces of a few hundred pico-Newtons can be generated which allow particles to be manipulated at speeds of tens of microns per second [49]. Optical tweezers are now commercially available [40, 41] and used widely in the biological community for purposes such as measuring the compliance of bacterial tails [53], the forces exerted by single muscle molecules [65] and the stretching of single strands of DNA [51]. Optical tweezers have also been combined with an additional laser to form optical scissors [73] or used as part of a fluorescence [74], confocal [75] or scanning force [76] probe.

Physicists have used optical tweezers as a tool to study the transfer of angular momentum from light to particles. For particles trapped on the beam axis, both the spin and orbital angular momentum have been shown to cause rotation of birefringent [21] and absorbing [22] particles respectively. For absorbing particles, spin and orbital angular momenta can be transferred simultaneously with the same efficiency so that the applied torque is proportional to the total angular momentum [19]. Most recently optical tweezers have been used to explore the intrinsic and extrinsic nature of a light beams angular momentum by examining the motion of particles trapped away from the beam axis [12][1]. However, it should be emphasised that the prime motivation behind that work lay in the study of the optical properties of the beams rather than specifically as a technical tool, see Chapter 8. The linear

[1]The research covered on this topic can be found in Chapter 8.

momentum or "radiation pressure" of a single beam has also been used to impart rotation to suitably shaped, micro-machined objects [77] or assemblies of partly silvered beads [78].

For practical applications, rotation within optical tweezers has a history dating back to 1991 when Sato used a rotating high-order Hermite-Gaussian mode to induce the rotation of red blood cells [8]. Often, rotation relies on the rectangular symmetry of the beam forcing the asymmetric cell to take up a particular orientation [79]. Rotation of the laser mode then leads to a direct rotation of the cell. Indeed, Ashkin himself observed that this inherent alignment of objects with the beam symmetry could cause rod shaped bacteria to stand upright, aligning themselves vertically along the trapping axis of the beam [48].

Optical tweezers have also been configured using multiple beams to trap more than one particle. These have been implemented by the rapid scanning of a single beam between two or more trap positions [80], or by using computer-generated holograms to give multiple beams simultaneously [81]. These multiple beam traps that allow independent positioning of different objects, or parts thereof, enable rotation of large objects. Dual beam traps have also been configured to create an interference pattern; the resulting intensity gradient gives rise to a trapping force [57]. Recently, by interfering beams with an azimuthal phase structure, this technique has been extended to induce rotation [58].

6.3 Experimental Procedure

Here I demonstrate a simplified method for rotational control within optical tweezers. A rectangular aperture clipping each side of the beam results in a focused spot that also has a rectangular symmetry.

I show that an asymmetric object trapped in the beam has its angular

orientation fixed such that rotation of the aperture results in a direct rotation of the particle. The experimental configuration used in this work is

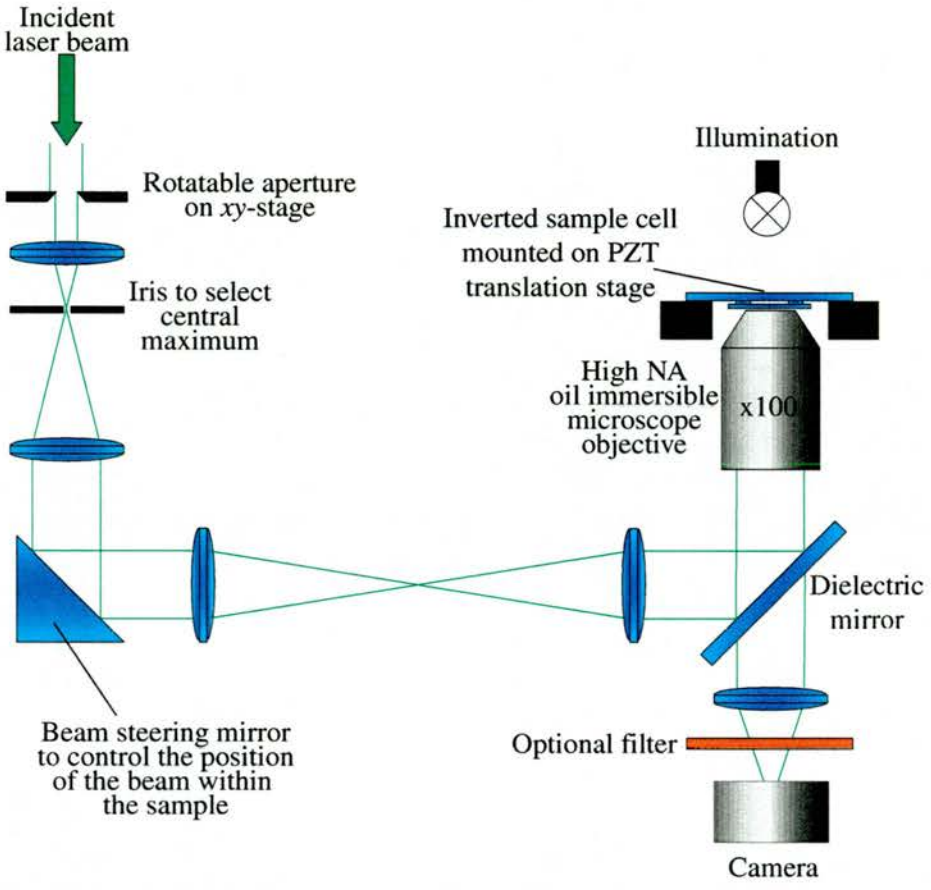

Figure 6.1: The configuration of the inverted optical tweezers set-up with rotatable slit aperture. An iris in the back focal plane of a lens transmitted only the slit's central, elliptical, far-field diffraction peak, which was then imaged onto the sample plane.

shown in Figure 6.1 and is based around an inverted optical tweezers geometry, with the trapping beam directed upwards. The objective lens is an infinity-corrected, Zeiss, Plan-Neofluar 1.3NA, $\times 100$, and the trapping laser is a commercial Nd:YVO_4 laser, frequency-doubled to give approximately 100mW at 532nm. A combination of relay lenses and beam steering mirrors couples this beam into the objective via a highly reflective dielectric mirror,

which separates the trapping and imaging optical paths. The sample cell is mounted on an xyz-piezoelectric (PZT) stage, which provides 100microns of travel in each direction. Beam steering mirrors allow the trapping beam to be positioned anywhere within the field of view of the microscope.

As previously discussed, rotation in optical tweezers has already been achieved using a high-order Hermite-Gaussian mode [8]. In that work, the long axis of the asymmetrically shaped cell aligned itself with the elongated direction of the beam cross section. The axis of the mode was then rotated using an aperture within the laser cavity and the cell was observed to rotate, at all times maintaining its alignment with the mode. Clearly, that technique relied upon a specialist laser and is therefore not readily adaptable. One alternative option for this approach, or indeed for achieving rotation by using a laser within an elliptical output mode [50], would be to create the asymmetric beam and then rotate the whole beam prior to the tweezers. Although simple in concept, the rotation of a beam exactly about its own axis is more difficult than might appear. For example, a rotating Dove prism is well known to rotate a transmitted image or beam, but such a prism requires precise angular and lateral alignment in a way that is difficult to achieve at optical wavelengths [82].

Perhaps the most obvious way to generate an asymmetric beam is to introduce an asymmetric aperture. Although almost any shape of aperture will suffice, and indeed some shapes would better match the symmetry of some objects, I chose a simple rectangular aperture as it is readily engineered to be adjustable. Mounting the aperture within a rotation stage that is itself mounted on an xy-translation stage means that its rotation axis is easily aligned to the beam axis. I found that inserting the aperture just about anywhere in the optical path has the desired effect. However, to minimise requirements on the mechanical stability and tolerance of the mounts I typically inserted the aperture in an expanded and collimated region of the

trapping beam. The output of the trapping laser was expanded to give a collimated Gaussian beam with a $\frac{1}{e}$ diameter of 10mm. Inserting a 4mm wide rectangular aperture (shown in Figure 6.2) at this point produced a diffraction pattern, in the far field, comprising of a central maximum containing approximately 45% of the original power and additional diffraction orders containing approximately a further 10% of the power. The subsequent iris

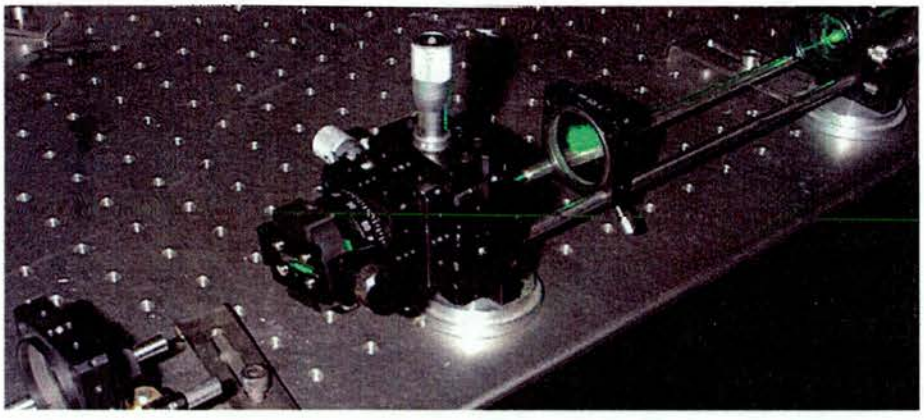

Figure 6.2: The rotational aperture is 4mm wide, and introduces an elongated beam by clipping a 10mm wide fundamental Gaussian.

removed these diffraction orders, such that only the central maximum was relayed to the sample plane. The central maximum is itself elliptical in cross-section with an aspect ratio of 1 : 2, and it is this ellipticity which was responsible for causing the asymmetric objects to align with respect to the beam.

Although the use of an aperture in this way is wasteful of laser power it should be appreciated that it is the potential for optical damage [83] rather than the available laser power which typically sets the upper limit to the power incident in the sample plane. In any event, an efficiency of 50% compares favourably with the efficiency of many computer-generated holograms used for beam shaping in optical tweezers [69] and other applications.

6.4 Results

To demonstrate the application of this technique, I prepared a sample of silica spheres of sizes between 1 and 5 microns suspended in water. Leaving the sample within the tweezers for an hour invariably results in a number of the spheres sticking together. The result is a collection of single spheres and asymmetric fused assemblies of silica spheres. Figure 6.3 shows the

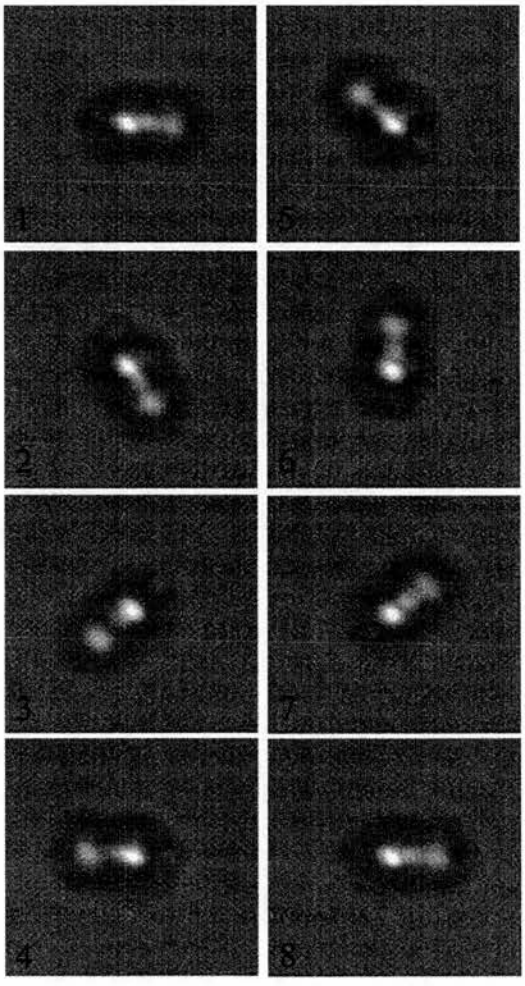

Figure 6.3: Synchronous rotation of a fused assembly of silica spheres using an aperture for the rotational control.

orientation of one such assembly of spheres trapped by the tweezers as the

Particle size	Q-LATERAL	Q-AXIAL
2μm	0.082 ± 0.004	0.079 ± 0.005
5μm	0.173 ± 0.004	0.152 ± 0.006

Table 6.1: Lateral and Axial Q-values using an apertured trapping beam.

aperture is rotated. In this case the trapping power in the sample plane was set to be 30mW. In this configuration the aperture was rotated by hand and therefore limited to a rotation rate of about 1Hz. However, some particles were held extremely tightly such that even sudden movements of the aperture were unable to shake the object free, suggesting that significantly higher rotation speeds are possible. In practice the maximum possible rotation speed is a complex function depending upon the asymmetry of the focal spot, the viscosity of the fluid, and the shape of the object. The ideal object would clearly be symmetrical in shape (thereby minimising the drag) but asymmetrical in terms of its refractive index.

I also assessed the impact of the aperture on the performance of the lateral and axial trapping efficiency of the tweezers. When used for trapping single spheres I measured lateral and axial Q-values for 2 and 5 micron diameter spheres, these are shown in Table 6.1. Such results lie well within the range of those reported by other groups that have used conventional non-apertured Gaussian beams [3], and agree closely with my earlier work on lateral and axial trapping efficiencies [6] described in Chapter 5. I used the method as described in Chapter 5 to obtain the results for lateral and axial Q-values given in this section, and hence the results here can be compared directly with those in Chapter 5 for the lateral and axial trapping of silica spheres. In Figures 6.4 and 6.5 we can see the lateral and axial Q-values for the apertured beam along with a direct comparison of the results shown in Chapter 5. It would be useful to know the magnitude of torques present

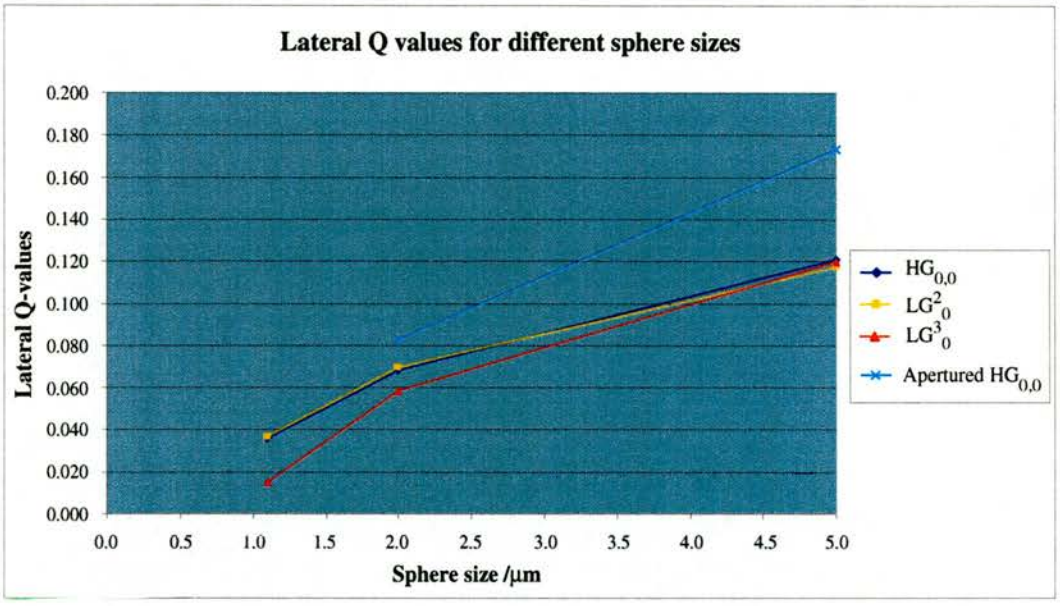

Figure 6.4: Lateral Q-values for a rotating aperture directly compared to previously obtained results (see Chapter 5).

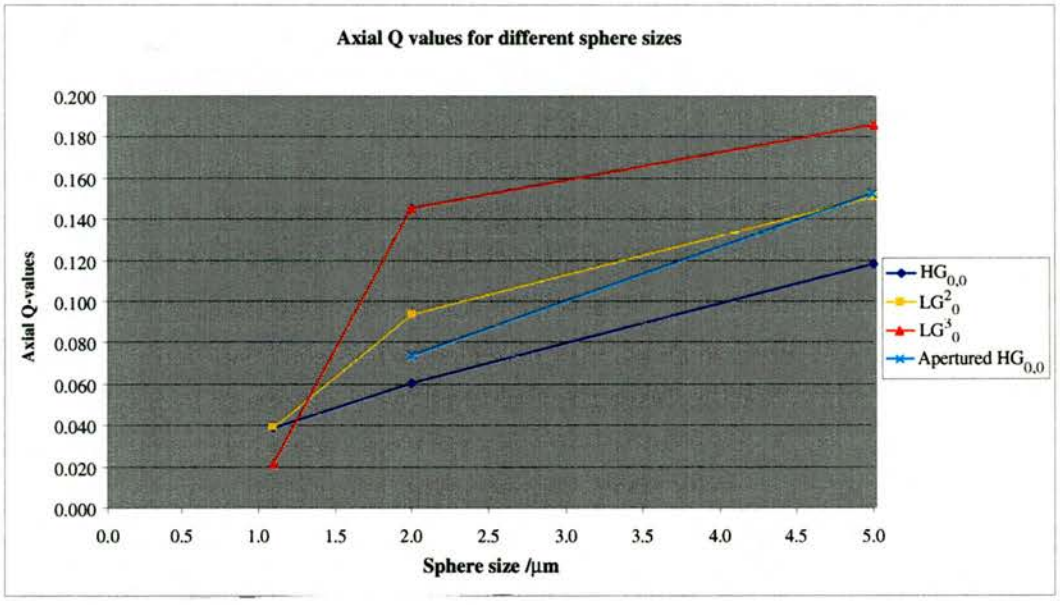

Figure 6.5: Axial Q-values for a rotating aperture directly compared to previously obtained results (see Chapter 5).

in the system. However, more experiments need to be performed to make a reliable estimation.

6.5 Conclusion

I have demonstrated a simple, but to my knowledge unreported, method for achieving rotational control within optical tweezers. The inclusion of an aperture in the trapping beam gives a focused spot with the same cross-sectional symmetry as the aperture. This results in the preferential rotational alignment of an irregular object with the beam. Rotating the aperture rotates the focal spot within the tweezers causing a synchronous rotation of the object. The technique can readily be applied to most existing tweezers experimental configurations allowing its use in all areas of tweezers activity. However, it is most likely to be of interest in the manipulation and control of micromachines where the potential use of rotational control is most apparent. Since rotational control may only be occasionally required in many applications, the aperture can be easily removed from this configuration, reverting simply to a standard optical tweezers set up.

Some of the content of this chapter has been the subject of a submission to Optics Letters [7].

Chapter 7

Metal Particle Trapping in Inverted Optical Tweezers

7.1 Introduction

During the investigation of metal particle trapping, a novel way of trapping silver particles was discovered. I found that a metal particle could be trapped on the outside of a Laguerre-Gaussian laser beam, this particle was then confined to the beam. This method of metal particle confinement allowed a particularly useful investigation of the properties of the laser beam. It allowed the discrimination of both the *spin* angular momentum and that of the *orbital* angular momentum of the beam. I termed this method *metal-particle confinement*:

- Particle trapped off-axis on the outside of a Laguerre-Gaussian beam.
- Particle rotated about the beam axis in either direction depending on the handedness of the phase fronts of the LG beam.
- Allowed investigation of angular momentum within the beam.

The general importance of this work was the distinctive nature of the metal trapping and how it alluded to the separability of spin and orbital angular momentum. This enabled further understanding of the angular momentum of light. Section 7.3 gives full details of this method.

7.2 Investigation into an appropriate suspension solution

The two types of metal particles which I trapped during my research were silver and nickel. Silver and nickel have very different densities, because of this they behaved very differently when 2μm particles were placed in water. Extensive investigations into suitable fluids for the efficient trapping of both particles types were performed.

Correct solution choice is important for the successful trapping of particles with different properties. Each particle, with its different properties, requires a specific solution for it to be suspended in. The largest stumbling block proved to be that of finding the best medium in which to suspend the different particles. The dielectric particles (silica and calcite) were trapped in water. However, the metallic particles needed something different. Silver particles were positively buoyant and floated on the surface of the water without mixing because the surface tension of the water prevented this. On the other hand, the nickel particles were too negatively buoyant and did not suspend in the solution for long enough to trap them, a method of reducing the speed with which they sank to the bottom was required.

Working with these tiny particles required some safety precautions to be taken into consideration. Whilst they remain in their powder form they are carcinogenic, and must not be inhaled. To prevent inhalation, gloves, mask, and goggles were worn during the preparation of the solutions.

The high surface tension forces prevented the suspension of the silver

particles in water. Many different solutions were tried, including methanol and propanol, but their composition proved too volatile: the heating of the particles by the laser beam resulted in the methanol and propanol evaporating off rapidly, immobilising the particles. The solution which worked most successfully was that of detergent and water. Ratio of detergent to water was 1 : 50; this detergent lowered the surface tension enough to suspend the silver in solution. The silver particles could then be trapped easily.

The problem with the nickel particles was the reverse; the particles sank too rapidly in water, resulting in a *dead* sample, since they were already resting on the microscope slide. Dead samples are extremely difficult to work with and get good results. Particles often get stuck on to the slide if they are stationary for too long which makes trapping them difficult. A very mobile sample with the particles jiggling around is much better to work with. Methanol and propanol were tried, but their viscosity was even lower than that of water, not to mention that they suffered the aforementioned side effects due to heating of the particles. Such solutions' usefulness was so limited that they were discarded as a viable option. Eventually, the best solution proved to be a sugar solution. One part glucose was dissolved in five parts water before the nickel was added. This resulted in a more viscous solution, and that meant that the nickel particles sank more slowly. They were held in suspension long enough for the particles to be trapped. Once trapped they no longer sank, allowing the particles to be moved around as required.

7.3 Transfer of Orbital Angular Momentum to Metal Particles Confined Using Optical Tweezers

7.3.1 Introduction

Using Laguerre-Gaussian beams in an inverted optical tweezers geometry I observe that silver particles 2μm in diameter are confined to an annulus around the outside of the beam. This annulus is situated 4μm below the beam waist where the upward scattering force counterbalances gravity. The scattering force results in a transfer of the orbital angular momentum content of the beam to the particle causing it to rotate about the beam axis.

In addition to the spin angular momentum associated with individual photons, which on a macroscopic scale corresponds to circular polarisation, it is now well established that light beams can also carry an orbital angular momentum that is associated with helical phase fronts. Beams with helical phase fronts, such as the Laguerre-Gaussian laser modes, are characterised by an azimuthal phase term of $\exp\{-il\varphi\}$. At all points in the beam, the azimuthal component to the momentum density is $p_\varphi = \frac{l\hbar}{r}$, giving an orbital angular momentum of $l\hbar$ per photon [17].

7.3.2 Background

As far back as the 1930s Beth demonstrated the transfer of spin angular momentum from a circularly polarised light beam to a birefringent wave plate suspended from a quartz fibre [20]. This experiment is made possible since the nature of spin angular momentum means that the axis of the wave plate defines the axis of the torque [84, 85]. However, orbital angular momentum transfer is more problematic since any misalignment between the suspension

axis of the test object and the propagation axis of the beam results in additional torque on the system from which the effect of the orbital angular momentum transfer is difficult to distinguish. A solution to this problem lies in the use of optical tweezers that were invented by Arthur Ashkin at Bell Laboratories in 1986 [2]. They rely upon the dipole force that acts on any transparent particle resulting in a force directed towards the beam focus. When the beam is tightly focused, it creates a three-dimensional trap for transparent objects. In this situation the resulting force is sufficient to overcome both the scattering force and that due to gravity. Optical tweezers are used to trap particles in a liquid that provides both a viscous damping force and the partial buoyancy of the particles. Optical tweezers have been configured using both Hermite-Gaussian, ($HG_{m,n}$) or Laguerre-Gaussian (LG_p^l) modes. Optical tweezers allow a particle to be held at the focus of a laser beam, exactly aligned with the beam axis.

Constraint of a partially absorbing particle to the beam axis using optical tweezers ensures exact alignment of the torque and suspension axes. Using Laguerre-Gaussian modes as the trapping beam has enabled a number of groups to transfer orbital angular momentum to particles held on the beam axis and to show that the on-axis rotation of the particle is related to the total angular momentum [22, 23, 19], i.e. spin AM plus orbital AM. The dipole force, however, depends only on the beam intensity and is not related either to the polarisation or the phase of the beam and a different transfer mechanism needs to be identified. In previous work, the transfer mechanism for both spin and orbital angular momenta was the partial absorption of light by the particles. In addition to the transfer of orbital angular momentum, it has also been demonstrated that transparent birefringent particles held in optical tweezers can be rotated by the spin angular momentum content of the beam; analogous to the Beth experiment [21]. In the latter case orbital angular momentum would not induce a rotation as propagation through a

birefringent medium does not change the helicity of the phase fronts. The equivalent mechanism for the transfer of orbital angular momentum alone lies elsewhere.

Metallic particles scatter and reflect much more strongly than the transparent particles normally held within optical tweezers. Consequently these particles cannot be trapped in the usual manner. Small Rayleigh particles (tens of nanometres in diameter) have been trapped in three dimensions; in that size regime, scattering from metals and dielectric particles is similar [54]. As shown previously in Table 4.1 larger Mie particles have been trapped in two dimensions, the forces arising from a creeping wave induced by a surface plasmon [64]. Metal particles have also been confined in two dimensions by scanning beams (see Table 4.1 [10]) or annular rings (see Table 4.1 [11]) and [70]. These methods rely on light scattering to produce a repulsive force and trap the particle. In this chapter I report a variant of this last trapping mechanism that occurs in inverted optical tweezers. In an inverted arrangement, shown in Figure 7.1, the trapping beam is directed upwards counteracting the gravitational force. Micron-sized metal particles are observed to be loosely confined to an annular region below the beam focus but external to the high intensity region of the beam. Furthermore, I observe that, if the trapping beam is a Laguerre-Gaussian mode with $|l| > 0$ then the orbital angular momentum induces a motion of the particle around the beam axis. The speed and direction of this rotation is dependent solely upon the orbital angular momentum and is not altered by the spin angular momentum of the beam.

7.3.3 Experimental Apparatus

Figure 7.1 and Figure 7.2 show the experimental apparatus, the former is a schematic, whilst the latter shows a photograph of the arrangement. Figure 7.3 shows the optics that were inserted into the arrangement to inves-

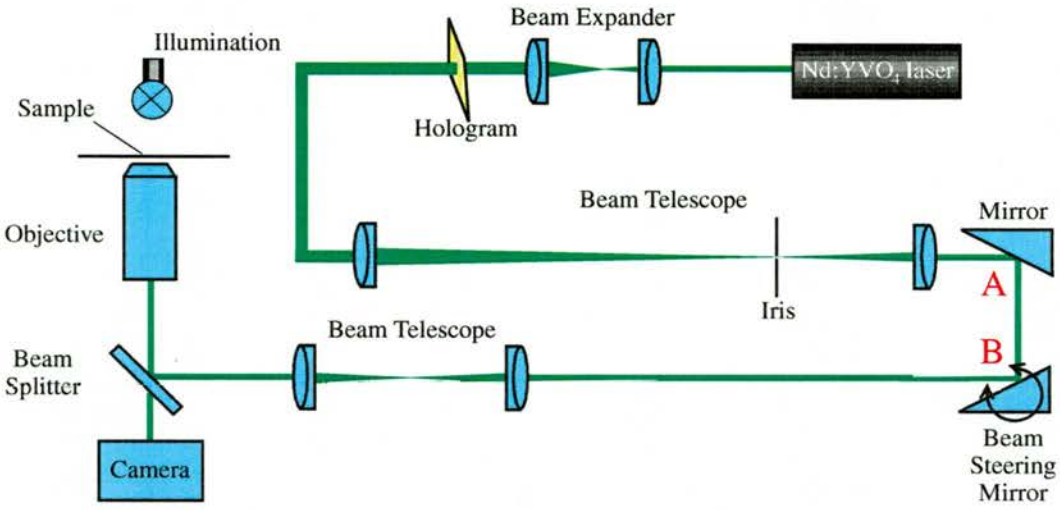

Figure 7.1: Experimental apparatus used for the trapping and rotation of metal particles. Between points A and B further optics were used to probe the trapping mechanism.

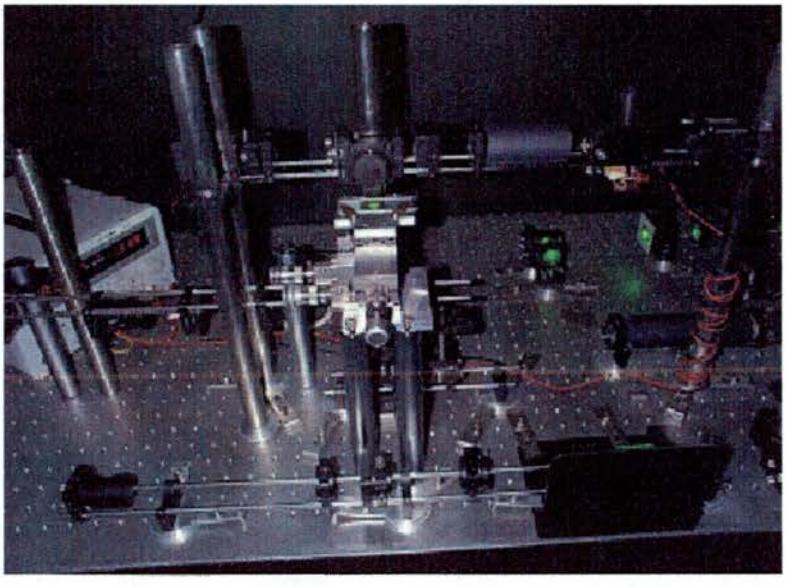

Figure 7.2: A photograph showing the actual experimental setup.

tigate the summing affect of the spin AM, in circularly polarised light, with the orbital AM of helical phase fronts. The trapping laser is a frequency-doubled diode-pumped Nd:YLF laser with single transverse mode output power of 100mW at 532nm. The beam is expanded, collimated and passed

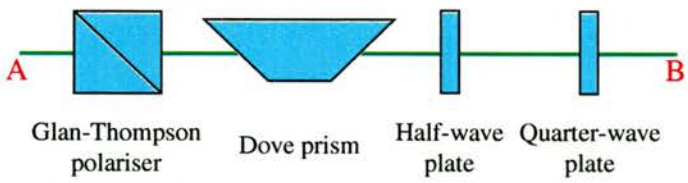

Figure 7.3: Here we can see the additional optics required in this experiment. The Glan Thompson polariser linearly polarises the light so it can then be circularly polarised (CP) by the quarter-wave plate. A half-wave plate can be added to change handedness of the CP light, and hence that of the spin AM. The Dove prism could be inserted and removed as required to change the handedness of the helical phase fronts.

through a computer-designed hologram containing a single on-axis fork dislocation [34]. A subsequent aperture can be translated to select either the zero-order beam, which has the same spatial profile as the laser, i.e. that of a $HG_{0,0}$ mode, or the first-order diffracted beam which closely resembles a Laguerre-Gaussian mode, (LG_0^1), and hence carries an orbital angular momentum of $+\hbar$ per photon. A quarter-wave plate can be introduced into the beam, which circularly polarises the light, giving a spin angular momentum of $+\hbar$ per photon. A Dove prism can be precisely inserted so as to reverse the handedness of the helical phase fronts and therefore reverse the sign of the orbital angular momentum without changing the propagation direction or polarisation of the beam, in this case giving us an orbital angular momentum of $-\hbar$ per photon. Similarly, the quarter-wave plate can be rotated to change the handedness of the circularly polarisation without changing the helicity of the phase front, resulting in a spin angular momentum of $-\hbar$ per photon. Hence, by appropriate positioning of prism and wave plate, the total angular momentum in the beam can be set at $\pm\hbar_{orbital} \pm \hbar_{spin}$. Hence one can obtain the following variation of Total AM values: $-2\hbar, -\hbar, 0, \hbar$, and $2\hbar$, some of these are represented pictorially in Figure 7.4. Beam-steering mirrors and associated relay optics ensure that the beam can be directed around the sample cell while still being centred on the back aperture of the

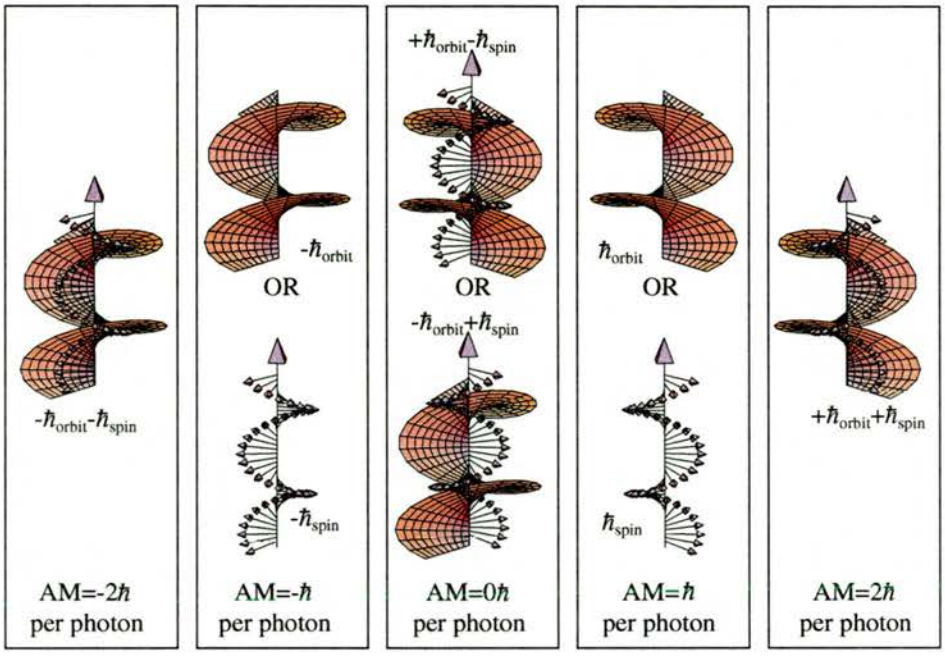

Figure 7.4: A pictorial representation of spin angular momentum summing with orbital angular momentum.

objective lens. The objective lens is a Zeiss $\times 100$ Plan-Neofluar (NA= 1.3), widely used by the optical tweezers community. The sample cell is formed from a microscope slide, a PTFE 70μm spacer and a thin coverslip to allow for the short working distance of the objective. The particles themselves are 2μm-diameter silver spheres which are suspended in water containing a small amount of detergent (1 part detergent:50 parts water), which reduces the surface tension so the particles are suspended in the solution. The particles can be observed as individual particles and in small clumps. After losses in the hologram, prism, wave plate and beam-steering mirrors, the power incident at the microscope objective is 10 mW, approximately 50% of which is transmitted to the sample.

7.3.4 Optical Confinement

Focusing of a Laguerre-Gaussian beam with any combination of spin and orbital angular momentum a few microns above the base of the sample cell allowed particles to be picked up. Single 2μm diameter silver particles, or clumps thereof, could be trapped and then moved in three dimensions. The radial and vertical motion of the particles is somewhat random but they remain within an annular region approximately 10μm in diameter centred on the beam axis but a few microns below the beam focus. When using a Laguerre-Gaussian beam of any polarisation, the azimuthal position of the confined particle evolves over time in a specific rotation direction, depending upon the helical phase fronts, around the beam axis. From the observation of the light scattered from the particle I deduce that every few seconds the force of gravity acting on the particle causes it to fall into a high-intensity region of the beam, in a plane below the focus where the light is highly converging. This results in a sudden impulse force on the particle pushing it both upwards and inwards towards the beam axis. After a few seconds the particle falls back again into the beam and the process repeats itself. I believe that the impulse force arises from the scattering of the light from the particle. Within the experimental configuration I measured the far-field, half-cone angle of the beam to be about 60°. Two microns below the focus of a 5 mW fundamental Gaussian mode the $\frac{1}{e}$ intensity is approximately 50 MW/m^2, giving both a radial and vertical scattering force on the 2-micron-diameter particle of order 1 x 10^{-12} N. This force is sufficient to overcome the weight, about 0.5 x 10^{-12} N, of the particle, supporting it against gravity and confining it near to the beam axis. In support of these estimates I find that if the power in the beam is halved then trapping is very difficult to maintain. Although, as reviewed above, metal particles have previously been confined, when it was published I believed that this was the first reported confinement of micron-sized metal particles in three dimensions.

7.3.5 Optical Rotation

When a Laguerre-Gaussian beam is used instead of a $HG_{0,0}$ beam, the behaviour of the confined particle changes. Firstly, the particles become easier to lift and confine. This is not surprising since for beams of the same numerical aperture and power, the peak intensity of a LG_0^1 mode is approximately three times higher than the $\frac{1}{e}$ intensity of a fundamental Hermite-Gaussian mode. Consequently, the scattering force associated with these off-axis regions of the beam is correspondingly increased. Secondly, over a period of several minutes the particle is seen to rotate around the beam axis. I believe this rotation arises from the azimuthal component of the Laguerre-Gaussian mode's momentum density and the corresponding azimuthal component of the scattering force. The relative size of the axial, radial and azimuthal components can be deduced from the form of the Poynting vector [17, 71]. The radial component scales in proportion to the radial position whereas the azimuthal component scales inversely with radius. Even for this degree of extreme focusing, it transpires that a couple of microns below the focus, at the radius corresponding to maximum intensity the azimuthal component of the Poynting vector, and hence scattering force, is 10 times smaller than its radial component. This explains the slow rate of observed rotation of the particle around the beam axis. However, as the particle approaches the beam axis the azimuthal component of the scattering force can dominate over the radial component. Consequently, in practice, the particle always stays on the outside of the beam and never reaches the beam axis from which point the intensity null may have enabled it to escape, see Figure 7.5.

Inserting a Dove prism into the beam changes the sense of the helical wave fronts, resulting in a reversal of the azimuthal scattering force and hence the direction of rotation. It was noted that in all cases the rotation sense and rate cannot be influenced by the sense of the circular polarisation. Specifically, a Laguerre-Gaussian beam with azimuthal mode index can be

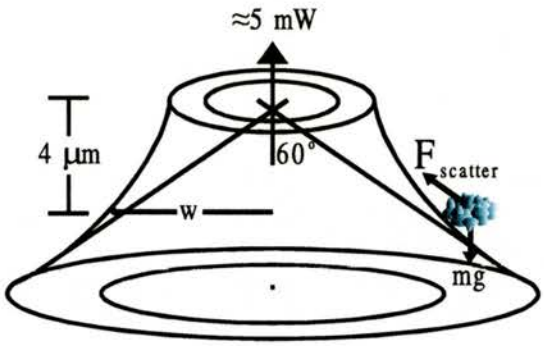

Figure 7.5: The trapped particles are confined to an annular region 4μm below the beam focus with a radius greater than that corresponding to the maximum intensity of the Laguerre-Gaussian beam.

circularly polarised in the opposite sense to give a beam with a total angular momentum of zero. However, such a beam still induces a rotation of the particle about the beam axis since the polarisation state and hence spin angular momentum has no influence on the scattering force. This confirms that the dominant force is indeed due to light scattering since absorption of the light would result in a transfer of spin angular momentum and a rotation of the particle. Figure 7.6 shows the time-recorded trajectories for a particle rotating in opposite directions around the beam axis depending on whether or not the Dove prism is inserted. In both cases, the Laguerre-Gaussian mode has an azimuthal mode index and a circular polarisation of the opposite handedness to give a total angular momentum of zero. When the Laguerre-Gaussian beam was replaced with a $HG_{0,0}$ Gaussian beam it was still possible (although much more difficult) to lift the metal particles but, irrespective of the polarisation state, the particles were not observed to rotate in any systematic way about the beam axis. This reinforces my belief that it is the orbital angular momentum content of the beam which is indeed responsible for the observed rotation. Figure 7.7 shows the Poynting vectors corresponding to the radius of maximum-intensity of a Laguerre-Gaussian beam; also shown is an example trajectory of the metallic particle

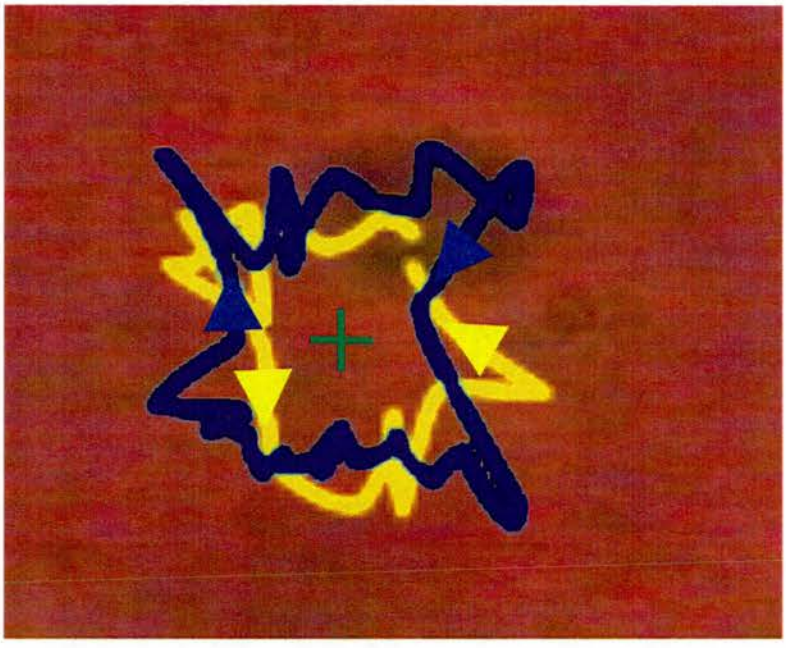

Figure 7.6: Clockwise and anticlockwise trajectories of the trapped particle as it is rotated around the beam axis.

as it moves around the outside of the beam.

Further to my investigations into the nature of angular momentum transfer, I also investigated the effect of higher l-values. Using appropriately designed holograms first-order diffracted beams approximating LG_0^2, LG_0^3, and LG_0^4 can be obtained. As expected, I observed that higher values result in faster rotation. The use of an LG_0^4 beam results in rotation that is approximately four times quicker about the beam axis than obtained using a LG_0^1 beam.

7.4 Summary

In this chapter I have discussed a range of insights into solutions required for trapping metal particles. This is often an area which is omitted in papers and it is useful to have the information. The method of optical confinement, shown in Table 7.1 and described within this chapter, allowed a deeper un-

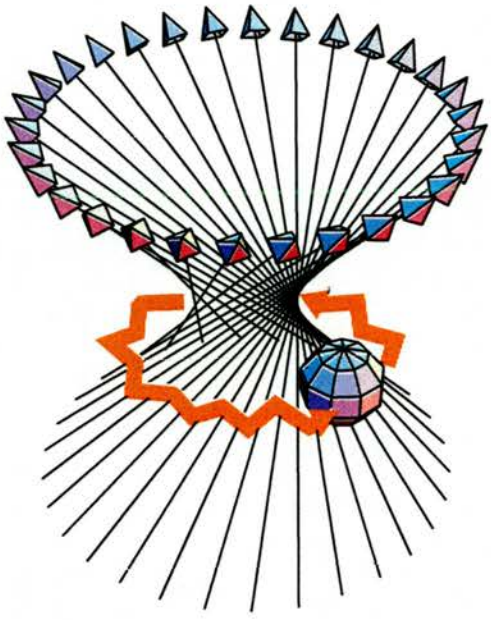

Figure 7.7: The metallic particle's path around the outside of Laguerre-Gaussian beam. The particle is confined 4μm below the beam focus. When the particle bounces too far into the beam the radiation pressure of the laser light ejects it. Despite this it continues to remain confined and continues on its path around the outside of the beam.

	O'Neil & Padgett 2000 [9] ANNULAR BEAM Mie (μm) particle 3D TRAPPING

Table 7.1: Optical confinement of metallic particles.

derstanding of angular momentum of light.

In Section 7.3.4 and 7.3.5 I have shown that within inverted optical tweezers, the force arising from light scattering can be used to confine micron-sized metallic particles to an annular region immediately below the beam focus. Compared with a fundamental Gaussian mode, the increased scattering force arising from the off-axis rays associated with the Laguerre-Gaussian beams gives more efficient trapping of metallic particles. The azimuthal component of the momentum density associated with Laguerre-Gaussian beams can also induce a rotation of the particle around the beam axis

7.5 Conclusion

The key result in this chapter was the effect of Spin angular momentum (AM) relative to Orbital AM on the particle. Equally interesting was the particle confinement issue. Previous experiments have shown that the spin and orbital angular momentum components of a beam can act in an equivalent and interchangeable manner, e.g. for an optical spanner [19, 21], and more recently in the rotational Doppler shift [86, 82]. By contrast, in this work I have emphasized that this interchangeability is not a general phenomenon but depends on the specific process. For example, in a Beth-type experi-

ment one would have no reason to anticipate that a helically phased beam would induce any torque on the suspended wave plate since the mechanism for angular momentum exchange relies upon birefringence, a phenomenon that does not affect the helical phase structure in any way. Similarly astigmatism can change the helicity of the beam and hence the orbital angular momentum, whereas it cannot change the polarisation state. In this case I rely upon the azimuthal component of the beam's momentum. Scattering of the light from the particle into a random direction results in a recoil force acting on the particle, thereby creating a torque around the beam axis.

Finally, my observation of the fact that the rotation of the particle cannot be influenced by the spin angular momentum of the beam demonstrates that, in this regime, it is indeed the scattering of light from the particle and not absorption that gives rise to the dominant force acting upon the metallic particle.

A paper based on the material in this chapter has been published in Optics Communications [9].

Chapter 8

Orbital and spin angular momentum acting on calcite particles

8.1 Introduction

In this chapter, I demonstrate the different actions of spin and orbital angular momentum on different-sized particles. The work presented here is based on experimentation with particles trapped off-axis in a Laguerre-Gaussian beam with a high azimuthal mode index, $l = 8$.

8.2 Background

Circularly polarised light has an angular momentum associated with it [20, 21], termed *spin* angular momentum, arising from the spin of individual photons. In 1936, Beth [20] demonstrated that he could exert a torque upon a birefringent wave plate suspended in the beam by the transfer of angular momentum, as stated in Chapter 2.

An orbital angular momentum component (also described in Chapter 2) is known to originate from the linear momentum of a light beam about a radius vector. Within the last ten years, Allen *et al.* [17] showed that for beams with helical phase fronts[1] the orbital angular momentum in the propagation direction has the discrete value of $l\hbar$ per photon, see Equation (2.12). As stated previously, beams possessing each of these types of angular momenta are used within optical tweezers to trap particles. The particles interact with the laser beams in distinct ways depending on the type of angular momentum present in the beam. The specific behaviour of the particles during this experiment supported initial intuition, of the expected actions of particles when acted on by spin and orbital angular momentum.

8.3 The transfer of spin and orbital angular momentum to small particles

A number of groups have used optical tweezers to investigate how the angular momentum of a light beam interacts with a small particle. Optical tweezers (see Chapter 4) are usually implemented using a high numerical-aperture microscope, and rely on the gradient force to confine a dielectric particle near the point of highest light intensity [2]. When particles are trapped on the beam axis, both the spin and orbital angular momentum have been shown to cause rotation of birefringent [21] and absorbing [22] particles, respectively.

For absorbing particles, both spin and orbital angular momentum are transferred with the same efficiency so that the applied torque is proportional to the total angular momentum [19], that is, $(\sigma + l)\hbar$ per photon[2]. The $\sigma\hbar$

[1]Beams with helical phase fronts can be characterised by an $\exp(il\varphi)$ azimuthal phase dependence.

[2]The types of angular momentum were originally discussed in Chapter 2, Equations (2.12) and (2.13)

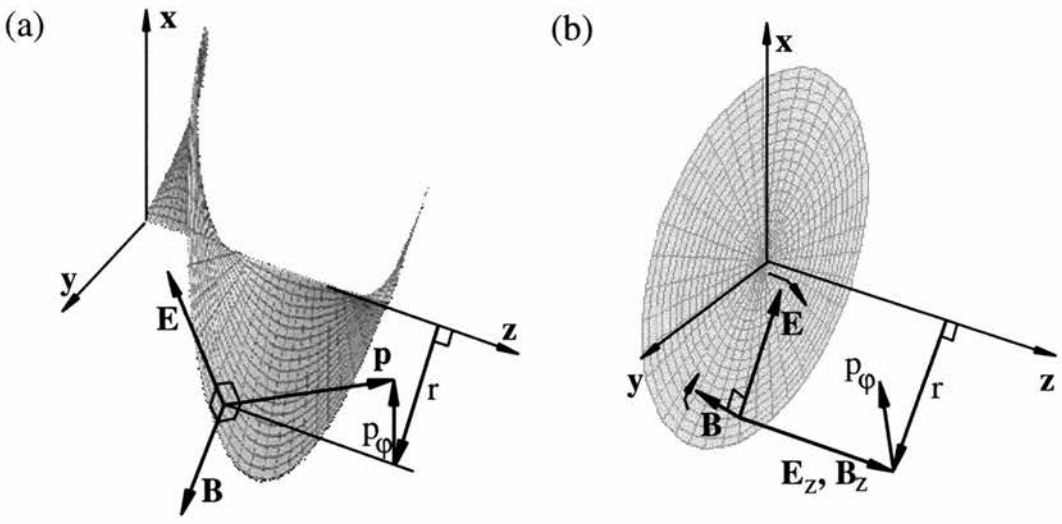

Figure 8.1: (a) The electric and magnetic fields for a linearly polarised helical wave. The inclination of the phase fronts results in field components in the propagation direction, a momentum contribution in the azimuthal direction and hence an angular momentum in the direction of propagation. (b) The electric and magnetic fields for a circularly polarised plane wave. A radial intensity gradient results in field components in the propagation direction, a momentum contribution in the azimuthal direction and hence an angular momentum in the direction of propagation.

term comes from the spin AM component introduced by circularly polarised light. The $l\hbar$ term comes from the orbital AM component due to the helical phase fronts of a Laguerre-Gaussian beam.

In Figure 8.1, we can see both the helical phase fronts of a Laguerre-Gaussian beam with its electric and magnetic fields, and a plane wave with its electric and magnetic fields. Angular momentum transfer with a birefringent particle arises from a re-phasing of orthogonal polarisation fields. In a similar way, the equivalent interaction for beams possessing orbital angular momentum is by the use of astigmatic optical components which re-phase orthogonal modes [24]. However, because micron-sized astigmatic optical components are not easily produced, such interactions between small astigmatic particles and light had not yet been observed.

8.4 Experimental Procedure

In this work, I used a circularly polarised Laguerre-Gaussian mode with a high azimuthal mode index, l. Initially using a $l = 4$ LG beam, the motion of the particle around the beam was difficult to distinguish, and I decided that a higher l was necessary. Subsequently, the specific mode order used in the experiments was $l = 8$, when the beam was focused down it still had a clear ring at the beam waist. This ensures that the rotation of the particle around the beam due to orbital angular momentum is observable. The insertion of a half-wave plate or a Dove prism allows the reversal of the handedness of the spin or the orbital angular momentum [36]. As in Chapters 5, 6 and 7, the experimental configuration consisted of an inverted optical tweezers with the trapping beam directed upwards, based on a 1.3NA, $\times 100$ objective lens. The 100mW output of a commercial Nd:YVO_4 laser was transformed, using a computer-generated hologram[3], to give a Laguerre-Gaussian ($l = 8$) mode of approximately 30mW, see Figure 8.2.

Calcite particles from about 1 to 3μm in diameter were used in this experiment. These particles were suspended in water to enable their trapping. Careful vertical alignment of the trapping beam is paramount for this experiment to be successful; the slightest misalignment of the trapping beam meant that the effect I was looking for failed. Additional alignment difficulties were also introduced by the need for such a high l-value. If the beam is skew when going into the back objective, the transfer of angular momentum is difficult and is hard to discern in the results.

Intuitively, one would think that, on interaction with orbital AM, the particle would move around the beam axis, as I found for silver particles [9] (see Chapter 7). However this time, since the particles are transparent, one would expect them to be held at the most intense part of the beam and not

[3]See Appendix A.

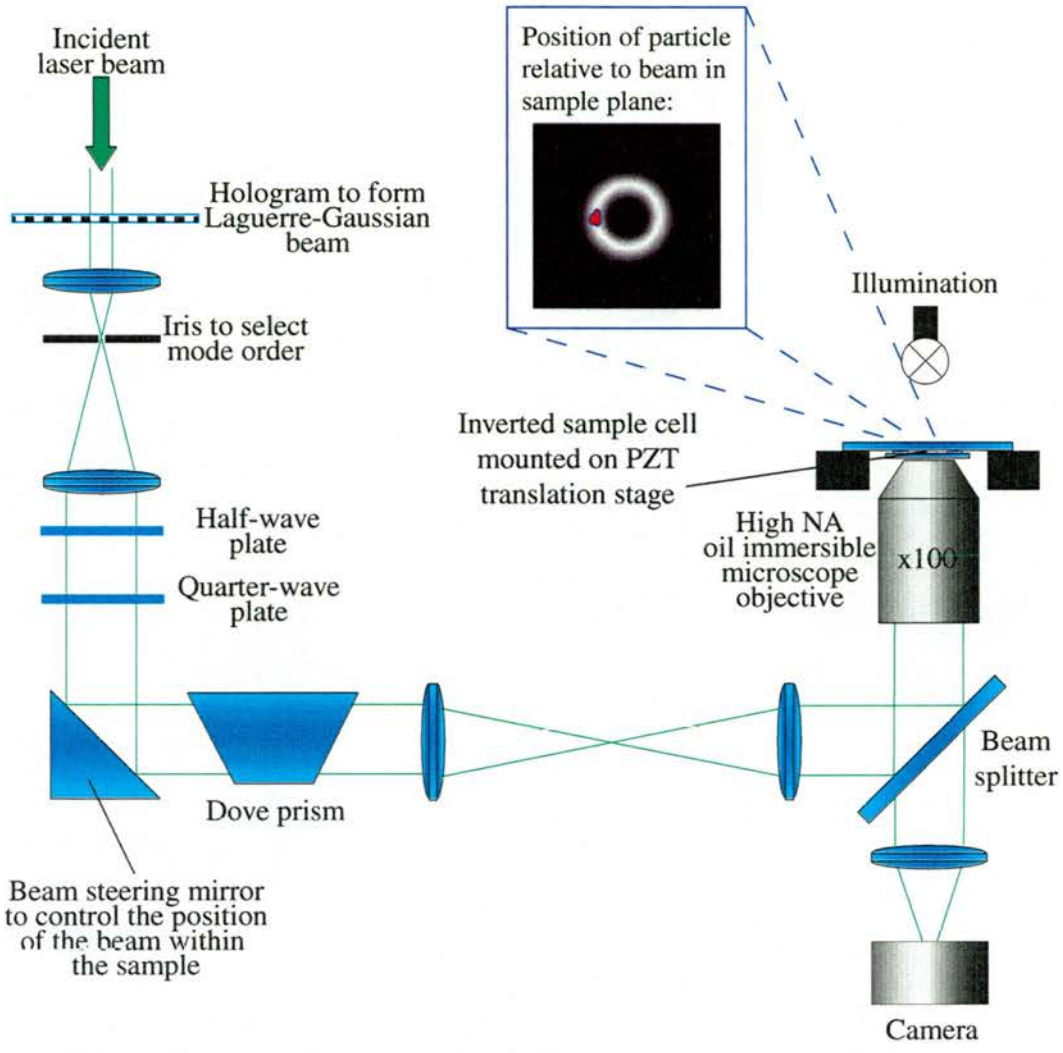

Figure 8.2: The set-up used for testing the particle's interaction with orbital AM and spin AM. The LG beam was circularly polarised using a half-wave plate then a quarter-wave plate to test the interaction with spin AM. The Dove prism could be used to change the sign of the orbital AM, thus resulting in rotation of the particle around the beam profile in the opposite direction.

to be ejected as was observed with the silver particles. As in the paper by Simpson *et al.* [19], I believed that the spin AM component would cause the particle to rotate on its own axis. Given that the beam profile was a large *doughnut* mode due to the high l-value, I thought that the particle would be

positioned off-axis at the most intense part of the beam, but still rotate on its own axis. Figure 8.3 displays LabVIEW calculations by Miles Padgett,

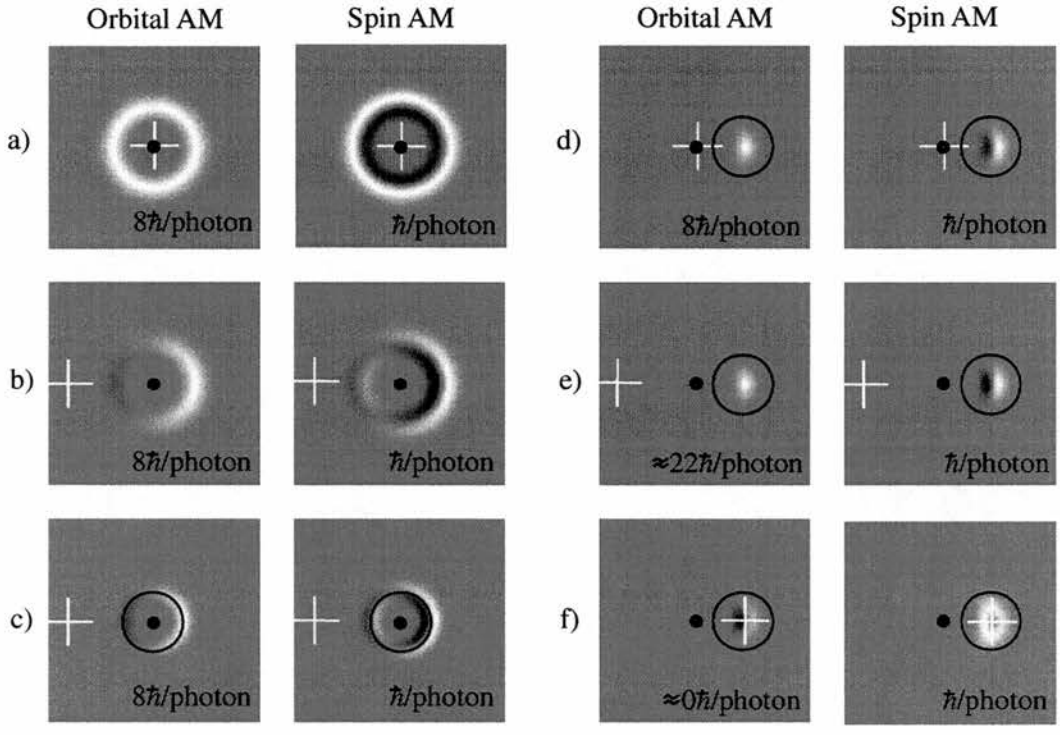

Figure 8.3: Numerically calculated local spin and orbital angular momentum densities in the direction of propagation for a $l = 8$ and $\sigma = 1$ Laguerre-Gaussian mode. A positive contribution is shown in white, grey represents zero and black a negative contribution: the black spot marks the axis of the original beam, the white cross marks the axis about which the angular momenta are calculated and, where appropriate, the black circle marks the position of a soft edged aperture. Note that the spin angular momentum is equivalent to $\sigma\hbar$ per photon irrespective of the choice of aperture or calculation axis, whereas the orbital angular momentum is only $l\hbar$ per photon if the aperture or calculation axes coincide with the axis of the original beam (calculation by Miles Padgett)

which show values of spin and orbital AM at various parts of the laser beam.

8.5 Results

Recall from Equation (5.2) in Chapter 5 that the radius of maximum intensity, $r_{I_{max}}$ of a Laguerre-Gaussian mode is given by [71],

$$r_{I_{max}} = \sqrt{\frac{z_R l}{k}}.$$

Even under the tight focusing associated with optical tweezers, the peak intensity ring of a Laguerre-Gaussian mode of high index l may be made several microns in diameter and consequently be much larger than the particles it is attempting to trap.

It is not surprising that, under these conditions, the particles are confined by the gradient force not on the beam axis, but at the radius of maximum light intensity. When a birefringent particle such as a calcite fragment is trapped, and circularly polarised light is converted to linear, the particle spins about its own axis. The sense of rotation is governed by the handedness of the circular polarisation.

For small particles the force arising from the light scattering, the momentum recoil force, becomes important. For a tightly focused Laguerre-Gaussian mode, the dominant component of the scattering force lies in the direction of beam propagation. The gradient force again constrains the particle to the annulus of maximum beam intensity. However, as the intensity distribution is cylindrically symmetric, the particle is not constrained azimuthally. Because the particle is trapped off the beam axis, the inclination of the helical phase fronts and the corresponding momentum result in a tangental force on the particle. For a small particle, although it is still contained within the annular ring of light, it orbits the beam axis in a direction determined by the handedness of the helical phase fronts; see Figure 8.4.

The small 1μm calcite particles, effectively spherical in nature, interacted with the orbital angular momentum and rotated around the beam profile as previously expected. The larger 3μm particles, which were asymmetric in

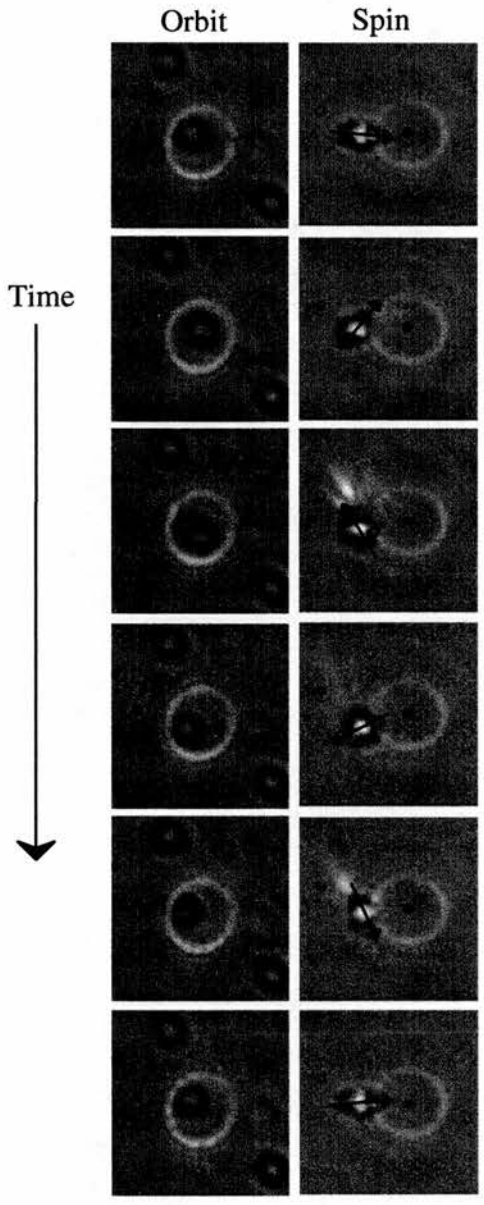

Figure 8.4: Successive frames of video of particles trapped near the focus of an $l = 8$ and $\sigma = 1$ Laguerre-Gaussian mode. Small particles are subject to a scattering force which allows them to exchange angular momentum with the orbital angular momentum of the beam and are set in motion, orbiting the beam axis. Larger, calcite fragments are birefringent and can exchange angular momentum with the spin angular momentum of the beam and are set spinning about their own axis.

shape, interacted with the spin AM and were held off-axis, rotating upon their own axis in a direction which depended upon the σ value of the circular polarisation.

8.6 Conclusion

From these observations it follows that the large and small calcite particles are interacting with spin and orbital angular momentum respectively. In principle, it should be possible to observe both the orbital and angular momentum acting simultaneously upon the same small birefringent particle. However, my results are inconclusive as birefringent particles which are small enough for the scattering force to induce a rotation about the beam axis are typically too small to see whether they are spinning about their own axis. Compounding the difficulty is the fact that they are often too spherical to be able to discern any rotation about the particle's own axis.

It would have been ideal to get both spin and orbital angular momentum working together on the same particle. A more exhaustive search on the geometry and particle size would be needed to find out what is required to allow this. I would suggest some intermediate geometry between 1 and 3μm in diameter, e.g. the asymmetric shape of the teflon particles used by Simpson *et al.* [19] would suffice.

These experiments, along with the numerical calculations which support them, has been the subject of a submission to Physical Review Letters [12].

Chapter 9

Conclusion

9.1 Introduction

In this chapter I present some overall conclusions to each of the research topics covered in this thesis. The thesis splits nicely into two sections; that of laser modes, and optical tweezers. At the end of the chapter I have general conclusions and future work relevant to the research project.

9.2 Laser Modes

9.2.1 The Variable Phase-shift Mode Converter

⋆ A. T. O'Neil and J. Courtial, Mode transformations in terms of the constituent Hermite-Gaussian or Laguerre-Gaussian modes and the variable-phase mode converter, *Opt. Commun.*, **181**, 35–45, (2000).

In this experiment I used various cylindrical lenses and Dove prisms to devise a system which allowed the transformation between different laser modes of the same mode order.

This system exploited the fact that one can draw parallels between various polarisations of light and certain types of laser mode. The previous knowl-

edge about polarisation allowed insight into the way first order laser modes behaved and could be transformed. This was directly applicable, and held, for higher order laser modes allowing many different types of laser modes to be efficiently produced including unusual, and previously unresearched, laser modes which might well be useful in the future study of quantum entanglement [38, 39].

9.3 Optical Tweezers

9.3.1 Lateral and Axial Trapping of silica spheres using Laguerre-Gaussian laser modes.

⋆ A. T. O'Neil and M. J. Padgett, Axial and lateral trapping efficiency of Laguerre-Gaussian laser modes in inverted optical tweezers, *Opt. Commun.* **193**, 45–50, (2001).

Lateral and axial trapping efficiencies (Q) were measured for optical tweezers. Various particle sizes and different laser modes were used in a method that measures both the lateral *and* axial Q-values for individual particles.

This research served to strengthen previous predictions as well as give a better coverage of reported results. The fact that for spheres larger than the focused beam size, the axial trapping efficiency increases when one implements a higher l LG mode was confirmed. However, not all my findings agreed with preliminary results. For example, I found no improvement in lateral trapping efficiency, this can be supported by the ray-optical model of the optical tweezers force. I discovered from these results that for smaller particles LG modes may, in fact, be less efficient than a fundamental Gaussian mode. Given these observations I can only suggest that one considers an LG mode if axial, rather than lateral trapping, is of paramount importance.

9.3.2 Rotational control within optical tweezers using a rotating aperture

⋆ A. T. O'Neil and M. J. Padgett, Rotational control within optical tweezers using a rotating aperture, submitted to *Opt. Lett.* in August 2001.

I presented a novel technique for rotational control of objects within optical tweezers. Simply, a rectangular aperture was placed in the laser beam resulting in a focused spot with its own rectangular symmetry. With an asymmetric object trapped in the beam, the particle itself aligns with the beam profile. Rotation of the aperture results in direct rotation of the particle.

This method can be readily applied to most existing optical tweezers arrangements. Its expected uses would be in the creation of micromachines were, clearly, precision rotational control is paramount. For other uses it can easily be removed to allow the original configuration for the optical tweezers set-up.

9.3.3 Using Inverted Optical Tweezers for Metal Particle Trapping

⋆ A. T. O'Neil and M. J. Padgett, Three-dimensional optical confinement of micron-sized metal particles and the de-coupling of the spin and orbital angular momentum within an optical spanner, *Opt. Commun.* **185**, 139–143, (2000).

During the course of this investigation I discovered a novel way of trapping silver particles. A metal particle could be trapped on the outside of a Laguerre-Gaussian laser beam. I observed that it rotated around the beam off-axis, and was confined within an annulus about the beam profile. This method of confinement allowed a deeper investigation into the properties of light. It allowed the discrimination of both the *spin* angular momentum and that of the *orbital* angular momentum of the beam.

The key result in this chapter was the effect of Spin AM relative to Orbital AM on the particle. Previously, the spin and orbital angular momentum components of a beam have been shown to act in an equivalent and interchangeable manner, e.g. for an optical spanner [19, 21], and more recently in the rotational Doppler shift [86, 82]. Conversely, I found that the interchangeability previously described is not a general phenomenon but depends on the specific process involved.

9.3.4 Orbital and spin angular momentum acting on calcite particles

⋆ A. T. O'Neil, I. MacVicar, L. Allen and M. J. Padgett, The intrinsic and extrinsic nature of the orbital angular momentum of a light beam, submitted to *Phys. Rev. Lett.* in June 2001, accepted in November 2001.

This work really leads on from the discoveries about spin and orbital AM made using silver particles. It is further investigation into the alternative actions of spin and orbital angular momentum on different-sized particles. The experimentation used particles trapped off-axis in a Laguerre-Gaussian beam with a high azimuthal mode index, $l = 8$.

The large calcite particles interact with spin AM, whilst the smaller, more spherical particles' motion was due to the orbital angular momentum. Both the orbital and spin angular momentum should were seen to act on the particles. When acted upon by the orbital angular momentum, the particle moved around off-axis at the most intense part of the beam. However, when acted on by the spin angular momentum, the motion was different, in that case the particle was positioned off-axis but instead of rotating around the beam it remained in one place and rotated on its own axis. Obviously, an asymmetrical particle is required to recognise this motion.

9.4 Future Work

9.4.1 Simultaneous acting of spin and orbital angular momentum on a particle

Building on my early results in which I was able to demonstrate more about spin and orbital angular momentum, there is a clear possibility of extending that work further. The ultimate results would be to obtain footage of *simultaneous* spin AM and orbital AM acting on a particle.

9.4.2 Mode converter used for quantum entanglement

In quantum entanglement experiments, people measure intermediate polarisations of individual photons. By analogy the mode converter work that I report produced intermediate modes, and may allow people to do the same for laser modes.

9.4.3 Rotation measurements

Within my thesis I obtained results on the rotation of particles. The results presented here are proof of principle, and development of this research would be useful. It would be useful to measure the magnitude of torques present in the system. Investigation into the mechanism at work, qualification of the rotation present and further research into applications like micromachines may develop this area further.

9.5 General Conclusions

Many areas have emerged that rely on optical tweezers as their basis. This thesis has described the fundamentals of this technique with a view to finding a wider range of applications in the future. I used optical tweezers to develop

knowledge of the spin and orbital angular momentum of light which enhances people's understanding for the future.

Appendix A

Holograms

A.1 Introduction

Holograms have been designed to address a wide range of distinctive applications. Rainbow holograms, for example, marked a major advance in display technology [87, 88]. These rainbow holograms are capable of transmitting the light and constructing a monochromatic image which is both bright and sharp. Rainbow holograms are widely used on credit cards as a security measure.

I used computer-generated holograms in my research. In this appendix, I describe the production of these holograms together with the sourcing of the required materials. Making holograms is a time-consuming business, and although their use forms a relatively small part of the research described in this thesis, the time spent creating them was disproportionately large. My hope is that this appendix will save future researchers from having to do time-consuming investigative procedures to find a good recipe for reliably producing effective holograms. Good reference books are Bjelkhagen [89] and Hariharan [90].

A.2 Computer-Generated Holograms

A description of how to produce Laguerre-Gaussian laser modes is given in Chapter 2 where I cited that the use of computer-generated holograms is one way of doing this. They offer an easy method for producing a variety of laser modes, although you do need to write a program to produce the desired "contact print" for the development process. By using special bleach solutions an amplitude profile can be changed to a phase hologram[1].

A.3 Blazing of Holograms

A diffraction grating converts a single laser mode to produce a mode with many different orders of equal powers. *Blazing* of a diffraction grating produces mode orders with preferential power levels in a particular order. Blazing is specified for a particular wavelength and usually designed for the first order. Blazing refers to the angling of the faces of each ruling on the hologram as shown in Figure A.1. For multiple-slit interference we get a diffraction pattern depending on the individual rulings we get light diffracted into specific orders and this specifies their strength. In Figure A.2 we can see the original binary pattern of an $l = 1$ hologram next to that of its blazed partner.

A.4 Hologram Production

First, the desired pattern is produced by writing a computer program to generate a `Tiff` file[2]. The `Tiff` file is written to a 35 mm slide which produces a greyscale image with values 0 to 255. The slide is used as a contact print on to either holographic film or glass plates with a layer of holographic emulsion

[1] As discussed in Section 2.4.2 phase holograms are much more efficient than the corresponding amplitude hologram.

[2] See Section A.5 for a diagram of the LabVIEW program used to write the `Tiff` file.

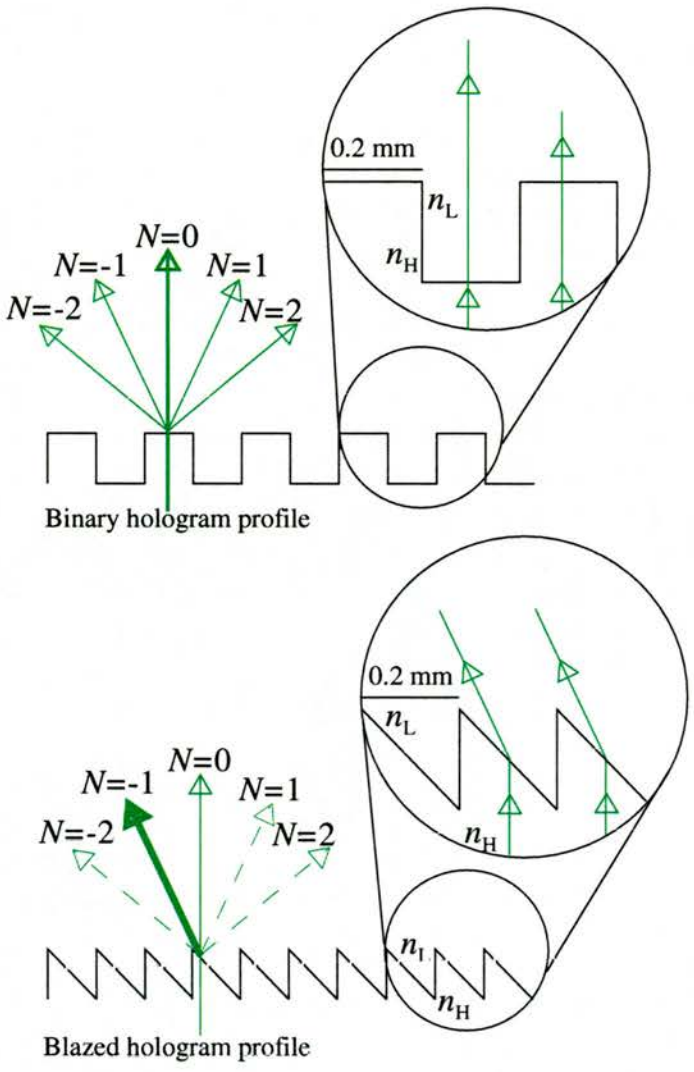

Figure A.1: This figure shows the difference in profile between a binary hologram and a blazed hologram. We can see that when light passes through the hologram in the blazed case it is preferentially directed into one order, it is not the case for binary holograms where one obtains many orders of low power and no preferential power direction.

applied to them. Once this has been done I go through the 'wet' development stage to create the finished hologram, Section A.6. Placing a hologram in the beam, alters its subsequent profile compared to that incident on the hologram.

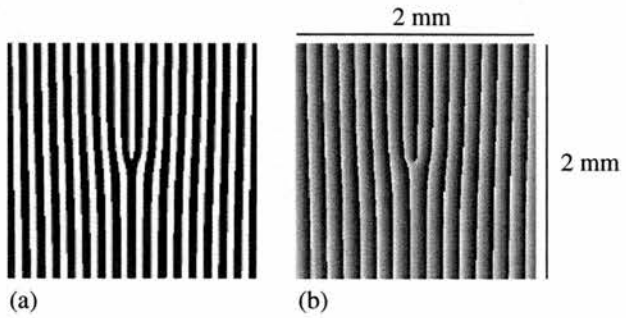

Figure A.2: Here we can see the difference between a binary hologram and a blazed hologram.

A.5 Program One

LabVIEW program for writing Computer-generated file to produce $p = 0$ Laguerre-Gaussian holograms. This produces a square array which can be saved as either a `Tiff` or a `Bitmap` image file. Given that the photographic film is 35×24 mm the maximum dimension for the array is 4096×2732 pixels. In Figure A.3 we can see the panel used to create the hologram with a specific l-value. In Figure A.4 we can see the code used to create the LabVIEW program.

A.6 The Development Procedure for Hologram Production

Jochen Arlt's original recipe [35] for transferral of a slide image onto holographic film is shown in Table A.1.

Since holographic film is not flat, I decided to use holographic plates, which can not be warped by the heat of the laser beam. I used AGFA MIL-

Process	Time
1. Exposure	
2. Develop (Kodak D-19)	4min
3. Rinse (5 ml acetic acid in 995 ml distilled water)	1 min
4. Fix (Kodak Max Fix)	4 min
5. Rinse (Distilled Water)	1 min
6. Rehalogenation bleach (see Table A.2)	5 min
7. Rinse (10 ml acetic acid in 990 ml distilled water)	10 min
8. Drying	

Table A.1: Processing of the holographic film, as used by Jochen Arlt [35].

Rehalogenation Bleach	
Potassium Dichromate	1.8 g
Potassium Bromide	4.0 g
Sulphuric Acid	1 ml
Distilled water to make	1.0 l

Table A.2: Chemistry for the rehalogenation bleach, as used by Jochen Arlt [35].

WARNING
Dichromate solutions are very hazardous to the environment, do NOT ever tip them down the sink! You must fill in COSHH forms stating the hazards involved.

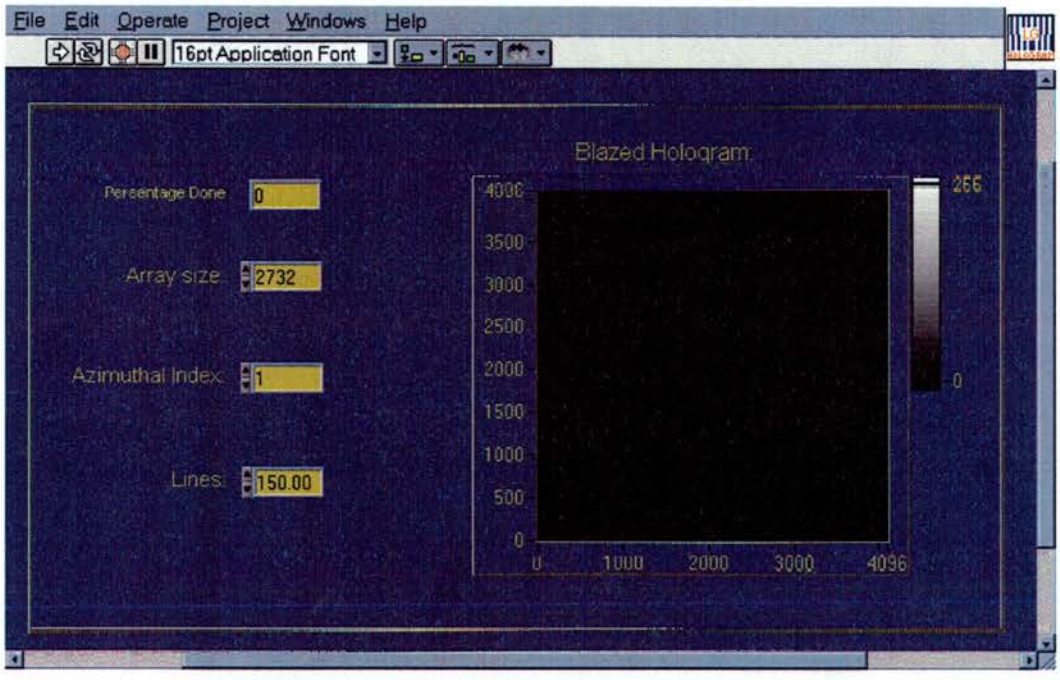

Figure A.3: Panel used for controlling the creation of holograms.

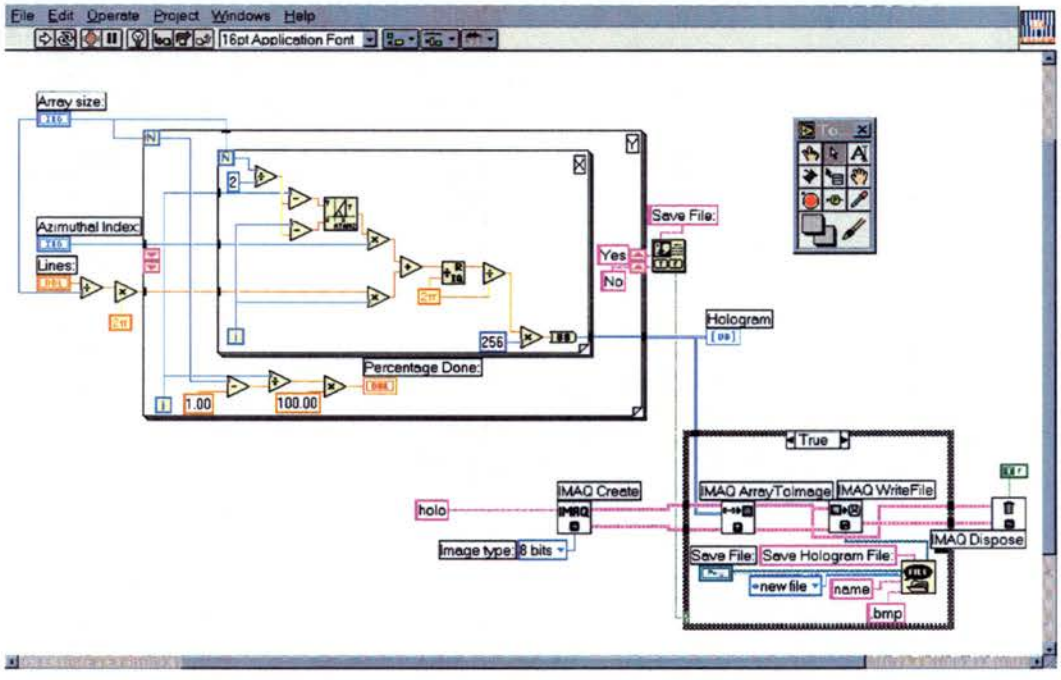

Figure A.4: Code used in LabVIEW for the creation of holograms.

LIMASK PLATES[3,4] with EMULSION FL5HD[5]. Whilst working on the recipe for these plates I tried various developers. Kodak (D-19) is the one routinely used, but is extremely contrasty (it makes the print more black and white, with little grey scale), a less harsh developer is Ilford Microphen (it has a better grey scale response and the blazing was much more effective). Ultimately I settled on `Ilford Perceptol` which retains the grey scale well, thus producing a far superior blaze and giving us better efficiencies as a result. I found that it was more important to make sure that the greyscale was full, from 0 to 255, than for the step height to be exact.

Table A.3 shows the recipe for holograms of greater than 30% efficiency[6]. Tables A.4, A.5 and A.6 give supplemental details needed for their creation.

[3]Supplier used for the Agfa Millimask Plates: LITHO SUPPLIES (UK) LTD, Scottish Region, Elphinstone Square, Deans Industrial Estate, Livingstone, West Lothian, EH54 8RG, Tel:01506 462555 Fax:01506 465678. Order Description: Millimask, Code: GSK8C, Emulsion: FL5HD, Dimensions: 7.6×7.6 cm.

[4]Always keep the holographic plates in the fridge (or preferably the freezer). Only take out the limited number you are going to use otherwise the emulsion degrades very quickly resulting in very low efficiencies.

[5]This emulsion is designed for use at green wavelengths. Its efficiency drops off greatly in the red ($\approx 50\%$ less than green).

[6]Adapted upon recipe by Chang and Winick [91].

Gelatine Hologram Method		
Method	**Time**	**Lighting**
1. Expose [4]	3′	
2. Develop in `Ilford Perceptol`	6′	None
3. Soak in **Stop Bath** (See Table A.4)	45″	
4. Rinse in Distilled H_2O	1′	
5. Soak in **Rehalogenation Bleach** (See Table A.5)	2′ 30″	
6. Rinse in Distilled H_2O	1′	
7. Soak in **Ammonium Dichromate Solution** (Table A.6)	5′	
8. Soak in hardening fixer $(0-2\%)$ [`Kodak Max Fix`]	5′	
9. Rinse in Running H_2O	10′	Light on
10. Rinse in Distilled H_2O	3′	
11. Dehydrate in 50% Isopropanol	5′	
12. Dehydrate in 100% Isopropanol	5′	
13. Dry in fast flowing air	30″	

Table A.3: The procedure for producing holograms using Agfa Millimask plates.

Stop Bath	
Acetic Acid	2.5 ml
Distilled water	497.5 ml

Table A.4: Chemistry for the stop bath.

Rehalogenation Bleach Stock Solutions:	
Stock solution A:	**Stock solution B:**
250 ml Distilled water	46 g Potassium bromide
10 g Ammonium Dichromate $(NH_4)_2Cr_2O_7$	500 ml Distilled water
7 ml concentrated sulphuric acid	
Distilled water to make 500 ml	
Working solution:	
Mix 1 part A with 10 parts distilled H_2O.	Then add 1 part B.

Table A.5: Chemistry for the stock solutions A and B for the rehalogenation bleach. The stock solutions are more stable, and if kept in the dark can be kept for a few weeks. The working solution is what is used for creating the hologram, it must only be used once.

Ammonium Dichromate solution:
Stock solution:
25 g Ammonium dichromate solution $(NH_4)_2Cr_2O_7$
500 ml Distilled water
Working solution:
Mix 1 part A with 9 parts distilled H_2O.

Table A.6: Chemistry for the ammonium dichromate solution. The stock solution is more stable, and if kept in the dark can be kept for a few weeks. The working solution is what is used for creating the hologram, it must only be used once.

Bibliography

[1] A. T. O'Neil and J. Courtial. Mode transformations in terms of the constituent Hermite-Gaussian or Laguerre-Gaussian modes and the variable-phase mode converter. *Opt. Commun.*, 181:35–45, 2000.

[2] A. Ashkin, J. M. Dziedzic, J. E. Bjorkholm, and S. Chu. Observation of a single-beam gradient force optical trap for dielectric particles. *Opt. Lett.*, 11:288–290, 1986.

[3] H. Felgner, O. Mueller, and M. Schliwa. Calibration of light forces in optical tweezers. *Appl. Opt.*, 34(6):977–982, 1995.

[4] W. H. Wright, G. J. Sonek, and M. W. Berns. Radiation trapping forces on microspheres in optical tweezers. *Appl. Phys. Lett.*, 63(6):715–717, 1993.

[5] N. B. Simpson, D. McGloin, K. Dholakia, L. Allen, and M. J. Padgett. Optical tweezers with increased axial trapping efficiency. *J. Mod. Opt.*, 45(9):1943–1949, 1998.

[6] A. T. O'Neil and M. J. Padgett. Axial and lateral trapping efficiency of Laguerre-Gaussian laser modes in inverted optical tweezers. *Opt. Commun.*, 193:45–50, 2001.

[7] A. T. O'Neil and M. J. Padgett. Rotational control within optical tweezers using a rotating aperture. submitted to Opt. Lett. in August 2001.

[8] S. Sato, M. Ishigure, and H. Inaba. Optical trapping and rotational manipulation of microscopic particles and biological cells using higher-order mode Nd-YAG laser-beams. *Elec. Lett.*, 27(20):1831–1832, 1991.

[9] A. T. O'Neil and M. J. Padgett. Three-dimensional optical confinement of micron-sized metal particles and the de-coupling of the spin and orbital angular momentum within an optical spanner. *Opt. Commun.*, 185:139–143, 2000.

[10] K. Sasaki, M. Koshioka, H. Kitamura, and H. Masuhara. Optical trapping of a metal-particle and a water droplet by a scanning laser-beam. *Appl. Phys. Lett.*, 60(7):807–809, 1992.

[11] S. Sato, Y. Harada, and Y. Waseda. Optical trapping of microscopic metal particles. *Opt. Lett.*, 19(22):1807–1809, 1994.

[12] A. T. O'Neil, I. MacVicar, L. Allen, and M. J. Padgett. The intrinsic and extrinsic nature of the orbital angular momentum of a light beam. to appear in Physics Review Letters.

[13] A. E. Siegman. *Lasers.* University Science Books, Mill Valley, California, 1986.

[14] G. B. Arfken and H. Weber. *Mathematical methods for physicists.* Academic Press, 4th edition, 1995.

[15] J. M. Vaughan and D. V. Willetts. Interference properties of a light beam having a helical wave surface. *Opt. Commun.*, 30:263–267, 1979.

[16] I. S. Gradshteyn and I. M. Ryzhik. *Tables Of Series, Products, And Integrals.* Berlin:VEB, 3rd. edition, 1957. Chapter 8, Eqn. 8.970 (1).

[17] L. Allen, M. W. Beijersbergen, R. J. C. Spreeuw, and J. P. Woerdman. Orbital angular momentum of light and the transformation of Laguerre-Gaussian modes. *Phys. Rev. A*, 45:8185–8189, 1992.

[18] I. V. Basistiy, V. Yu. Bazhenov, M. S. Soskin, and M. V. Vasnetsov. Optics of light beams with screw dislocations. *Opt. Commun.*, 103:422–428, 1993.

[19] N. B. Simpson, K. Dholakia, L. Allen, and M. J. Padgett. Mechanical equivalence of spin and orbital angular momentum of light: an optical spanner. *Opt. Lett.*, 22:52–54, 1997.

[20] R. A. Beth. Mechanical detection and measurement of the angular momentum of light. *Phys. Rev.*, 50:115–125, 1936.

[21] M. E. J. Friese, T. A. Nieminen, N. R. Heckenberg, and H. Rubinsztein-Dunlop. Optical alignment and spinning of laser-trapped microscopic particles. *Nature*, 394(6691):348–350, 1998.

[22] H. He, M. E. J. Friese, N. R. Heckenberg, and H. Rubinsztein-Dunlop. Direct observation of transfer of angular momentum to absorptive particles from a laser beam with a phase singularity. *Phys. Rev. Lett.*, 75:826–829, 1995.

[23] M. E. J. Friese, J. Enger, H. Rubinsztein-Dunlop, and N. R. Heckenberg. Optical angular-momentum transfer to trapped absorbing particles. *Phys. Rev. A*, 54:1593–1596, 1996.

[24] M. W. Beijersbergen, L. Allen, H. E. L. O. van der Veen, and J. P. Woerdman. Astigmatic laser mode converters and transfer of orbital angular momentum. *Opt. Commun.*, 96:123–132, 1993.

[25] N. R. Heckenberg, R. McDuff, C. P. Smith, and A. G. White. Generation of optical-phase singularities by computer-generated holograms. *Opt. Lett.*, 17:221–223, 1992.

[26] N. R. Heckenberg, R. McDuff, C. P. Smith, H. Rubinsztein-Dunlop, and M. J. Wegener. Laser beams with phase singularities. *Opt. and Quant. Electron.*, 24:S951–S962, 1992.

[27] J. Arlt, K. Dholakia, L. Allen, and M. J. Padgett. The production of multiringed Laguerre-Gaussian modes by computer-generated holograms. *J. Mod. Opt.*, 45:1231–1237, 1998.

[28] M. W. Beijersbergen, R. P. C. Coerwinkel, M. Kristensen, and J. P. Woerdman. Helical-wavefront laser beams produced with a spiral phaseplate. *Opt. Commun.*, 112:321–327, 1994.

[29] G. A. Turnbull, D. A. Robertson, G. M. Smith, L. Allen, and M. J. Padgett. The generation of free-space Laguerre-Gaussian modes at millimetre-wave frequencies by use of a spiral phaseplate. *Opt. Commun.*, 127:183–188, 1996.

[30] R. Oron, N. Davidson, A. A. Friesem, and E. Hasman. Efficient formation of pure helical laser beams. *Opt. Commun.*, 182:205–208, 2000.

[31] E. Abramochkin, N. Losevsky, and V. Volostnikov. Generation of spiral-type laser beams. *Opt. Commun.*, 141(1–2):59–64, 1997.

[32] S. Chavez-Cerda. personal communication, 2001.

[33] M. J. Padgett, J. Arlt, N. B. Simpson, and L. Allen. An experiment to observe the intensity and phase structure of Laguerre-Gaussian laser modes. *Am. J. Phys.*, 64:77–82, 1996.

[34] H. He, N. R. Heckenberg, and H. Rubinsztein-Dunlop. Optical particle trapping with higher-order doughnut beams using high efficiency computer generated holograms. *J. Mod. Opt.*, 42(1):217–223, 1995.

[35] Jochen Arlt. *Applications of Laguerre-Gaussian beams and Bessel beams to both nonlinear optics and atom optics.* PhD thesis, University of St Andrews, December 1999.

[36] M. J. Padgett and J. Courtial. A Poincaré-sphere equivalent for light beams containing orbital angular momentum. *Opt. Lett.*, 24:430–432, 1999.

[37] L. Allen, J. Courtial, and M. J. Padgett. Matrix formulation for the propagation of light beams with orbital and spin angular momenta. *Phys. Rev. E*, 60:7497–7503, 1999.

[38] S. M. Barnett. personal communication, 2000.

[39] S. Franke-Arnold, S. M. Barnett, M. J. Padgett, and L. Allen. Two-photon entanglement of orbital angular momentum states. To appear in Phys. Rev. A, 2001.

[40] Cell Robotics International Inc., Albuquerque USA.

[41] P.A.L.M. GmbH, Bernried, Germany.

[42] A. Ashkin. Acceleration and trapping of particles by radiation pressure. *Phys. Rev. Lett.*, 24(4):156–159, 1970.

[43] E. G. Rawson and A. D. May. Propulsion and angular stabilization of dust particles in a laser cavity. *Appl. Phys. Lett.*, 8(4):93–95, 1966.

[44] A. D. May, E. G. Rawson, and E. H. Hara. Propulsion and angular stabilization of dust particles in a laser cavity. ii. *J. Appl. Phys.*, 38(13):5290–5292, 1967.

[45] A. Ashkin. The pressure of laser light. *Scient. Amer.*, 226:63–71, 1972.

[46] A. Ashkin. Atomic beam deflection by resonance-radiation pressure. *Phys. Rev. Lett.*, 25(19):1321–1324, 1970.

[47] A. Ashkin. Trapping of atoms by resonance radiation pressure. *Phys. Rev. Lett.*, 40(12):729, 1978.

[48] A. Ashkin, J. M. Dziedzic, and T. Yamane. Optical trapping and manipulation of single cells using infrared-laser beams. *Nature*, 330(6150):769–771, 1987.

[49] S. M. Block. *Non-invasive Techniques in Cell Biology*, volume 9, chapter 15, pages 375–402. Wiley-Liss, New York, 1990.

[50] S. Sato and H. Inaba. Optical trapping and manipulation of microscopic particles and biological cells by laser beams. *Opt. Quant. Electr.*, 28:1–16, 1996.

[51] M. D. Wang, H. Yin, R. Landick, J. Gelles, and S. M. Block. Stretching DNA with optical tweezers. *Biophysical J.*, 72(3):1335–1346, 1997.

[52] J. Conia, B. S. Edwards, and S. Voelkel. The micro-robotic laboratory: Optical trapping and scissing for the biologist. *J. Clin. Lab. Anal.*, 11(1):28–38, 1997.

[53] S. M. Block, D. F. Blair, and H. C. Berg. Compliance of bacterial flagella measured with optical tweezers. *Nature*, 338:514–518, 1989.

[54] K. Svoboda and S. M. Block. Optical trapping of metallic Rayleigh particles. *Opt. Lett.*, 19(13):930–932, 1994.

[55] N. B. Simpson, L. Allen, and M. J. Padgett. Optical tweezers and optical spanners with Laguerre-Gaussian modes. *J. Mod. Opt.*, 43:2485–2491, 1996.

[56] S. Sato, E. Higurashi, Y. Taguchi, and H. Inaba. Achievement of laser fusion of biological cells using UV pulsed dye-laser beams. *Appl. Phys. B.*, 54(6):531–533, 1992.

[57] A. E. Chiou, W. Wang, G. J. Sonek, J. Hong, and M. W. Berns. Interferometric optical tweezers. *Opt. Commun.*, 133(1–6):7–10, 1997.

[58] L. Paterson, M. P. MacDonald, J. Arlt, W. Sibbett, P. E. Bryant, and K Dholakia. Controlled rotation of optically trapped microscopic particles. *Science*, 292:912–914, 2001.

[59] A. Ashkin. Applications of laser radiation pressure. *Science*, 210(4474):1081–1088, 1980.

[60] A. L. Schawlow and C. H. Townes. Infrared and optical masers. *Phys. Rev.*, 112(6):1940–1949, 1958.

[61] T. H. Maiman. Stimulated optical radiation in ruby. *Nature*, 187(4736):493–494, 1960.

[62] S. Chu, J. E. Bjorkholm, A. Ashkin, and A. Cable. Experimental observation of optically trapped atoms. *Phys. Rev. Lett.*, 57(3):314–317, 1986.

[63] C. S. Adams and E. Riis. Cooling and trapping of neutral atoms. *Prog. Quantum Electron.*, 21(1):1–79, 1997.

[64] H. Furukawa and I. Yamaguchi. Optical trapping of metallic particles by a fixed Gaussian beam. *Opt. Lett.*, 23(3):216–218, 1998.

[65] J. T. Finer, R. M. Simmons, and J. A. Spudich. Single myosin molecule mechanics — piconewton forces and nanometer steps. *Nature*, 368(6467):113–119, 1994.

[66] A. Ashkin. Forces of a single-beam gradient laser trap on a dielectric sphere in the ray optics regime. *Biophys. J.*, 61(2):569–582, 1992.

[67] R. Gussgard, T. Lindmo, and I. Brevik. Calculation of the trapping force in a strongly focused laser beam. *J. Opt. Soc. Amer. B*, 9(10):1922–1930, 1992.

[68] J-S Kim and S-W Kim. Dynamic motion analysis of optically trapped nonspherical particles with off-axis position and arbitrary orientation. *Appl. Opt.*, 39(24):4327–4332, 2000.

[69] K. T. Gahagan and G. A. Swartzlander Jr. Simultaneous trapping of low-index and high-index microparticles observed with an optical-vortex trap. *J. Opt. Soc. B*, 16(4):533–537, 1999.

[70] Min Gu, D. Morrish, and Pu Chun Ke. Enhancement of transverse trapping efficiency for a metallic particle using an obstructed laser beam. *Appl. Phys. Lett.*, 77(1):34–36, 2000.

[71] M. J. Padgett and L. Allen. The Poynting vector in Laguerre-Gaussian laser modes. *Opt. Commun.*, 121:36–40, 1995.

[72] M. E. J. Friese, H. Rubinsztein-Dunlop, N. R. Heckenberg, and E. W. Dearden. Determination of the force constant of a single-beam gradient trap by measurement of backscattered light. *Appl. Opt.*, 35(36):7112–7116, 1996.

[73] H. Liang, W. H. Wright, C. L. Rieder, E. D. Salmon, G. Profeta, J. Andrews, Y. G. Liu, G. J. Sonek, and M. Berns. Directed movement of chromosome arms and fragments in mitotic newt lung-cells using optical scissors and optical tweezers. *Exp. Cell Res.*, 213(1):308–312, 1994.

[74] Y. Liu, G. J. Sonek, M. W. Berns, K. Konig, and B. J. Tromberg. 2-photon fluorescence excitation in continuous-wave infrared optical tweezers. *Opt. Lett.*, 20(21):2246–2248, 1995.

[75] K. Visscher and G. J. Brakenhoff. Single beam optical trapping integrated in a confocal microscope for biological applications. *Cytometry*, 12(6):486–491, 1991.

[76] L. P. Ghislain and W. W. Webb. Scanning-force microscope based on an optical trap. *Opt. Lett.*, 18(19):1678–1680, 1993.

[77] E. Higurashi, H. Ukita, H. Tanka, and O. Ohguchi. Optically induced rotation of anisotropic micro-objects fabricated by surface micromachining. *Appl. Phys. Lett.*, 64(17):2209–2210, 1994.

[78] Z. P. Luo, Y. L. Sun, and K. N. An. An optical spin micromotor. *Appl. Phys. Lett.*, 76(13):1779–1781, 2000.

[79] R. C. Gauthier, M. Ashman, and C. P. Gover. Experimental confirmation of the optical-trapping properties of cylindrical objects. *Appl. Opt.*, 38(22):4861–4869, 1999.

[80] G. J. Brakenhoff K. Visscher and J. J. Krol. Micromanipulation by multiple optical traps created by a single fast scanning trap integrated with the bilateral confocal scanning laser microscope. *Cytometry*, 14(2):105–114, 1993.

[81] M. Reicherter, T. Haist, E. U. Wagemann, and H. J. Tiziani. Optical particle trapping with computer-generated holograms written on a liquid-crystal display. *Opt. Lett.*, 24(9):608–610, 1999.

[82] J. Courtial, D. A. Robertson, K. Dholakia, L. Allen, and M. J. Padgett. Rotational Doppler shift of a light beam. *Phys. Rev. Lett.*, 81:4828–4830, 1998.

[83] I. A. Vorobjev, L. Hong, W. H. Wright, and M. W. Berns. Optical trapping for chromosome manipulation - a wavelength dependence of induced chromosome bridges. *Biophys J.*, 64(2):533–538, 1993.

[84] J. W. Simmons and M. J. Guttman. *States, Waves and Photons.* Addison-Wesley, 1970.

[85] L. Allen and M. J. Padgett. The Poynting vector in Laguerre-Gaussian beams and the interpretation of their angular momentum density. *Opt. Commun.*, 184(1–4):67–71, 2000.

[86] J. Courtial, K. Dholakia, D. A. Robertson, L. Allen, and M. J. Padgett. Measurement of the rotational frequency shift imparted to a rotating light beam possessing orbital angular momentum. *Phys. Rev. Lett.*, 80:3217–3219, 1998.

[87] S. A. Benton. Hologram reconstructions with extended incoherent sources. *J. Opt. Soc. Am.*, 59:1545–6, 1969.

[88] S. A. Benton, Editors: E. Marom, A. A. Friesem, and E. Wiener-Avnear. *Applications of Holography & Optical Data Processing*, chapter White transmission/reflection holographic imaging, pages 401–409. Oxford: The Pergamon Press, 1977.

[89] H. I. Bjelkhagen. *Silver-Halide Recording Materials.* Springer, second ed. edition, 1995.

[90] P. Hariharan. *Optical Holography: Principles, Techniques and Applications.* Cambridge University Press, first ed. edition, 1986.

[91] B. J. Chang and K. Winick. Silver-halide gelatin holograms. In T. C. Lee and P. N. Tamura, editors, *Proc. of SPIE: Recent Advances in Holography*, volume 215, pages 172–177, 1980.